

Fingerprints of classical memory in quantum hysteresis

Francesco Caravelli^{1,2}

¹*Los Alamos National Laboratory, Los Alamos, New Mexico 87545, USA*

²*Dipartimento di Fisica dell'Università di Pisa, Largo Bruno Pontecorvo 3, I-56127 Pisa, Italy*

(Dated: January 29, 2026)

We present a simple framework for classical and quantum “memory” in which the Hamiltonian at time t depends on past values of a control Hamiltonian through a causal kernel. This structure naturally describes finite-bandwidth or filtered control channels and provides a clean way to distinguish between memory in the control and genuine non-Markovian dynamics of the state. We focus on models where $H(t) = H_0 + \int_{-\infty}^t K(t-s) H_1(s) ds$, and illustrate the framework on single-qubit examples such as $H(t) = \sigma_z + \Phi(t) \sigma_x$ with $\Phi(t) = \int_{-\infty}^t K(t-s) u(s) ds$. We derive basic properties of such dynamics, discuss conditions for unitarity, give an equivalent time-local description for exponential kernels, and show explicitly how hysteresis arises in the response of a driven qubit.

I. INTRODUCTION

¹ High-fidelity coherent control is a basic requirement across quantum information science, from gate synthesis and dynamical decoupling to calibration, characterization, and error mitigation.[1–4] In the idealized description used in much of the theory, the experimenter prescribes a time-dependent Hamiltonian and the device follows it exactly. This abstraction is analytically convenient and often accurate at the level of first principles, but it hides an important practical layer: the Hamiltonian experienced by the quantum system is not programmed directly. Instead, it is generated and delivered by a classical control stack, as for instance room-temperature electronics, wiring, attenuators, bias tees, packaging, and on-chip filters, with finite bandwidth and its own internal dynamics.[5] This issue is particularly timely in view of recent evidence of memory effects in out-of-equilibrium protocols on quantum annealers by Pelofske and collaborators [6, 7].

A simple intuition comes from elementary electronics. Driving an RC circuit with a time-dependent voltage does not produce an output that tracks the input instantaneously; rather, the output relaxes toward it with a characteristic time constant, leading to smoothing and a phase lag that depend on the drive history. Analogous effects appear broadly in quantum-control platforms: control lines act as low-pass filters, cables and packaging introduce dispersion, bias tees and amplifiers contribute dynamical response, and resonator-mediated actuation adds latency and ringing.[5, 8, 9] As a result, the field that actually reaches the device can carry substantial *classical memory*, even when the device itself is perfectly isolated and its intrinsic evolution is unitary.

This distinction matters both conceptually and operationally. Classical memory in the control channel can generate signatures that resemble dissipation or non-Markovianity, for example, hysteresis loops when plotting an observable against the commanded waveform,

despite the absence of any environmental memory in the quantum state evolution.[10–12] Conversely, genuine quantum memory originates in system–environment coupling and must be diagnosed by observables that are insensitive to purely classical distortions.[10–12] Separating these mechanisms is therefore essential for interpreting data and for designing robust control protocols.

Motivated and inspired by these experimental works, we adopt a minimal framework in which the commanded waveform $u(t)$ generated at room temperature is mapped to an in-situ realized field $\Phi(t)$ by a causal filter,

$$\begin{aligned} \Phi(t) &= \Phi_0 + (K * u)(t) \\ &= \Phi_0 + \int_{-\infty}^t K(t-s) u(s) ds, \end{aligned} \quad (1)$$

and $\Phi(t)$ is the control amplitude that enters the device Hamiltonian. This kernel inside the Hamiltonian has been used sporadically in the past, and it is used in the quantum-control literature to model hardware distortion, finite bandwidth, and ringdown.[9, 13, 14] In particular, Hincks *et al.* incorporate explicit distortion dynamics (including nonlinearities) directly into optimal-control synthesis, so that the optimized command $u(t)$ implements a target unitary under the *realized* waveform that reaches the device.[13] Related approaches appear in resonator-limited control [9] and in integrated calibration/optimization toolchains for superconducting circuits.[14]

While we adopt the same physical separation between commanded and realized control, our goal is not pulse design under a known distortion model. Instead, we use the filtered-control viewpoint to develop a *memory diagnostics* program based on geometric loop measures. Concretely, we treat the control as a dynamical memory system in its own right and quantify its hysteretic response by loop areas such as $\mathcal{A}_{u\Phi} = \oint \Phi du$; as a result, we show that even when the device responds adiabatically to the *realized* trajectory (so that $O(t) \approx f(\Phi(t))$ and $\mathcal{A}_{\Phi O} \approx 0$), a nonzero commanded-loop area $\mathcal{A}_{uO} = \oint O du$ can persist as a deterministic fingerprint of classical filtering, with controlled small-amplitude relations linking \mathcal{A}_{uO} to $\mathcal{A}_{u\Phi}$; we then use $\mathcal{A}_{\Phi O}$ as a diagnostic that separates

¹ caravelli@lanl.gov * guest affiliations.

classical control memory from genuinely state-history-dependent effects (e.g. coherent nonadiabaticity) at fixed realized field. In this sense, our framework is aimed at the interpretation and separation of mechanisms, rather than at the inversion of the distortion map.

In the second part of the manuscript, and to keep the control memory both experimentally grounded and analytically tractable, we connect the kernel K to (classical) passive RC line models to build the intuition. Classical network-synthesis constraints imply that passive RC ladders have transfer functions with poles on the negative real axis, so their impulse responses are sums (or mixtures) of decaying exponentials. This motivates the exponential mode embedding used throughout the paper and provides a concrete physical meaning for the rates as relaxation time scales of the control. Dissipation in the control stack is most commonly modeled by treating the channel as an *open* quantum system, i.e., by coupling it to uncontrolled degrees of freedom and describing the reduced channel dynamics with an effective Gorini-Kossakowski-Sudarshan-Lindblad, or GKLS generator (see for instance [15] for a review). From a complementary microscopic viewpoint, however, eliminating the environmental degrees of freedom leads to a generalized Langevin description [16] in which *memory and fluctuations arise together*: the same bath modes that generate a retarded friction (memory) kernel also produce stochastic forces, whose correlations are constrained by the fluctuation-dissipation theorem [17, 18]. In this work we focus on the deterministic memory kernel governing the mean input-output response of the channel; the accompanying noise, while essential for a fully consistent description, is not modeled explicitly here but is nevertheless linked to the kernel through the corresponding fluctuation-dissipation relations.

We also give a microscopic derivation (in the Kubo linear response formalism) in which the control is modeled as a (possibly large) quantum channel driven at an input port by the classical source $u(t)$. In linear response, the realized field is a retarded susceptibility convolved with the command, and we show that under weak coupling conditions the device evolves under an effective filtered-control Hamiltonian, with fluctuations entering only as a separate weak correction. We highlight that the classical and quantum framework are mutually consistent in the presence of dissipation.

The manuscript is organized as follows. Section II introduces the kernel-filtered control model and the standing assumptions ensuring unitary device evolution at the level treated here. Section III shows how common causal kernels admit a time-local embedding via a finite set of auxiliary filter modes. Section IV defines loop measures in the (u, Φ) , (u, O) , and (Φ, O) planes and introduces the adiabatic response function $f(\Phi)$. Section V treats the nonadiabatic regime and clarifies why loop areas alone do not certify open-system quantum memory. Sections VI-VII connect the kernel description to RC-network control lines and work out single-qubit case studies (including an

exactly solvable commuting benchmark). Section VIII presents numerical experiments mapping the frequency dependence of the loop measures, and Sec. IX concludes. Most technical derivations are collected in the appendices.

II. HAMILTONIANS WITH A MEMORY KERNEL

In this first part of the manuscript, we discuss a simple model of the control. We provide a general treatment of filtered Hamiltonians, discussed in [9, 13].

A. Model and standing assumptions

We consider closed-system dynamics generated by Hamiltonians whose control component is processed through a causal response function. Concretely, we consider

$$\hat{H}(t) = \hat{H}_A + \hat{H}'_c(t) \quad (2)$$

$$\equiv \hat{H}_A + \int_{-\infty}^t K(t-s) \hat{H}_c(s) ds, \quad (3)$$

where \hat{H}_A is a fixed (time-independent) drift Hamiltonian and $\hat{H}'_c(s)$ is a Hermitian control Hamiltonian. The scalar function K is a kernel encoding the impulse response of a classical control channel.[19, 20] Unless stated otherwise, we assume that K is *causal*, e.g.

$$K(\tau) = 0 \quad \text{for } \tau < 0, \quad (4)$$

so that $\hat{H}(t)$ depends only on past values of the control.

The convolution in Eq. (3) is understood as an operator-valued integral (intended as a Bochner integral [21]). A simple set of sufficient conditions for well-posedness is that $K \in L^1(\mathbb{R}_+)$ and that $\sup_{s \in \mathbb{R}} \|\hat{H}_c(s)\| < \infty$, which guarantees that the integral exists and defines a bounded operator for each t .[22, 23] These assumptions are mild and encompass the kernels typically used to model finite bandwidth or linear filtering (e.g. sums of decaying exponentials).[19]

It is convenient to introduce the filtered control operator

$$\hat{H}'_c(t) := \int_{-\infty}^t K(t-s) \hat{H}_c(s) ds, \quad (5)$$

so that $\hat{H}(t) = \hat{H}_A + \hat{H}'_c(t)$. In this form, all history dependence is confined to the map $\hat{H}_c(\cdot) \mapsto \hat{H}'_c(\cdot)$, which is linear and time-translation invariant. In other words, the control channel acts as a classical LTI filter on an operator-valued input.[19, 24] A direct generalization of this integral is the case of K promoted to an operator is not proportional to the identity. This phenomenological Hamiltonian can be justified both via a classical and quantum treatment, that we discuss later in Sec. IV.

Now, we note that causality implies that specifying the control trajectory $\hat{H}_c(s)$ for $s \leq t$ uniquely determines the instantaneous generator $\hat{H}(t)$. The resulting dynamics is nevertheless local in the state: once $\hat{H}(t)$ is fixed, the Schrödinger equation retains its standard first-order form and does not involve the past history of the quantum state.[23] In this sense, the “memory” described by K is classical and resides in the actuation mechanism, not in the quantum dynamics of the system itself.

The RC circuit provides a useful archetype. A voltage command applied at the input of an RC filter produces an output that relaxes toward the command with a characteristic time constant.[20] At the Hamiltonian level, this corresponds to replacing the commanded control by a smoothed and phase-lagged realized control, obtained by convolution with an exponentially decaying kernel.[19] More general kernels represent more elaborate linear responses, including multi-timescale relaxation (sums of exponentials) and resonant features (damped oscillatory responses), while still maintaining a simple, causal description at the Hamiltonian level.[19, 25]

For the evolution generated by Eq. (3) to be unitary, the instantaneous Hamiltonian must be Hermitian for all t . Since \hat{H}_A and $\hat{H}_c(s)$ are assumed Hermitian, one has

$$\hat{H}(t)^\dagger = \hat{H}_A + \int_{-\infty}^t K(t-s)^* \hat{H}_c(s) ds. \quad (6)$$

Thus, for a scalar kernel acting multiplicatively on a Hermitian operator input, a transparent sufficient condition for Hermiticity is that the kernel be real-valued,

$$K(\tau) \in \mathbb{R} \quad \text{for all } \tau, \quad (7)$$

so that the filtered control $\hat{H}'_c(t)$ is a real linear combination of Hermitian operators. Under Eq. (7), the propagator is unitary for each fixed control trajectory.[22, 23]

We emphasize that Eq. (7) is a condition on the effective description rather than a fundamental constraint: in applications, K is typically identified with a classical impulse response (hence real), or with the real part of a causal response function inferred from calibration data.[5, 8, 19] In either case, the framework provides a compact way to incorporate finite-bandwidth distortions while maintaining a strictly unitary closed-system description.[1, 23]

The discussion simplifies dramatically for the case of a scalar control $\hat{H}_c(t) = u(t)\hat{M}$ filtered through a causal kernel: the realized drive is $w(t) = (K * u)(t)$ and the Hamiltonian reads $\hat{H}(t) = \hat{H}_A + w(t)\hat{M}$. Above, $u(t)$ is the *commanded* control parameter, e.g. what an experimenter would set on the software or the voltage generator. In App.A we provide general statements for the unitary evolution operator based on the properties of the kernel $K(\tau)$.

Before we continue, let us now briefly comment on the units. With $\hbar = 1$, Hamiltonians have units of inverse time. Since the filtered control enters as a causal

convolution $\hat{H}'_c(t) = \int_{-\infty}^t K(t-s) \hat{H}_c(s) ds$, dimensional consistency requires $[K][\hat{H}_c][\text{time}] = [\hat{H}]$. In the convention we use here where the control term is written as $\hat{H}_c(s) = u(s)\hat{M}$ with a fixed dimensionless generator \hat{M} (e.g. Pauli operators), the drive amplitude u carries the physical energy scale, and one has $[K] = 1/\text{time}$ so that $u_{\text{eff}}(t) = \int_{-\infty}^t K(t-s)u(s) ds$ has the same units as u . In this convention the integrated weight $g = \int_0^\infty K(\tau) d\tau$ is dimensionless, and the Markov/instantaneous limit $K(\tau) \rightarrow g\delta(\tau)$ corresponds to a memoryless rescaling $u_{\text{eff}}(t) \rightarrow g u(t)$.

Later, when we interpret $u(t)$ as a laboratory control such as a voltage waveform $V(t)$ (rather than an already-calibrated energy amplitude), an additional conversion factor is implicitly present: the device couples to an electrical potential through an appropriate charge-like scale (e.g. e or an effective charge/lever arm set by circuit geometry), so the Hamiltonian drive takes the schematic form $\hat{H}_c(t) \sim (\text{coupling}) \times V(t) \times \hat{M}$. One may adopt “electrical natural units” in which this charge scale is set to unity (informally $e = 1$), absorbing the conversion into the definition of u . Restoring physical units then amounts to re-inserting the appropriate factor (for example e times a dimensionless lever arm, or more generally the relevant calibration constant mapping volts to energy) so that the product has units of energy. Which prefactor appears depends on the experimental realization (gate voltage, flux bias, piezo drive, etc.), but once this mapping $V \mapsto u$ is fixed, the kernel units follow as above and the convolution remains dimensionally consistent.

B. Time-local embedding for scalar filtered control

A key advantage of kernel-filtered Hamiltonians is that broad and physically relevant classes of causal kernels admit an equivalent *time-local* realization once one introduces a small set of auxiliary classical variables. This converts the nonlocal convolution in the Hamiltonian into an ordinary differential equation (ODE) for the realized field, coupled to the usual Schrödinger equation.[19, 26] The quantum evolution remains unitary (for Hermitian instantaneous Hamiltonians), while the control channel becomes an explicit finite-dimensional dynamical system.

We focus on the case in which the filtered control enters as a scalar amplitude multiplying a fixed Hermitian operator,

$$\hat{H}(t) = \hat{H}_A + \Phi(t)\hat{M}, \quad \Phi(t) = \int_{-\infty}^t K(t-s)u(s) ds, \quad (8)$$

with real command $u(t)$ and causal kernel $K(\tau)$. In this setting, $\Phi(t)$ is the *realized field*, e.g. the effective drive amplitude reaching the device. While this choice will be motivated shortly, it is evident from its form that it is a form of classical memory in the Hamiltonian control.

A particularly convenient class is given by kernels representable as finite (or truncated) sums of decaying exponentials,

$$K(\tau) = \sum_{k=1}^{K_{\max}} c_k e^{-\nu_k \tau} \Theta(\tau), \quad \nu_k > 0, \quad c_k \in \mathbb{R}. \quad (9)$$

As we show in the example later, this is motivated by the physics of a control line, where passive RC ladders and lossy transmission channels naturally generate multi-exponential impulse responses.[25, 27] This includes, as special cases, the single-mode RC kernel, where the decay rates ν_k form a ladder $\nu_k = 2\pi k/\beta$.

Defining auxiliary filter modes

$$\Phi_k(t) := \int_{-\infty}^t c_k e^{-\nu_k(t-s)} u(s) ds, \quad \Phi(t) = \sum_{k=1}^{K_{\max}} \Phi_k(t), \quad (10)$$

one finds that each mode satisfies a first-order ODE,

$$\dot{\Phi}_k(t) = -\nu_k \Phi_k(t) + c_k u(t), \quad k = 1, \dots, K_{\max}. \quad (11)$$

Consequently, the kernel-filtered Schrödinger dynamics is equivalent to the time-local coupled system

$$\begin{cases} i \frac{d}{dt} |\psi(t)\rangle = \left(\hat{H}_A + \left[\sum_{k=1}^{K_{\max}} \Phi_k(t) \right] \hat{M} \right) |\psi(t)\rangle, \\ \dot{\Phi}_k(t) = -\nu_k \Phi_k(t) + c_k u(t), \quad k = 1, \dots, K_{\max}. \end{cases} \quad (12)$$

The structure of these equations are similar, in spirit, to those of circuits with memory [28–30].

In this representation the memory kernel is replaced by a finite number of classical state variables $\{\Phi_k\}$ that store the control history.[19, 26] We will argue below why this representation is general enough in the case of a dissipative (and classically treated) *control* channel.[20, 25]

The model of eqns (12) also makes precise the case in which there is the absence of memory. In the strictly memoryless case, one expects $\Phi(t)$ to track the command $u(t)$ instantaneously, $\Phi(t) = g u(t)$ for some (static) gain g . At the kernel level, this corresponds to

$$K(\tau) \longrightarrow g \delta(\tau), \quad (13)$$

so that the convolution in (8) collapses to $\Phi(t) = g u(t)$.[19, 31]

For the exponential family (9), the δ -limit is obtained by sending all filter time-scales to zero while keeping the total gain fixed. A convenient sufficient condition is

$$\nu_k \rightarrow \infty \quad \text{for all } k, \quad \frac{c_k}{\nu_k} \rightarrow g_k, \quad g := \sum_{k=1}^{K_{\max}} g_k < \infty, \quad (14)$$

with g_k finite constants. Under (14), $K(\tau)$ converges to $g \delta(\tau)$ in the distributional sense on \mathbb{R}_+ ,[31, 32] and hence $\Phi(t) \rightarrow g u(t)$ for sufficiently regular inputs.[32]

There are several ways to derive this limit. A direct derivation follows by expanding the ODEs. From (11) one may write

$$\Phi_k(t) = \frac{c_k}{\nu_k} u(t) - \frac{1}{\nu_k} \dot{\Phi}_k(t). \quad (15)$$

Summing over k and using $\Phi = \sum_k \Phi_k$ yields

$$\Phi(t) = \sum_{k=1}^{K_{\max}} \frac{c_k}{\nu_k} u(t) - \sum_{k=1}^{K_{\max}} \frac{1}{\nu_k} \dot{\Phi}_k(t). \quad (16)$$

If $\nu_k \rightarrow \infty$ while $c_k/\nu_k \rightarrow g_k$ and the $\dot{\Phi}_k$ remain bounded on the time window of interest, the second term vanishes and one obtains the instantaneous relation

$$\Phi(t) \longrightarrow g u(t), \quad g = \sum_{k=1}^{K_{\max}} g_k. \quad (17)$$

Equivalently, the kernel converges to a delta distribution with weight g . Indeed, for the single-mode case $K(\tau) = c e^{-\nu \tau} \Theta(\tau)$, if one sets $c = \nu$ then $K(\tau) = \nu e^{-\nu \tau} \Theta(\tau)$ is an approximate identity on \mathbb{R}_+ and converges to $\delta(\tau)$ as $\nu \rightarrow \infty$.[31, 32]

While we will discuss later the physical origin of this model, let us discuss what truncating the series implies. First, truncations yield finite sums of exponentials with rates ν_k growing linearly with k ; the memoryless limit corresponds to pushing all relevant rates far above the drive bandwidth. In the frequency domain, this is the familiar condition that the transfer function of the filter becomes approximately constant over the support of the protocol, so that the realized control is proportional to the command with negligible phase lag.[19, 26]

C. Measures of hysteresis

Let us now move on to the notion of “memory” between a control and an observable. We use the term *hysteresis* in an operational sense: a driven protocol is hysteretic whenever the relationship between two time-dependent quantities fails to be single-valued over a cycle. This definition is directly analogous to the standard use of hysteresis in magnetism, where a multivalued relation between magnetic induction B and applied field H over a cycle produces a characteristic loop, and where the loop area quantifies the energy dissipated per cycle.[33–35]

In the present setting, such multivalued behavior can arise from multiple mechanisms. One is *classical memory* in the control channel, encoded by a causal kernel K , which makes the realized field $\Phi(t)$ depend on the history of the commanded signal $u(t)$. A second is *state-lag* relative to the realized Hamiltonian: even in a closed system this can occur through non-adiabatic (finite-rate) driving and produces a purely *dynamical* hysteresis that vanishes in the quasi-static limit.[36–38] More generally, additional physical sources of loops may appear (e.g., due

to ergodicity breaking or open-system effects), and the goal is to disentangle control-channel memory from these state-dynamics contributions.

A useful feature of the scalar filtered-control model adopted throughout the paper is that control-channel and state-dynamics effects can be separated experimentally and numerically by comparing hysteresis measures in the (u, Φ) plane (control channel only) and in the (Φ, O) plane (state response to the realized Hamiltonian). The notation here is consistent with the model introduced earlier:

$$\begin{aligned}\hat{H}(t) &= \hat{H}_A + \Phi(t) \hat{M}, \\ \Phi(t) &= \int_{-\infty}^t K(t-s) u(s) ds,\end{aligned}\quad (18)$$

with real-valued command $u(t)$ and causal kernel K .[19, 26] Throughout, the observable $O(t)$ is always computed from the evolution under $\hat{H}(t)$ with the *realized* field $\Phi(t)$.

Assume a periodic protocol with period T after transients have died out, so that

$$u(t+T) = u(t). \quad (19)$$

The drive channel determines a closed parametric curve in the (u, Φ) plane,

$$\Gamma_{u\Phi} : t \in [0, T] \mapsto (u(t), \Phi(t)). \quad (20)$$

If the channel is memoryless, $\Phi(t)$ is (approximately) an instantaneous function of $u(t)$ and $\Gamma_{u\Phi}$ collapses to a single-valued curve. With memory, the same value of u can occur at two different times in the cycle with different values of Φ , producing a loop, in direct analogy with B - H hysteresis loops in ferromagnets or in capacitors/inductors.[33, 34]

We quantify this *control-channel hysteresis* by the oriented area enclosed by $\Gamma_{u\Phi}$,

$$\mathcal{A}_{u\Phi} := \oint_{\Gamma_{u\Phi}} \Phi du = \int_0^T \Phi(t) \dot{u}(t) dt. \quad (21)$$

A nonzero $\mathcal{A}_{u\Phi}$ is an intrinsic signature of memory in the map $u \mapsto \Phi$: it vanishes whenever Φ is a single-valued function of u along the cycle. In the embedding of Sec. II B, this area measures the extent to which the auxiliary filter variables $\{\Phi_k(t)\}$ lag the command $u(t)$, in the same way that magnetic hysteresis-loop area measures lag between B and H in classical Preisach-type descriptions.[24, 34, 35]

To probe hysteresis originating from the *state response* to the realized field, we analogously consider the closed curve in the (Φ, O) plane,

$$\Gamma_{\Phi O} : t \in [0, T] \mapsto (\Phi(t), O(t)), \quad (22)$$

and define the corresponding oriented area

$$\mathcal{A}_{\Phi O} := \oint_{\Gamma_{\Phi O}} O d\Phi = \int_0^T O(t) \dot{\Phi}(t) dt. \quad (23)$$

In the quasi-static limit for a closed system, $O(t)$ becomes (approximately) a single-valued function of $\Phi(t)$ and $\mathcal{A}_{\Phi O} \rightarrow 0$, whereas finite-rate (non-adiabatic) driving can produce $\mathcal{A}_{\Phi O} \neq 0$ as a form of dynamical hysteresis.

Finally, it is useful to note that an “apparent” loop can arise if one plots O against the *command* u rather than against the realized field Φ . Define

$$\mathcal{A}_{uO} := \oint O du = \int_0^T O(t) \dot{u}(t) dt. \quad (24)$$

Even when the state has no hysteresis with respect to the realized field (so that $\mathcal{A}_{\Phi O} = 0$), one may still obtain $\mathcal{A}_{uO} \neq 0$ purely from control-channel memory.

A minimal example is given by pure control-lag produces an apparent loop. Consider the lag kernel

$$K(t) = \delta(t - t_{\text{lag}}), \quad (25)$$

so that

$$\Phi(t) = \int_{-\infty}^t \delta(t-s-t_{\text{lag}}) u(s) ds = u(t-t_{\text{lag}}). \quad (26)$$

Assume the system response is strictly memoryless with respect to the realized field, i.e., $O(t) = f(\Phi(t))$ for a single-valued function f . Then the curve $\Gamma_{\Phi O}$ is single-valued and $\mathcal{A}_{\Phi O} = 0$ identically. Nevertheless, the parametric curve $t \mapsto (u(t), O(t)) = (u(t), f(u(t-t_{\text{lag}})))$ can enclose a nonzero area \mathcal{A}_{uO} and thus display a seemingly hysteretic loop in the (u, O) plane. For concreteness, one may take, e.g.,

$$f(\Phi) = \tanh(a\Phi), \quad (27)$$

which yields a pronounced loop in (u, O) for cyclic drives $u(t)$ despite the absence of any state memory.¹

More generally, it is easy to see that the exponential kernel

$$K(\tau) = \alpha e^{-\alpha\tau} \Theta(\tau), \quad (28)$$

the realized field obeys $\dot{\Phi} = \alpha(u - \Phi)$. For a sinusoidal command $u(t) = u_0 \sin(\omega t)$, the steady-state response takes the form

$$\Phi(t) = u_0 \frac{\alpha}{\sqrt{\alpha^2 + \omega^2}} \sin(\omega t - \delta), \quad \delta = \arctan \frac{\omega}{\alpha}. \quad (29)$$

The resulting curve $\Gamma_{u\Phi}$ is an ellipse, and the loop area is

$$|\mathcal{A}_{u\Phi}| = \pi u_0^2 \frac{\alpha\omega}{\alpha^2 + \omega^2}. \quad (30)$$

Thus control hysteresis is largest when ω is comparable to the filter rate α , and it vanishes both for $\omega \ll \alpha$ (negligible lag) and for $\omega \gg \alpha$ (strong attenuation), exactly as

¹ The author is indebted to P. Sathe for suggesting this example.

in classical single-pole low-pass responses in electronics and control.[19, 26]

Let \hat{O} be a time-independent observable and define

$$O(t) := \langle \hat{O} \rangle_t. \quad (31)$$

Plotting the observable against the command produces a closed loop

$$\Gamma_{uO} : t \in [0, T] \mapsto (u(t), O(t)), \quad (32)$$

and we define its oriented area as in eqn. (24). In general, \mathcal{A}_{uO} can be nonzero for two reasons: because the control channel is hysteretic ($u \mapsto \Phi$ is history dependent), or because the quantum state itself exhibits dynamical lag relative to the realized Hamiltonian, as in generic non-adiabatic or non-Markovian evolution.[11, 36, 37, 39]

To isolate the quantum contribution, it is natural to “factor out” the control channel by plotting the same observable against the realized field $\Phi(t)$, defining

$$\Gamma_{\Phi O} : t \in [0, T] \mapsto (\Phi(t), O(t)), \quad (33)$$

and the corresponding loop area as in eqn. (23). By construction, $\mathcal{A}_{\Phi O}$ is insensitive to purely classical filtering when the quantum response is effectively instantaneous in Φ . In that regime, residual hysteresis in the (Φ, O) plane reflects genuine quantum dynamical effects rather than distortions in the control channel.

A few results can be proved in this setting that are well known, but that we report here for completeness. For a closed cycle $\Phi(0) = \Phi(T)$ we write the loop area as the integral $A_{uO} := \oint O d\Phi$; when Φ is absolutely continuous this reduces to $A_{uO} = \int_0^T O(u) \Phi'(u) du$. A key consequence is that if the response is *single-valued* in the realized field, $O(u) = f(\Phi(u))$, then $A_{uO} = \oint f(\Phi) d\Phi = 0$, i.e. a nonzero A_{uO} necessarily implies multibranch (history-dependent) behavior. Independently of uniqueness, boundedness of O yields an a priori variation bound

$$|A_{uO}| \leq \frac{O_{\max} - O_{\min}}{2} \int_0^T |\Phi'(u)| du, \quad (34)$$

and, under a single turning-point sweep, a two-branch representation $A_{uO} = \int_{\Phi_{\min}}^{\Phi_{\max}} (O_{\uparrow} - O_{\downarrow}) d\Phi$ that immediately gives lower bounds when the branch gap has a definite sign. All proofs and precise assumptions are collected in Appendix D.

D. Classical memory fingerprint in the adiabatic regime

In this section we address the regime in which the quantum dynamics is adiabatic with respect to the *realized* Hamiltonian path generated by the filtered control $\Phi(t)$. In this limit the quantum response carries essentially no additional “memory” beyond the instantaneous value of Φ , and any hysteresis observed in the (u, O) plane

can be understood as the image, under a static nonlinear map $O = f(\Phi)$, of the purely classical hysteresis already present in the control channel (u, Φ) .[36–38]

We use the scalar filtered-control model,

$$\hat{H}(t) = \hat{H}_A + \Phi(t) \hat{M}, \quad \Phi(t) = \int_{-\infty}^t K(t-s) u(s) ds, \quad (35)$$

and consider protocols for which transients have decayed so that u and Φ are periodic with period T .

It is convenient to view the Hamiltonian as a one-parameter family

$$H(\Phi) = \hat{H}_A + \Phi \hat{M}, \quad (36)$$

and to interpret the drive as prescribing a path $\Phi(t)$ in parameter space. Assume that along the relevant range of Φ the spectrum splits into energy levels separated by a strictly positive gap. Denote by $\Pi(\Phi)$ the spectral projector onto a chosen band and assume $\Phi \mapsto \Pi(\Phi)$ is smooth.[38]

A convenient formulation of adiabatic following is the Kato form: there exists an intertwiner $W(t)$ solving

$$\dot{W}(t) = [\dot{\Pi}(t), \Pi(t)] W(t), \quad W(0) = \mathbb{1}, \quad (37)$$

where $\Pi(t) := \Pi(\Phi(t))$.[37, 38, 40] The operator $W(t)$ transports the instantaneous spectral subspace along the path, in the sense that

$$\Pi(t) = W(t) \Pi(0) W^\dagger(t). \quad (38)$$

In the adiabatic regime, the exact unitary $\hat{U}(t)$ generated by $\hat{H}(t)$ remains close to a product of the dynamical phase within each band and the intertwiner $W(t)$, and transitions between distinct levels are suppressed. Rigorous adiabatic theorems provide quantitative bounds on this approximation in terms of the gap and time scales of the protocol.[38, 41] For the present purposes, this means that expectation values of observables are well approximated by functions of the instantaneous spectral data of $H(\Phi(t))$, rather than by functionals of the entire past history of Φ . In other words, in the adiabatic limit $\mathcal{A}_{\Phi O}$ becomes a purely geometric and spectral quantity, while \mathcal{A}_{uO} retains the imprint of classical memory in the control channel via the map $u \mapsto \Phi$.

The relevant small parameter controlling adiabaticity is set by the speed of the realized protocol compared to the instantaneous gap.[37, 38, 41] Since $\Phi(t)$ is itself produced by a filter, the adiabatic condition should be formulated in terms of $\dot{\Phi}(t)$ (not $\dot{u}(t)$): memory in the control can slow down or phase-shift Φ relative to u , thereby modifying adiabaticity even at fixed command frequency.

E. Adiabatic response function $f(\Phi)$ and vanishing of $\mathcal{A}_{\Phi O}$

Let \hat{O} be a time-independent observable and define $O(t) = \langle \hat{O} \rangle_t$. In the adiabatic regime with respect to

the realized Hamiltonian path, the state remains (to a good approximation) confined to the instantaneous spectral decomposition of $H(\Phi)$ with negligible inter-band transitions. A convenient representation that fixes notation is the adiabatic diagonal ensemble associated with the initial state, closely related to the diagonal ensembles used to describe relaxation in isolated quantum systems.[42, 43]

Let $H(\Phi)$ have instantaneous spectral projectors $\Pi_i(\Phi)$ associated with eigenvalues $\varepsilon_i(\Phi)$, with constant ranks along the path. Define the initial band weights

$$p_i = \text{Tr}(\Pi_i(\Phi(0)) \rho(0)), \quad \sum_i p_i = 1, \quad (39)$$

and introduce the adiabatic reference state

$$\rho_{\text{ad}}(\Phi) = \sum_i p_i \frac{\Pi_i(\Phi)}{\text{Tr} \Pi_i(\Phi)}. \quad (40)$$

For nondegenerate energy levels, this reduces to frozen populations in instantaneous eigenstates, consistent with standard adiabatic theorems.[36–38] The corresponding adiabatic response function is

$$f(\Phi) = \text{Tr}(\rho_{\text{ad}}(\Phi) \hat{O}) = \sum_i \frac{p_i}{\text{Tr} \Pi_i(\Phi)} \text{Tr}(\Pi_i(\Phi) \hat{O}). \quad (41)$$

Along an adiabatic trajectory $\Phi(t)$ one then has

$$O(t) \approx f(\Phi(t)). \quad (42)$$

Since $f(\Phi)$ is single-valued, the oriented loop area in the (Φ, O) plane vanishes,

$$\mathcal{A}_{\Phi O} = \oint O d\Phi \approx \oint f(\Phi) d\Phi = 0. \quad (43)$$

Thus, once Φ is taken as the independent variable, adiabatic quantum evolution does not generate additional hysteresis beyond what is already present in the control channel.

Even though $\mathcal{A}_{\Phi O}$ vanishes in the adiabatic regime, the loop in the (u, O) plane is generically nontrivial whenever the *control channel* is hysteretic. Combining the loop-area definitions with the adiabatic approximation (42) yields

$$\mathcal{A}_{u O} = \oint O du \approx \int_0^T f(\Phi(t)) \dot{u}(t) dt. \quad (44)$$

Thus, in the adiabatic regime the observable loop is the image of the classical loop $t \mapsto (u(t), \Phi(t))$ under the nonlinear transformation $\Phi \mapsto f(\Phi)$.

A transparent consequence is obtained in the weak-modulation limit. Suppose the command is scaled as $u(t) = \varepsilon u_1(t)$ with $\varepsilon \ll 1$. By linearity of the filter, $\Phi(t) = \varepsilon \Phi_1(t)$, and expanding $f(\Phi)$ about $\Phi = 0$ gives

$$f(\Phi) = f(0) + f'(0) \Phi + O(\Phi^2). \quad (45)$$

The constant term drops out of (44) because the cycle is closed, $\int_0^T \dot{u}(t) dt = u(T) - u(0) = 0$, leaving

$$\mathcal{A}_{u O} \approx f'(0) \int_0^T \Phi(t) \dot{u}(t) dt = f'(0) \mathcal{A}_{u \Phi} + O(\varepsilon^3). \quad (46)$$

Equation (46) separates roles: the control memory enters only through the classical loop area $\mathcal{A}_{u \Phi}$, while the quantum system contributes a static factor $f'(0)$ determined by spectral properties of $H(\Phi)$ and by the choice of observable and initial state.

Differentiating (41) yields a projector expression for $f'(0)$ (assuming \hat{O} has no explicit Φ dependence),

$$f'(0) = \sum_i \frac{p_i}{\text{Tr} \Pi_i(0)} \text{Tr} \left((\partial_\Phi \Pi_i(\Phi))_{\Phi=0} \hat{O} \right), \quad (47)$$

which can be made fully explicit using standard resolvent identities for $\partial_\Phi \Pi_i$ when the gap is nonzero.[38] As we show in App. C, introducing the reduced resolvent on the complement of the i th band,

$$R_i(0) = (\mathbb{1} - \Pi_i(0)) (H(0) - \varepsilon_i(0))^{-1} (\mathbb{1} - \Pi_i(0)),$$

one has the Kato-type identity[37]

$$(\partial_\Phi \Pi_i(\Phi))_{\Phi=0} = R_i(0) \hat{M} \Pi_i(0) + \Pi_i(0) \hat{M} R_i(0),$$

and therefore

$$f'(0) = 2 \sum_i \frac{p_i}{\text{Tr} \Pi_i(0)} \text{Re} \text{Tr} \left(\Pi_i(0) \hat{O} R_i(0) \hat{M} \Pi_i(0) \right).$$

Equivalently, expanding $R_i(0)$ over the remaining energy levels yields the sum-over-levels (first-order perturbation) form[44]

$$f'(0) = 2 \sum_i \frac{p_i}{\text{Tr} \Pi_i(0)} \sum_{j \neq i} \frac{\text{Re} \text{Tr} \left(\Pi_i(0) \hat{O} \Pi_j(0) \hat{M} \Pi_i(0) \right)}{\varepsilon_i(0) - \varepsilon_j(0)},$$

which makes the dependence of the proportionality factor $f'(0)$ on the spectrum of $H(0)$ and on the matrix elements of \hat{O} and \hat{M} explicit.

F. Nonadiabatic response: separating control-channel memory from quantum information backflow

Section II D treated the regime in which the observable response can be expressed as a single-valued function of the realized control field, $O(t) \simeq f(\Phi(t))$, so that the loop in the (Φ, O) plane collapses and $\mathcal{A}_{\Phi O} \simeq 0$. We now move beyond this limit.

Outside the adiabatic regime, the state does not remain confined to an instantaneous eigenspace of $H(\Phi(t))$. Even though the qubit is still closed and the control memory is still classical, the observable acquires dependence on the history of Φ through coherent transitions

and phase accumulation. Operationally, the loop area $\mathcal{A}_{\Phi O}$ becomes the relevant diagnostic: it vanishes when O is (approximately) single-valued in Φ , and it becomes nonzero when the same realized field value Φ can correspond to different quantum states depending on where one is on the cycle.

A systematic analytic treatment can be built from an adiabatic perturbation theory in the instantaneous eigenbasis of $H(\Phi)$ that, however, goes beyond the scope of this work. Nonetheless, for an initial ground-state preparation, the leading nonadiabatic correction is controlled by the off-diagonal coupling $\langle e(\Phi) | \partial_t g(\Phi) \rangle$, which is proportional to $\dot{\Phi}$ and suppressed by the gap. This suggests the scaling structure

$$\mathcal{A}_{\Phi O} \sim \ell(\hat{O}) \times \int_0^T \frac{\dot{\Phi}(t)^2}{\Delta(\Phi(t))^3} dt, \quad (48)$$

where $\ell(\hat{O})$ is a prefactor depending on the choice of observable, so that, at fixed realized amplitude A , nonadiabatic loop effects grow with frequency and are suppressed by a large gap. The precise prefactor and functional form depend on the chosen observable and on the initial state, and can be evaluated explicitly for $\hat{O} = \sigma_x, \sigma_z$ once the instantaneous eigenvectors are fixed.

In the exponential kernel model, increasing ω simultaneously (i) increases the classical phase lag and (ii) decreases the realized amplitude A . These effects compete:

$$\text{classical hysteresis } |\mathcal{A}_{u\Phi}| \text{ peaks at } \omega\tau_c \approx 1, \quad (49)$$

while

$$\text{nonadiabaticity (at fixed } A\text{) typically grows with } \omega. \quad (50)$$

Because $A = A(\omega)$ decreases with ω for a fixed command amplitude u_0 , the net nonadiabatic signature can exhibit a crossover: as ω increases from zero, classical hysteresis first grows; at larger ω , classical hysteresis decays, but nonadiabatic corrections may remain visible if the realized sweep rate $\omega A(\omega)$ is still large enough relative to the gap scale. This is exactly the regime where $\mathcal{A}_{\Phi O}$ becomes essential: it isolates state-history effects that cannot be attributed to the control filter alone.

In the nonadiabatic regime the state no longer follows instantaneous spectral subspaces of $\hat{H}(t) = \hat{H}_A + \Phi(t)\hat{M}$, and the mapping $\Phi \mapsto O$ can become history dependent even when the only source of *physical* memory is the classical filtering relation $\Phi = K * u$. Consequently, $\mathcal{A}_{\Phi O}$ can be nonzero purely because of coherent unitary dynamics, as in standard studies of nonadiabatic work and dissipation in driven closed systems [45, 46].

Beyond these general comments, this section has two aims. First, we state an exact identity that rewrites cyclic “work-like” integrals as commutator-weighted functionals of the control, without any adiabatic approximation. Second, we explain why such nonadiabatic hysteresis measures, while operationally useful, do not by themselves certify *quantum memory* in the open-system sense

of information backflow [47, 48]. The technical derivations and bounds are deferred to Appendix E.

We consider a cyclic protocol of duration T in steady periodic response,

$$u(T) = u(0), \quad \rho(T) = \rho(0),$$

and define the loop functional

$$I = \oint dt \text{Tr}(\rho(t)\hat{O}) \dot{u}(t); \quad (51)$$

for simplicity, we consider a time-independent observable \hat{O} . For unitary evolution, $\dot{\rho}(t) = -i[\hat{H}(t), \rho(t)]$, integration by parts yields the exact identity

$$I = i \oint dt u(t) \langle [\hat{O}, \hat{H}(t)] \rangle_t. \quad (52)$$

We specialize to the scalar filtered-control model used throughout the paper,

$$\hat{H}(t) = \hat{H}_A + \Phi(t)\hat{M}, \quad \Phi(t) = \int_0^t K(t-s) u(s) ds, \quad (53)$$

with real causal kernel K and real command u . Introducing the time-dependent commutator weights

$$a(t) = \langle [\hat{O}, \hat{H}_A] \rangle_t, \quad b(t) = \langle [\hat{O}, \hat{M}] \rangle_t, \quad (54)$$

one obtains an exact decomposition

$$I = i \oint_0^T dt u(t) a(t) + i \oint_0^T dt u(t) \Phi(t) b(t). \quad (55)$$

The first term is present even in the instantaneous-control limit and depends on correlations between the command waveform and the internal “bias” quantity $a(t)$. The second term is the contribution in which the control history enters explicitly through the convolution $\Phi = K * u$. When $b(t)$ is slowly varying or approximately constant over a cycle, the second term reduces to a quadratic functional of u (as in the adiabatic discussion), but Eq. (55) remains exact in the fully nonadiabatic unitary regime.

A compact estimate that makes the kernel dependence explicit is obtained by bounding the two contributions separately. Writing $\|u\|_2 = \|u\|_{L^2(0,T)}$ and $\|K\|_1 = \|K(\tau)\Theta(\tau)\|_{L^1(\mathbb{R}_+)}$, Appendix E shows that

$$|I| \leq \|u\|_2 \|a\|_2 + \|b\|_\infty \|K\|_1 \|u\|_2^2, \quad (56)$$

where $\|b\|_\infty = \sup_{t \in [0,T]} |b(t)|$. The first term is independent of the kernel and scales linearly with the drive amplitude, while the second term is the kernel-mediated contribution and scales quadratically, with explicit dependence on the control-channel memory strength through $\|K\|_1$.

III. RESULTS

A. Properties of the decay channels

We begin with the minimal control-channel model: a single passive first-order low-pass element relating the commanded waveform $u(t)$ to the realized field $\Phi(t)$ at the device node,

$$\tau_c \dot{\Phi}(t) + \Phi(t) = u(t), \quad \tau_c > 0. \quad (57)$$

Equivalently, $\Phi = (K * u)$ with the causal kernel

$$K(\tau) = \frac{1}{\tau_c} e^{-\tau/\tau_c} \Theta(\tau), \quad (58)$$

so τ_c sets the classical memory time of the control line.

In steady periodic operation, a sinusoidal command $u(t) = u_0 \sin(\omega t)$ produces a single-harmonic realized response,

$$\begin{aligned} \Phi(t) &= A \sin(\omega t - \delta), \\ A &= \frac{u_0}{\sqrt{1 + (\omega \tau_c)^2}}, \quad \delta = \arctan(\omega \tau_c), \end{aligned} \quad (59)$$

as follows from the transfer function $G(i\omega) = 1/(1 + i\omega\tau_c)$. Thus the channel memory has two experimentally accessible signatures: amplitude roll-off A/u_0 and a phase lag δ . Both will reappear below as the frequency dependence of loop areas.

The ideal instantaneous-channel limit corresponds to the kernel concentrating at $\tau = 0$ so that $\Phi(t) \rightarrow u(t)$. For the single-pole model this is achieved by $\tau_c \rightarrow 0$ at fixed static gain. Operationally, for band-limited commands with characteristic frequency ω , the condition $\omega\tau_c \ll 1$ implies

$$\Phi(t) = u(t) + \mathcal{O}(\omega\tau_c), \quad (60)$$

and the classical control hysteresis vanishes in this limit.

After transients die out, the pair $(u(t), \Phi(t))$ traces a closed curve in the (u, Φ) plane over one period $T = 2\pi/\omega$. We quantify the resulting classical control hysteresis by the oriented loop area

$$\mathcal{A}_{u\Phi} := \oint \Phi du = \int_0^T \Phi(t) \dot{u}(t) dt. \quad (61)$$

For the single-pole response (59), direct evaluation gives

$$\mathcal{A}_{u\Phi} = -\pi u_0^2 \frac{\omega \tau_c}{1 + (\omega \tau_c)^2}, \quad (62)$$

i.e. $|\mathcal{A}_{u\Phi}|$ is maximized at $\omega\tau_c = 1$ and decays for both $\omega\tau_c \ll 1$ (negligible lag) and $\omega\tau_c \gg 1$ (strong attenuation). This nonmonotone dependence is the classical “memory resonance” of a first-order low-pass element.

For a measured observable $O(t) = \langle \psi(t) | \hat{O} | \psi(t) \rangle$ we define

$$\begin{aligned} \mathcal{A}_{uO} &:= \oint O du = \int_0^T O(t) \dot{u}(t) dt, \\ \mathcal{A}_{\Phi O} &:= \oint O d\Phi = \int_0^T O(t) \dot{\Phi}(t) dt. \end{aligned} \quad (63)$$

In an adiabatic regime with respect to the realized Hamiltonian path $H(\Phi) = \sigma_z + \Phi\sigma_x$, and for preparations that follow an instantaneous eigenspace (e.g. ground-state following), $O(t)$ becomes a single-valued function of the realized field,

$$O(t) \approx f(\Phi(t)). \quad (64)$$

Consequently the (Φ, O) loop collapses to a curve and

$$\mathcal{A}_{\Phi O} \approx 0. \quad (65)$$

This provides a clean operational separation: in the adiabatic regime any hysteresis observed in the commanded plane (u, O) is not evidence of intrinsic quantum memory, but rather a deterministic consequence of the classical filter $u \mapsto \Phi$ together with the static nonlinear map $\Phi \mapsto f(\Phi)$.

If the drive amplitude is small enough that $\Phi(t)$ remains near 0, then

$$f(\Phi) = f(0) + f'(0)\Phi + \mathcal{O}(\Phi^2). \quad (66)$$

Since $\int_0^T \dot{u}(t) dt = 0$, the constant term does not contribute to \mathcal{A}_{uO} , and we obtain

$$\mathcal{A}_{uO} = f'(0) \mathcal{A}_{u\Phi} + \mathcal{O}(\text{amplitude}^3). \quad (67)$$

In particular, for ground-state response with $\hat{O} = \sigma_x$ in the Hamiltonian of eqn. (123), one has $f'(0) = -1$, so to leading order

$$\mathcal{A}_{uO} \approx -\mathcal{A}_{u\Phi}, \quad (68)$$

and hence inherits the characteristic single-pole frequency dependence

$$|\mathcal{A}_{uO}| \propto \frac{\omega \tau_c}{1 + (\omega \tau_c)^2} \quad (\text{adiabatic, weak-drive regime}). \quad (69)$$

A convenient sufficient adiabaticity criterion compares the rate of change of the Hamiltonian to the instantaneous gap. For $H(\Phi) = \sigma_z + \Phi\sigma_x$ the gap is

$$\Delta(\Phi) = 2\sqrt{1 + \Phi^2}, \quad (70)$$

and a typical condition has the form

$$\frac{|\dot{\Phi}(t)|}{\Delta(\Phi(t))^2} \ll 1 \quad \text{uniformly on the cycle.} \quad (71)$$

For the steady-state filtered sinusoid (59), $|\dot{\Phi}| \leq \omega A$, so low frequency and/or strong filtering (small A) both promote adiabaticity. This observation will be used to organize the adiabatic versus nonadiabatic regimes in later sections.

The single-exponential kernel (58) corresponds to the impulse response of one lumped RC element, i.e. a single relaxational degree of freedom in the control line. In realistic cryogenic wiring, however, the command generated

at room temperature traverses a *distributed* passive network with many internal charge-storage and dissipation mechanisms: distributed capacitance to ground, resistive losses (including thermalized attenuators), bias tees and low-pass sections, connectors and packaging parasitics, and on-chip filtering. A standard circuit idealization of such a channel is an *RC ladder* (a lossy line discretized into many RC sections), which is still linear and passive but typically high order.

For passive RC networks the transfer function $G(s) = \Phi(s)/u(s)$ is stable and, for ladder families of interest, has poles on the negative real axis; in particular, for a finite ladder G is rational with real negative poles. Consequently the impulse response is a superposition of decaying exponentials. Appendix F derives this explicitly for an N -stage ladder and relates it to classical RC realizability/synthesis results [25, 27]. In the time domain this motivates representing the control kernel as a finite exponential-mode expansion,

$$K(\tau) = \sum_{k=1}^{K_{\max}} c_k e^{-\nu_k \tau} \Theta(\tau), \quad \nu_k > 0, \quad (72)$$

which is *exact* whenever the channel admits a finite RC-ladder realization (and remains a controlled approximation for distributed lines).

Introducing auxiliary mode variables

$$\begin{aligned} \Phi_k(t) &:= \int_{-\infty}^t c_k e^{-\nu_k(t-s)} u(s) ds, \\ \Phi(t) &= \sum_{k=1}^{K_{\max}} \Phi_k(t), \end{aligned} \quad (73)$$

turns the convolutional memory into the time-local realization

$$\dot{\Phi}_k(t) = -\nu_k \Phi_k(t) + c_k u(t), \quad k = 1, \dots, K_{\max}. \quad (74)$$

For an actual finite ladder, the rates $\{\nu_k\}$ are precisely the relaxation rates of the circuit modes (the poles of G), while the weights $\{c_k\}$ encode the input-output coupling of each mode (Appendix F).

This representation also yields an explicit expression for the classical control-channel hysteresis area under harmonic drive. For $u(t) = u_0 \sin(\omega t)$ in steady state, linearity implies that $\Phi(t)$ is again purely sinusoidal at frequency ω , with complex gain

$$G(i\omega) = \frac{\Phi(i\omega)}{u(i\omega)} = \sum_{k=1}^{K_{\max}} \frac{c_k}{\nu_k + i\omega}. \quad (75)$$

Equivalently, writing $G(i\omega) = |G(i\omega)| e^{-i\delta(\omega)}$ with $\delta(\omega) \in [0, \pi/2)$, one has $\Phi(t) = u_0 |G(i\omega)| \sin(\omega t - \delta(\omega))$. The oriented loop area in the (u, Φ) plane,

$$\mathcal{A}_{u\Phi} = \oint \Phi du = \int_0^T \Phi(t) \dot{u}(t) dt, \quad T = \frac{2\pi}{\omega}, \quad (76)$$

can then be evaluated in closed form:

$$\mathcal{A}_{u\Phi} = -\pi u_0^2 |G(i\omega)| \sin \delta(\omega) = \pi u_0^2 \operatorname{Im} G(i\omega). \quad (77)$$

We anticipate that the formula above, derived from a classical approximation to the drive channel, has a quantum analog derived in a later section.

Using (75) this becomes an explicit sum over relaxation channels,

$$\mathcal{A}_{u\Phi}^{K_{\max}} = -\pi u_0^2 \omega \sum_{k=1}^{K_{\max}} \frac{c_k}{\nu_k^2 + \omega^2}. \quad (78)$$

In particular, each mode contributes a negative (lag-induced) area of magnitude $\propto \omega / (\nu_k^2 + \omega^2)$, peaking near $\omega \simeq \nu_k$ and vanishing both for $\omega \ll \nu_k$ (negligible lag) and for $\omega \gg \nu_k$ (strong attenuation). Thus a multi-mode RC channel generically produces a superposition of “memory resonances” across the hierarchy of relaxation rates. For the hysteresis of the quantum observable, we obtain then that in the adiabatic regime we have

$$\mathcal{A}_{uO} \approx f'(0) \mathcal{A}_{u\Phi}^{K_{\max}}. \quad (79)$$

B. Single-qubit case

This section collects two analytically controlled qubit examples that we use as reference points before turning to numerics. The first illustrates the adiabatic regime for the transverse-drive model used throughout the paper, where the qubit response becomes an (approximately) single-valued function of the *realized* field $\Phi(t)$. The second is an exactly solvable (commuting) model in which the control enters longitudinally; it provides a closed-form benchmark for how a classical control filter can generate a hysteretic (u, Φ) loop even when the unitary evolution requires no time ordering.

Throughout we adopt the notation of Secs. II and II C: the commanded waveform is $u(t)$, the realized field is $\Phi(t) = (K * u)(t)$ (or its time-local embedding in Sec. II B), and hysteresis is quantified by loop areas such as $\mathcal{A}_{u\Phi} = \oint \Phi du$ and $\mathcal{A}_{uO} = \oint O du$.

1. Single-qubit illustration and the exponential kernel

Let us compute the adiabatic map $f(\Phi)$ in a simple qubit example. Fix $\Phi \in \mathbb{R}$ and consider the instantaneous Hamiltonian

$$H(\Phi) = \sigma_z + \Phi \sigma_x = \mathbf{h}(\Phi) \cdot \boldsymbol{\sigma}, \quad \mathbf{h}(\Phi) = (\Phi, 0, 1), \quad (80)$$

with eigenvalues $\pm \|\mathbf{h}(\Phi)\|$ and gap $2\|\mathbf{h}(\Phi)\|$, where

$$\|\mathbf{h}(\Phi)\| = \sqrt{1 + \Phi^2}. \quad (81)$$

For any Pauli-vector Hamiltonian $H = \mathbf{h} \cdot \boldsymbol{\sigma}$, the ground state has Bloch vector antiparallel to \mathbf{h} ,

$$\mathbf{n}_g(\Phi) := (\langle \sigma_x \rangle_{g(\Phi)}, \langle \sigma_y \rangle_{g(\Phi)}, \langle \sigma_z \rangle_{g(\Phi)}) = -\frac{\mathbf{h}(\Phi)}{\|\mathbf{h}(\Phi)\|}. \quad (82)$$

Therefore

$$\langle \sigma_x \rangle_{g(\Phi)} = -\frac{h_x(\Phi)}{\|\mathbf{h}(\Phi)\|} = -\frac{\Phi}{\sqrt{1+\Phi^2}}. \quad (83)$$

In the adiabatic-following regime (slow variation of $\Phi(t)$ relative to the instantaneous gap), a state prepared in $|g(\Phi(0))\rangle$ remains close to $|g(\Phi(t))\rangle$ up to phases, hence

$$O(t) = \langle \sigma_x \rangle_t \approx \langle \sigma_x \rangle_{g(\Phi(t))} = -\frac{\Phi(t)}{\sqrt{1+\Phi(t)^2}} \equiv f(\Phi(t)), \quad (84)$$

in agreement with the standard Bloch-sphere description of driven two-level systems.[1] If $O(t) \approx f(\Phi(t))$ with single-valued f , then the (Φ, O) loop collapses to a curve and

$$\mathcal{A}_{\Phi O} = \oint O d\Phi \approx \oint f(\Phi) d\Phi = \oint dF(\Phi) = 0, \quad (85)$$

for $F'(\Phi) = f(\Phi)$ and cyclic protocols.

2. Transverse filtered drive: instantaneous eigenbasis and adiabatic response

We consider the transverse-drive qubit used in the main text,

$$\hat{H}(t) = \Omega_z \sigma_z + \Phi(t) \sigma_x, \quad \Phi(t) = (K * u)(t), \quad (86)$$

with $\Omega_z > 0$. Writing $\hat{H}(t) = \hat{H}(t) \cdot \boldsymbol{\sigma}$ gives

$$\hat{H}(t) = (\Phi(t), 0, \Omega_z), \quad E(t) = \|\hat{H}(t)\| = \sqrt{\Omega_z^2 + \Phi(t)^2}. \quad (87)$$

The instantaneous eigenvalues are $\pm E(t)$, and the instantaneous ground-state Bloch direction is

$$\mathbf{n}_g(t) = -\frac{\hat{H}(t)}{\|\hat{H}(t)\|} = -\frac{1}{\sqrt{\Omega_z^2 + \Phi(t)^2}} (\Phi(t), 0, \Omega_z). \quad (88)$$

3. Transverse filtered drive: adiabatic reduction and small-amplitude loop areas

Assume periodic steady state, $u(t+T) = u(t)$ and $\Phi(t+T) = \Phi(t)$. The loop areas introduced in Sec. II C are

$$\begin{aligned} \mathcal{A}_{u\Phi} &= \oint \Phi du = \int_0^T \Phi(t) \dot{u}(t) dt, \\ \mathcal{A}_{uO} &= \oint O du = \int_0^T O(t) \dot{u}(t) dt, \\ \mathcal{A}_{\Phi O} &= \oint O d\Phi = \int_0^T O(t) \dot{\Phi}(t) dt. \end{aligned} \quad (89)$$

In the adiabatic regime with respect to the realized trajectory $\Phi(t)$, and for preparations diagonal in the instantaneous eigenbasis at $\Phi(0)$, the expectation of any fixed observable \hat{O} is (to leading adiabatic order) a single-valued function of Φ ,

$$O(t) = \langle \hat{O} \rangle_t \approx f(\Phi(t)). \quad (90)$$

This is the standard structure of the adiabatic theorem in gapped systems [37, 38, 40]. For ground-state following,

$$\langle \sigma_x \rangle_t \approx -\frac{\Phi(t)}{\sqrt{\Omega_z^2 + \Phi(t)^2}}, \quad \langle \sigma_z \rangle_t \approx -\frac{\Omega_z}{\sqrt{\Omega_z^2 + \Phi(t)^2}}. \quad (91)$$

In particular, (90) implies

$$\mathcal{A}_{\Phi O} = \oint O d\Phi \approx \oint f(\Phi) d\Phi = 0, \quad (92)$$

so any nonzero $\mathcal{A}_{\Phi O}$ indicates nonadiabaticity (or additional degrees of freedom), not the classical filter alone.

a. Weak-drive expansion. Assume an amplitude scaling

$$u(t) = \varepsilon u_1(t), \quad 0 < \varepsilon \ll 1, \quad (93)$$

with u_1 fixed, T -periodic, and not identically constant. By linearity,

$$\Phi(t) = (K * u)(t) = \varepsilon \Phi_1(t), \quad \Phi_1(t) = (K * u_1)(t), \quad (94)$$

so $\mathcal{A}_{u\Phi} = \varepsilon^2 \mathcal{A}_{u_1\Phi_1}$. If f is smooth at $\Phi = 0$,

$$f(\Phi) = f(0) + f'(0)\Phi + \frac{1}{2}f''(0)\Phi^2 + \mathcal{O}(\Phi^3). \quad (95)$$

Using $\int_0^T \dot{u}(t) dt = 0$, inserting into \mathcal{A}_{uO} yields

$$\begin{aligned} \mathcal{A}_{uO} &= f'(0) \int_0^T \Phi(t) \dot{u}(t) dt \\ &\quad + \frac{1}{2} f''(0) \int_0^T \Phi(t)^2 \dot{u}(t) dt + \mathcal{O}(\varepsilon^4), \end{aligned} \quad (96)$$

hence

$$\mathcal{A}_{uO} = f'(0) \mathcal{A}_{u\Phi} + \mathcal{O}(\varepsilon^3). \quad (97)$$

For ground-state following, define

$$f_x(\Phi) = -\frac{\Phi}{\sqrt{\Omega_z^2 + \Phi^2}}, \quad f_z(\Phi) = -\frac{\Omega_z}{\sqrt{\Omega_z^2 + \Phi^2}}, \quad (98)$$

with small- Φ expansions

$$\begin{aligned} f_x(\Phi) &= -\frac{1}{\Omega_z} \Phi + \frac{1}{2\Omega_z^3} \Phi^3 + \mathcal{O}(\Phi^5), \\ f_z(\Phi) &= -1 + \frac{1}{2\Omega_z^2} \Phi^2 + \mathcal{O}(\Phi^4). \end{aligned} \quad (99)$$

(i) *Observable loop for $O = \sigma_x$.* Since $f'_x(0) = -1/\Omega_z \neq 0$,

$$\mathcal{A}_{u,\sigma_x} = -\frac{1}{\Omega_z} \mathcal{A}_{u\Phi} + \mathcal{O}(\varepsilon^3). \quad (100)$$

(ii) *Observable loop for $O = \sigma_z$.* Here $f'_z(0) = 0$, so

$$\mathcal{A}_{u,\sigma_z} = \frac{1}{2\Omega_z^2} \int_0^T \Phi(t)^2 \dot{u}(t) dt + \mathcal{O}(\varepsilon^4) = \mathcal{O}(\varepsilon^3). \quad (101)$$

b. *Single-pole kernel under harmonic command.* Take the kernel

$$K(\tau) = \alpha e^{-\alpha\tau} \Theta(\tau), \quad \alpha > 0, \quad (102)$$

and harmonic command

$$u(t) = u_0 \sin(\omega t), \quad T = \frac{2\pi}{\omega}. \quad (103)$$

In steady state,

$$\begin{aligned} \Phi(t) &= A \sin(\omega t - \delta), \\ A &= u_0 \frac{\alpha}{\sqrt{\alpha^2 + \omega^2}}, \quad \delta = \arctan\left(\frac{\omega}{\alpha}\right). \end{aligned} \quad (104)$$

Then

$$\mathcal{A}_{u\Phi} = \int_0^T \Phi(t) \dot{u}(t) dt = -\pi u_0 A \sin \delta, \quad (105)$$

so

$$|\mathcal{A}_{u\Phi}| = \pi u_0^2 \frac{\alpha \omega}{\alpha^2 + \omega^2}. \quad (106)$$

Combining (100) and (106) gives

$$|\mathcal{A}_{u,\sigma_x}| = \frac{\pi u_0^2}{\Omega_z} \frac{\alpha \omega}{\alpha^2 + \omega^2} + \mathcal{O}(u_0^3). \quad (107)$$

These relations quantify how the classical memory scale (here α^{-1}) imprints itself onto commanded loop areas even when $\mathcal{A}_{\Phi O} \approx 0$.^[38, 49] We next depart from the adiabatic reduction and treat the nonadiabatic regime, where $\mathcal{A}_{\Phi O}$ becomes a nontrivial diagnostic of coherent state-history dependence.

To contrast with the transverse-drive model (86), consider the commuting (longitudinal) control case

$$\hat{H}(t) = (\Omega_z + \Phi(t))\sigma_z, \quad \Phi(t) = (K * u)(t). \quad (108)$$

Since $[\hat{H}(t), H(t')] = 0$, time ordering is unnecessary and

$$\hat{U}(t) = \exp(-i\sigma_z \theta(t)), \quad \theta(t) = \int_0^t (\Omega_z + \Phi(\tau)) d\tau. \quad (109)$$

This is a standard exactly solvable setting.^[1]

c. *Closed-form expectations from a simple preparation.* Prepare $|+\rangle$ (the +1 eigenstate of σ_x). The Bloch vector rotates about the z axis by angle $2\theta(t)$, giving

$$\langle \sigma_x \rangle_t = \cos(2\theta(t)), \quad \langle \sigma_y \rangle_t = -\sin(2\theta(t)), \quad \langle \sigma_z \rangle_t = 0. \quad (110)$$

Thus, once the classical realized signal $\Phi(t)$ is known, the unitary response is explicit for arbitrary protocols.

d. *Single-pole kernel under harmonic command.* For the single exponential kernel and $u(t) = u_0 \sin(\omega t)$, the steady-cycle realized field is

$$\Phi(t) = u_0 \frac{\alpha}{\sqrt{\alpha^2 + \omega^2}} \sin(\omega t - \delta), \quad \delta = \arctan\left(\frac{\omega}{\alpha}\right), \quad (111)$$

so

$$\theta(t) = \Omega_z t - \frac{u_0 \alpha}{\omega \sqrt{\alpha^2 + \omega^2}} [\cos(\omega t - \delta) - \cos \delta], \quad (112)$$

and $\langle \sigma_x \rangle_t = \cos(2\theta(t))$ follows in closed form.

The transverse model (86) is the relevant setting for separating control-channel memory from coherent nonadiabaticity using loop measures: in the adiabatic regime $\mathcal{A}_{\Phi O} \approx 0$, while a nonzero \mathcal{A}_{uO} can persist as a consequence of $\mathcal{A}_{u\Phi} \neq 0$. The longitudinal model (108) provides a clean analytic benchmark where (u, Φ) hysteresis can coexist with fully explicit unitary dynamics.

We now turn to numerical simulations (Sec. III C) that interpolate between adiabatic and nonadiabatic regimes for the transverse model while holding the same classical control filter fixed.

We now turn to numerical simulations (Sec. III C) that interpolate between adiabatic and nonadiabatic regimes for the transverse model while holding the same classical control filter fixed.

C. Numerical experiments

In this section we report time-domain simulations designed to separate the two mechanisms that can generate cyclic hysteresis in commanded measurements. The first is *classical control-channel memory*: a finite-bandwidth drive chain maps the commanded waveform $u(t)$ to a realized field $\Phi(t)$ with a frequency-dependent lag, yielding a nonzero loop area $\mathcal{A}_{u\Phi} = \oint \Phi du$. The second is *coherent nonadiabatic response* of the qubit under the realized drive, which can produce genuine state-history dependence at fixed $\Phi(t)$ and hence a nonzero $\mathcal{A}_{\Phi O} = \oint O d\Phi$. Our numerical observables are the oriented areas in the (u, Φ) , (u, O) , and (Φ, O) planes, evaluated after the dynamics reaches a steady cycle.

The protocol follows the standard experimental logic used in cyclic-drive studies of superconducting qubits: a periodic control waveform is applied for many cycles, initial transients are discarded, and the final cycle is analyzed through parametric loops and their oriented areas.^[5, 50] The distinctive modeling assumption here is that *all* nonlocality is confined to the classical drive chain, while the qubit itself evolves unitarily under the realized field $\Phi(t)$.

We simulate a transverse-driven two-level system,

$$\hat{H}(t) = \Omega_z \sigma_z + \Phi(t) \sigma_x, \quad (113)$$

where Ω_z is the qubit splitting and $\Phi(t)$ is the realized control amplitude delivered at the device node. The commanded waveform $u(t)$ is filtered by a causal, dissipative

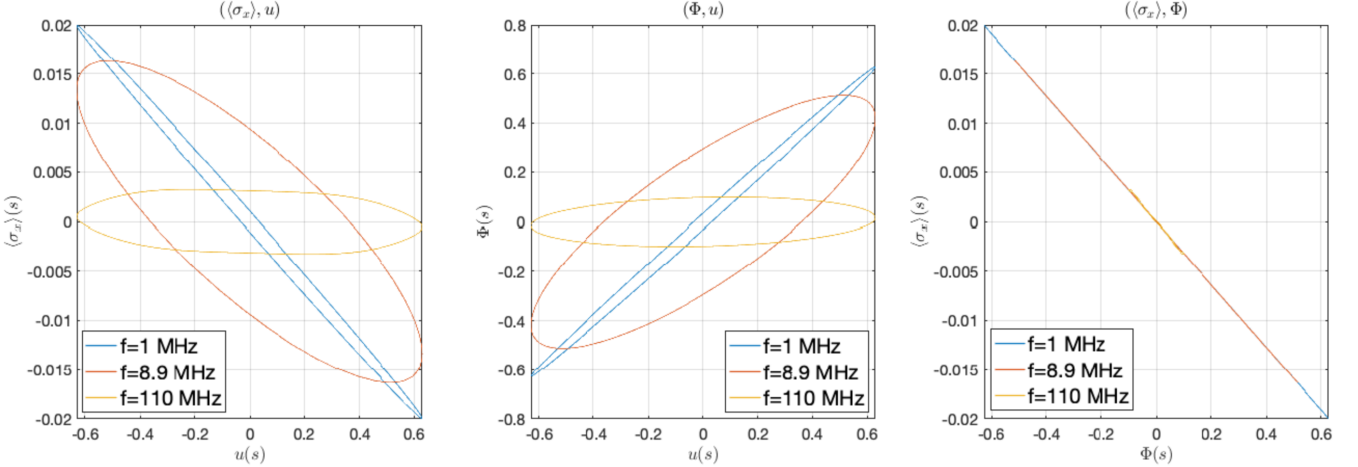


FIG. 1. **Representative steady-cycle parametric loops for a filtered transverse drive.** A periodic command $u(t)$ (triangle protocol in the example shown) is applied for many cycles; after discarding transients, the final cycle is plotted parametrically as three loops: (left) the *control-channel loop* (u, Φ) quantifying classical filtering and phase lag; (middle) the *commanded observable loop* (u, O) with $O(t) = \langle \sigma_z \rangle_t$; (right) the *realized-drive loop* (Φ, O) which isolates state history dependence at fixed realized field. The (u, Φ) loop is nontrivial whenever the control channel has memory ($\mathcal{A}_{u\Phi} \neq 0$). In contrast, a nontrivial (Φ, O) loop indicates nonadiabatic quantum response under the realized drive; in the adiabatic-following regime it collapses toward a single-valued curve and $\mathcal{A}_{\Phi O} \approx 0$.

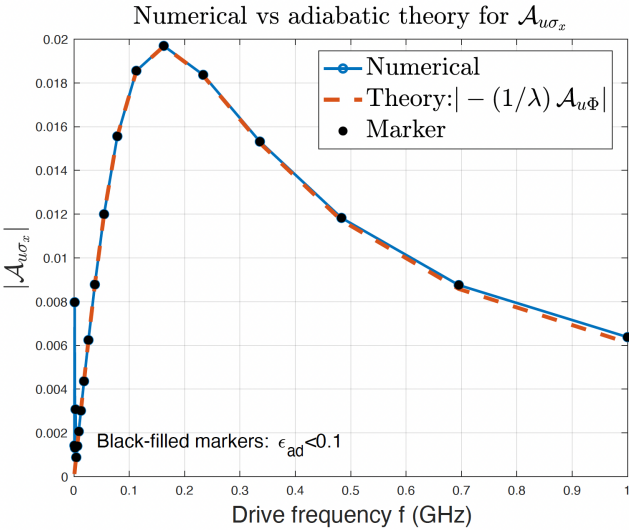


FIG. 2. **Testing the adiabatic ‘classical-memory imprint’ prediction.** The numerically extracted commanded-area $\tilde{\mathcal{A}}_{uO}$ (markers) is compared to the adiabatic small-amplitude prediction obtained from the control-channel area $\tilde{\mathcal{A}}_{u\Phi}$ via $\tilde{\mathcal{A}}_{uO} \approx f'(\Phi) \tilde{\mathcal{A}}_{u\Phi}$ (dashed curve), where $f(\Phi)$ is the adiabatic response function of the qubit observable. Points satisfying the adiabaticity diagnostic $\epsilon_{ad}^{max} < \epsilon_0$ are highlighted. Agreement holds in the regime where both (i) the realized field varies slowly compared to the instantaneous gap and (ii) the amplitude is sufficiently small for linearization of $f(\Phi)$ about $\Phi = 0$.

control channel. For the numerical experiments we adopt

the single-pole (single-RC) embedding,

$$\dot{\Phi}(t) = \frac{1}{\tau_c} (u(t) - \Phi(t)), \quad (114)$$

which is the minimal time-local realization of a causal exponential kernel and makes the control memory scale explicit (Sec. II B).

The qubit state is represented by its Bloch vector $r(t) \in \mathbb{R}^3$, $r_j(t) = \langle \sigma_j \rangle_t$. For unitary evolution one has the precession equation

$$\dot{r}(t) = \Omega(t) \times r(t), \quad \Omega(t) = (\Phi(t), 0, \Omega_z), \quad (115)$$

which is equivalent to the Schrödinger equation for pure states.[51, 52] Unless otherwise noted we initialize in the $|+\rangle$ state, $r(0) = (1, 0, 0)$, so that $\langle \sigma_z \rangle$ is generated dynamically by the transverse drive.

To separate the filter timescale from qubit frequencies we work in dimensionless variables

$$\begin{aligned} s &= \frac{t}{\tau_c}, & \tilde{u}(s) &= \tau_c u(t), \\ \tilde{\Phi}(s) &= \tau_c \Phi(t), & \lambda &= \Omega_z \tau_c. \end{aligned} \quad (116)$$

The coupled dynamics becomes

$$\begin{aligned} \frac{d\tilde{\Phi}}{ds} &= -\tilde{\Phi} + \tilde{u}(s), & \frac{dr}{ds} &= \tilde{\Omega}(s) \times r, \\ \tilde{\Omega}(s) &= (\tilde{\Phi}(s), 0, \lambda). \end{aligned} \quad (117)$$

The dimensionless drive frequency is $\tilde{\omega} = 2\pi f \tau_c$. In these units the control-channel response depends primarily on $\tilde{\omega}$, while the degree of adiabaticity is controlled by $(\lambda, \tilde{\Phi})$ through the instantaneous gap and the realized slew rate.

We integrate (117) using a fixed-step fourth-order Runge–Kutta method on a uniform grid in s , with an integer number of steps per drive period. For each drive frequency we run many cycles, discard an initial transient window, and compute loop areas from the final cycle. Because the filter equation is strictly stable, this “last-cycle” procedure isolates the frequency-dependent steady response of the classical channel and the coherent qubit dynamics.

We consider periodic commands $u(t)$ with zero mean, emphasizing sinusoidal and piecewise-linear (triangle) protocols. For each run we record the commanded waveform $u(t)$, the realized field $\Phi(t)$, and the qubit observable $O(t)$ (typically $O(t) = \langle \sigma_z \rangle_t$). From the final cycle we compute the oriented areas

$$\mathcal{A}_{u\Phi} = \oint \Phi du, \quad \mathcal{A}_{uO} = \oint O du, \quad \mathcal{A}_{\Phi O} = \oint O d\Phi, \quad (118)$$

which quantify, respectively, hysteresis internal to the control channel, the experimentally accessible commanded hysteresis, and the residual state-history dependence at fixed realized drive. Numerically these are evaluated as discrete line integrals along the parametric curve using a trapezoidal rule with explicit loop closure,

$$\oint y dx \approx \sum_{n=1}^{N-1} \frac{y_{n+1} + y_n}{2} (x_{n+1} - x_n), \quad (119)$$

applied to $(x, y) = (u, \Phi)$, (u, O) , or (Φ, O) over one steady cycle. In the dimensionless implementation we report $\tilde{\mathcal{A}}_{u\Phi} = \oint \tilde{\Phi} d\tilde{u}$ and $\tilde{\mathcal{A}}_{uO} = \oint O d\tilde{u}$, with straightforward conversion to physical units via $\tilde{u} = \tau_c u$ and $\tilde{\Phi} = \tau_c \Phi$.

For the transverse Hamiltonian $\hat{H}(t) = \Omega_z \sigma_z + \Phi(t) \sigma_x$ the instantaneous gap is $\Delta(t) = 2\sqrt{\Omega_z^2 + \Phi(t)^2}$. A standard adiabatic parameter is

$$\epsilon_{\text{ad}}(t) := \frac{|\langle e(t) | \dot{\hat{H}}(t) | g(t) \rangle|}{\Delta(t)^2}, \quad (120)$$

with $\dot{\hat{H}}(t) = \dot{\Phi}(t) \sigma_x$. [37, 38] Evaluating the matrix element yields

$$\epsilon_{\text{ad}}(t) = \frac{|\dot{\Phi}(t)| \Omega_z}{4(\Omega_z^2 + \Phi(t)^2)^{3/2}}. \quad (121)$$

In dimensionless variables, using $d\tilde{\Phi}/ds = -\tilde{\Phi} + \tilde{u}(s)$, this becomes

$$\epsilon_{\text{ad}}(s) = \frac{|\lambda d\tilde{\Phi}/ds|}{4(\lambda^2 + \tilde{\Phi}(s)^2)^{3/2}}. \quad (122)$$

We summarize adiabaticity for a given run by $\epsilon_{\text{ad}}^{\text{max}}$, the maximum over the final cycle, and use a threshold $\epsilon_{\text{ad}}^{\text{max}} < \epsilon_0$ (with $\epsilon_0 = 0.1$) to highlight the region where adiabatic-following predictions are expected to hold.

Figure 1 visualizes the operational separation between control-channel memory and intrinsic state-history dependence. The (u, Φ) loop directly reports the phase lag generated by the filter and therefore persists even when the qubit response is adiabatic. In contrast, the (Φ, O) loop isolates history dependence of the observable at fixed realized drive: in the adiabatic-following regime $O(t) \approx f(\Phi(t))$ is (approximately) single-valued, so the loop collapses and $\mathcal{A}_{\Phi O} \approx 0$, whereas departures from this collapse signal coherent nonadiabatic response under $\Phi(t)$. The commanded loop (u, O) combines both effects and is therefore generically nontrivial whenever either $\mathcal{A}_{u\Phi} \neq 0$ or $\mathcal{A}_{\Phi O} \neq 0$.

A key analytic consequence of adiabatic following developed in Sec. II D is that, for small amplitudes, the commanded observable area is proportional to the control-channel area. Figure 2 compares the numerically extracted $\tilde{\mathcal{A}}_{uO}$ (markers) with the prediction obtained from $\tilde{\mathcal{A}}_{u\Phi}$ (dashed curve). Agreement is observed precisely in the region labeled adiabatic by the independent diagnostic $\epsilon_{\text{ad}}^{\text{max}} < \epsilon_0$ and breaks down once the realized field varies rapidly compared to the instantaneous gap, consistent with the interpretation that deviations originate from coherent nonadiabatic dynamics rather than from additional (open-system) memory.

To connect with a realistic control line, we take τ_c on the order of a nanosecond, $\tau_c \sim 1$ ns, representative of a well-engineered drive chain bandwidth. The qubit splitting is chosen in the few-GHz range, e.g. $\Omega_z/2\pi \sim 5$ GHz, so that $\lambda = \Omega_z \tau_c = \mathcal{O}(10)$. Sweeping the drive frequency across several decades therefore spans $\tilde{\omega} \ll 1$ (quasi-static tracking), $\tilde{\omega} \sim 1$ (maximal control lag), and $\tilde{\omega} \gg 1$ (attenuated realized drive), enabling a direct visualization of the crossover from classical memory-dominated hysteresis to regimes where coherent nonadiabatic response is prominent.

IV. PHYSICAL BASIS FOR THE MEMORY IN THE CONTROL CHANNEL

In this second part of the manuscript, we provide a more physical rationale why the kernel approach is grounded both classically and quantum mechanically, as shown in the diagram of Fig. 3. Specifically, this section motivates the exponential-mode control kernel introduced in Sec. II B from the physics of a typical superconducting-qubit control wiring and bias circuitry. The key point is that the waveform $u(t)$ generated by room-temperature electronics is not applied directly to the device. Instead, it propagates through a passive, dissipative, approximately linear network (for instance, attenuators, bias tees, wiring, packaging, and often deliberately inserted low-pass elements), so that the device experiences a *realized* field $\Phi(t)$ that is a filtered version of the command. This type of finite-bandwidth and distortion modeling is standard in superconducting-qubit hardware stacks and calibration workflows [5, 53, 54]. This

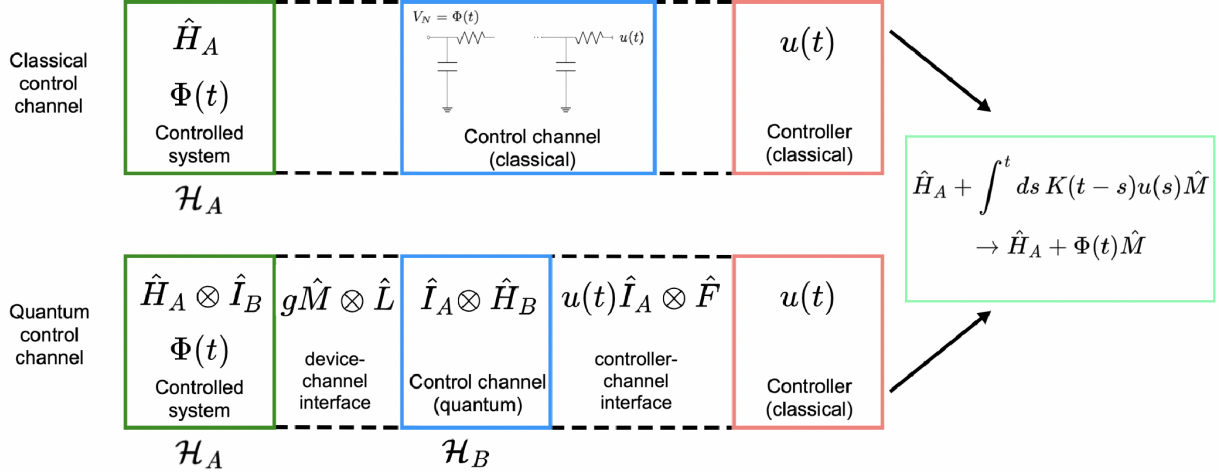


FIG. 3. Schematic connection between a phenomenological *classical* control filter and a microscopic *quantum* control-channel model. **Top:** the room-temperature controller outputs a command $u(t)$, which is distorted by a passive control line (e.g. an RC ladder) into a realized in-situ field $\Phi(t) = (K * u)(t)$ that drives the device A via $\hat{H}_A + \Phi(t)\hat{M}$. **Bottom:** the same architecture is modeled microscopically by a channel B with Hamiltonian \hat{H}_B , driven at the input port by the classical source $u(t)$ through an operator \hat{F} and coupled at the device port through $g\hat{M} \otimes \hat{L}$. In the weak-coupling regime (Born/Oppenheimer) limit and linear response (Kubo), the delivered field is the channel expectation $\Phi(t) = \langle \hat{L} \rangle_t = \int_{-\infty}^t \chi_{LF}(t-s) u(s) ds$, yielding the effective filtered Hamiltonian $\hat{H}_A + \int^t ds K(t-s)u(s) ds \hat{M} \equiv \hat{H}_A + \Phi(t)\hat{M}$ with K identified as the retarded susceptibility of the control.

point of view can also be relaxed, as we show later, with the quantum treatment of the kernel K .

We consider, as an example, a single-qubit effective description (e.g. a two-level truncation of a transmon or a flux qubit) driven by one near-resonant control quadrature [55, 56]:

$$\hat{H}(t) = \hat{H}_A + \Phi(t)\hat{M}, \quad \hat{H}_A = \sigma_z, \quad \hat{M} = \sigma_x, \quad (123)$$

where $\Phi(t)$ denotes the in situ drive amplitude at the device node. (For flux-type control one may have $\hat{M} = \sigma_z$; nothing below depends on this choice.) The classical filtering $u \mapsto \Phi$ is treated as an ordinary signal processing stage. In particular, we assume it does not induce open-system quantum memory in the sense of a non-Markovian bath: in our model the qubit evolution remains unitary once $\Phi(t)$ is specified. This is an idealization, but it is appropriate for isolating the role of *classical* channel memory in the hysteresis measures defined in Sec. II C.

A. Classical treatment of $\Phi(t)$.

In the small-signal regime relevant for waveform transfer (and after selecting a single effective quadrature), the control line can be modeled as a passive, stable, linear time-invariant (LTI) two-port mapping the commanded waveform $u(t)$ to the device-node field $\Phi(t)$. Causality motivates the convolution form

$$\Phi(t) = \int_{-\infty}^t K(t-s)u(s) ds, \quad K(\tau) = 0 \text{ for } \tau < 0, \quad (124)$$

equivalently $\Phi(s) = G(s)u(s)$ in the Laplace domain, with transfer function $G(s) := \Phi(s)/u(s)$ analytic for $\text{Re}(s) > 0$.

The distinctive feature of the experimental setting is that much of the relevant filtering is well described by *relaxational* (RC-type) dynamics rather than high- Q resonances: thermalized attenuators and resistive wiring introduce loss, while distributed capacitances to ground (and intentional shunt capacitances in bias tees and low-pass sections) provide storage. In such circumstances an RC network is a natural effective description at the frequencies that shape the envelope of typical control pulses.

Classical network-synthesis theory then severely restricts the analytic structure of $G(s)$. For passive RC networks the transfer function is real, stable, and (for ladder families of interest) has poles on the negative real axis, generically simple; realizability/synthesis criteria and proofs for RC ladders are classical [25, 27]. Appendix F summarizes the relevant statements and derives the exponential-mode representation directly for an RC ladder model.

These pole restrictions translate immediately into an exponential-mode impulse response. If $G(s)$ is rational (finite ladder approximation), one can write

$$G(s) = g_\infty + \sum_{k=1}^K \frac{c_k}{s + \nu_k}, \quad \nu_k > 0, \quad (125)$$

so that the causal kernel is

$$K(\tau) = g_\infty \delta(\tau) + \sum_{k=1}^K c_k e^{-\nu_k \tau} \Theta(\tau). \quad (126)$$

For a distributed (diffusive) RC line, $G(s)$ is no longer rational, but it remains passive and stable and admits an integral mixture of exponentials; Appendix F gives an explicit example and the corresponding long-tailed kernel. In either case, the essential consequence is that $K(\tau)$ is non-oscillatory and generated by a hierarchy of relaxation rates $\{\nu_k\}$.

The exponential representation (126) is equivalent to the finite-dimensional time-local embedding used in Sec. II B. Defining auxiliary modes

$$\begin{aligned}\Phi_k(t) &:= \int_{-\infty}^t c_k e^{-\nu_k(t-s)} u(s) ds, \\ \Phi(t) &= g_\infty u(t) + \sum_{k=1}^K \Phi_k(t),\end{aligned}\quad (127)$$

one obtains

$$\dot{\Phi}_k(t) = -\nu_k \Phi_k(t) + c_k u(t), \quad k = 1, \dots, K. \quad (128)$$

In the ODE and time-local representation, the initial conditions are associated to the initial state of the shunted capacitances. For a finite RC ladder this representation is not an approximation: it is simply the modal form of the ladder state-space dynamics (Appendix F). Physically, the modes correspond to internal charge-storage degrees of freedom of the line/bias network, and the slowest rate ν_{\min} sets the dominant memory time $\tau_{\text{mem}} \sim \nu_{\min}^{-1}$.

The simplest nontrivial instance is a single series resistance R feeding a device-side shunt capacitance C . Writing the device-node voltage as $\Phi(t)$, Kirchhoff's laws give

$$\begin{aligned}C \dot{\Phi}(t) &= \frac{u(t) - \Phi(t)}{R} \iff \tau_c \dot{\Phi}(t) + \Phi(t) = u(t), \\ \tau_c &:= RC,\end{aligned}\quad (129)$$

with kernel

$$K(\tau) = \frac{1}{\tau_c} e^{-\tau/\tau_c} \Theta(\tau). \quad (130)$$

This is precisely the single-pole truncation of (126), corresponding to retaining only the slowest relaxational channel. In the limit $\tau_c \rightarrow 0$, the kernel concentrates at $\tau = 0$ and $\Phi(t) \rightarrow u(t)$ for protocols that do not vary on vanishing time scales, recovering the memoryless control idealization.

The exponential-mode description is particularly convenient for the hysteresis framework developed earlier in the manuscript. It provides an explicit classical memory channel with a controlled hierarchy of time scales, and also a clean separation between hysteresis inherited from the filter (visible in $\mathcal{A}_{u\Phi}$ and thus potentially in \mathcal{A}_{uO}) and genuinely nonadiabatic/state-history effects in the quantum dynamics (diagnosed by $\mathcal{A}_{\Phi O}$). This separation was exploited in Secs. III B 1–III B 3 and in the numerical study of Sec. III C.

B. Quantum Kubo treatment of $\Phi(t)$.

Throughout the paper we model the *realized* control field $\Phi(t)$ seen by the device as a causal convolution of the room-temperature command $u(t)$, $\Phi(t) = (K * u)(t)$. This might seem unjustified from a quantum perspective. Appendix H provides a microscopic quantum derivation of this structure and clarifies when the kernel K admits the exponential-mode forms used in Sec. II B and in the RC examples (Appendix F). Here we summarize the key steps and consequences. First, we treat the control hardware (wiring, attenuators, bias tees, filters, packaging) as a *physical dynamical system*, in the most microscopic description, a quantum many-body “channel” B with Hilbert space \mathcal{H}_B and Hamiltonian \hat{H}_B . The room-temperature electronics provide a prescribed waveform $u(t)$, which we model as a classical (c-number) *generalized force* applied at an *input port* of the channel. Microscopically, such forcing is represented by a Hamiltonian term linear in a channel operator \hat{F} , i.e. a work term $-u(t)\hat{F}$, exactly as in the standard Kubo formulation of linear response and the fluctuation–dissipation framework [17, 57, 58]. The device A couples to the channel at an *output port* through a (generally distinct) channel operator \hat{L} , which represents the local field/coordinate delivered to the device node. This separation between input forcing and output readout is also the natural language of quantum network and input–output theory for driven electromagnetic environments [16, 59–62].

We aim to show that a minimal bipartite Hamiltonian capturing these roles is

$$\hat{H}(t) = \hat{H}_A \otimes \mathbb{I}_B + \mathbb{I}_A \otimes \hat{H}_B + g \hat{M} \otimes \hat{L} - u(t) \mathbb{I}_A \otimes \hat{F}, \quad (131)$$

where \hat{M} is the device operator that couples to the delivered field, and g is a (an assumed) small coupling parameter quantifying how strongly the device perturbs the control channel. The structure (131) is the direct analogue of standard system–bath models in which a distinguished system couples to a large environment via a bilinear interaction, with the environment itself subject to external driving [63–65]. In particular, eliminating (or coarse-graining) channel degrees of freedom in such models generically produces retarded response functions and memory kernels, as in the classic derivations of generalized Langevin dynamics for assemblies of coupled oscillators [66] and in the Caldeira–Leggett description of dissipative quantum environments [67]. In our setting, however, we emphasize that it is related to the transmission conductance, closer to Kubo's [17] *two-port* viewpoint, i.e. \hat{F} encodes how the commanded signal injects energy into the control, while \hat{L} encodes the field that is actually delivered at the device node and therefore enters the effective device Hamiltonian.

This microscopic setup is precisely tailored to the kernel description used in the main text: in linear response, the realized field $\Phi(t) := \langle \hat{L}(t) \rangle$ is a causal convolution of the command $u(t)$ with the retarded susceptibility

$\chi_{LF}(\tau)$ [17, 57]. Moreover, when \hat{F} and \hat{L} are chosen as standard circuit port variables (e.g. charge/flux at a port and current/voltage at a readout node), $\chi_{LF}(\omega)$ coincides with familiar circuit response functions such as admittances or transfer admittances, and its dissipative component is constrained by passivity and linked to equilibrium noise via fluctuation–dissipation [58, 60–62].

As we show in the Appendix, the realized classical field is identified with the channel mean at the output port,

$$\Phi(t) := \langle \hat{L} \rangle_t = \text{Tr}_B(\hat{\rho}_B(t)\hat{L}), \quad (132)$$

so $\Phi(t)$ is a c-number functional of the applied waveform $u(\cdot)$. Differentiating $\hat{\rho}_A(t) = \text{Tr}_B\hat{\rho}(t)$ yields an exact identity in which the device couples to the operator-valued field $\text{Tr}_B[(\mathbb{I}_A \otimes \hat{L})\hat{\rho}(t)]$ (Appendix H). In the weak-coupling regime one may neglect device-induced disturbance of the channel to leading order, so that $\hat{\rho}(t) \approx \hat{\rho}_A(t) \otimes \hat{\rho}_B^{(u)}(t)$ and the field factorizes as $\text{Tr}_B[(\mathbb{I}_A \otimes \hat{L})\hat{\rho}(t)] \approx \Phi(t)\hat{\rho}_A(t)$. This yields the effective reduced generator

$$\dot{\hat{\rho}}_A(t) = -i[\hat{H}_A + g\Phi(t)\hat{M}, \hat{\rho}_A(t)] + \mathcal{O}(g^2), \quad (133)$$

i.e. the device is driven *coherently* by the classical realized field $\Phi(t)$, while channel fluctuations and backaction enter only at higher order.

For a stationary reference state of the unforced channel, the response of $\Phi(t)$ to a weak source $u(t)$ is given by a Kubo retarded susceptibility. In the closed (unitary) case,

$$\begin{aligned} \Phi(t) &= \Phi_0 + \int_{-\infty}^t \chi_{LF}(t-s)u(s)ds + \mathcal{O}(u^2), \text{ where} \\ \chi_{LF}(\tau) &= i\Theta(\tau)\langle[\hat{L}_I(\tau), \hat{F}_I(0)]\rangle_B, \end{aligned} \quad (134)$$

so the kernel used in the main text is a Kubo-like causal response function $K(\tau) \equiv \chi_{LF}(\tau)$ to leading order (Appendix H), between the input and output port operators on \mathcal{H}_B . This identifies the classical filter as a two-port quantum response function of the control. We see that in this regime (and up to order g^2), the evolution of the reduced density matrix is consistent with the time evolution of eqn. (3). Implicitly, this structure was also partly suggested in [7] (see App. D) where, however, it was not identified as a convolution kernel *a lá* Kubo as in here.

The structure of the kernel function K depends on the physical assumptions. First, we show that the time-domain structure of $\chi_{LF}(\tau)$ depends qualitatively on whether the channel is lossless or dissipative. For a finite-dimensional unitary channel, $\chi_{LF}(\tau)$ admits a Lehmann expansion as a finite sum of oscillatory terms $e^{i\omega_{nm}\tau}$ and does not generically decay. Thus, without dissipation (or a macroscopic continuum limit), one should not expect a relaxational sum of decaying exponentials. However, if the channel is an open system with a stable GKLS generator \mathcal{L}_0 (dissipation *on* B), the Kubo formula is obtained by replacing unitary evolution with the adjoint semigroup $e^{\mathcal{L}_0^\dagger\tau}$. This yields a mode expansion

$\chi_{LF}(\tau) = \Theta(\tau) \sum_k c_k e^{\lambda_k \tau}$ with $\text{Re}(\lambda_k) \leq 0$. In the over-damped (RC-like) regime relevant for passive wiring and filters, the dominant λ_k are real and negative, $\lambda_k = -\nu_k$, giving

$$K(\tau) \equiv \chi_{LF}(\tau) \approx \sum_{k=1}^{K_{\max}} c_k e^{-\nu_k \tau} \Theta(\tau), \quad \nu_k > 0, \quad (135)$$

which is consistent with the exponential-mode embedding used in Sec. II B and earlier in this section. Thus, the same exponential structure follows from classical network synthesis: passive RC ladders have transfer functions with poles on the negative real axis, implying impulse responses that are sums (or mixtures) of decaying exponentials. Appendix F makes this connection explicit and provides the circuit-level interpretation of the rates ν_k as relaxation modes of the line.

A standard subtlety in Kubo linear response is that the assumption that the channel is thermal in the remote past is inconsistent with applying a finite perturbation for all times: if the source $u(t)$ were nonzero forever, the state at $t \rightarrow -\infty$ would not be an equilibrium state of \hat{H}_B . The conventional resolution is to assume that the perturbation is switched on adiabatically from the far past, either by sending the initial time $t_0 \rightarrow -\infty$ together with a convergence factor, or equivalently by replacing the perturbation by $-u(t)e^{\eta t}\hat{F}$ and taking $\eta \downarrow 0^+$ at the end (the “adiabatic switching” or “ $i0^+$ retarded prescription”). [17, 18, 68, 69] Concretely, in the derivation of Appendix H 1 one may keep the factor explicitly:

$$\begin{aligned} \Phi(t) - \Phi_0 &= \int_{-\infty}^t ds \chi_{LF}^{(\eta)}(t-s)u(s), \\ \chi_{LF}^{(\eta)}(\tau) &= i\Theta(\tau)e^{-\eta\tau}\langle[\hat{L}_I(\tau), \hat{F}]\rangle_B, \quad \eta > 0, \end{aligned} \quad (136)$$

so that $\chi_{LF}(\tau) = \lim_{\eta \downarrow 0^+} \chi_{LF}^{(\eta)}(\tau)$ in the usual retarded sense. In general, the representation above is well known to not lead to an RC-like kernel as it is quasi-periodic (see for instance App. H 2). In the fully closed case, the strictly closed thermal Lehmann sum representation for the kernel

$$\chi_{LF}(\tau) = i\Theta(\tau) \sum_{m,n} (p_n - p_m) L_{nm} F_{mn} e^{i(E_n - E_m)\tau}. \quad (137)$$

is quasi-periodic in time and, for a finite-dimensional B , does not generically decay as $\tau \rightarrow \infty$ (Appendix H 3).

In frequency space, the same η appears as the infinitesimal imaginary part selecting the retarded analytic continuation:

$$\begin{aligned} \chi_{LF}^R(\omega) &= -i \int_0^\infty d\tau e^{i(\omega+i0^+)\tau} \langle[\hat{L}_I(\tau), \hat{F}]\rangle_B, \\ \chi_{LF}^{(\eta)}(\omega) &= -i \int_0^\infty d\tau e^{i(\omega+i\eta)\tau} \langle[\hat{L}_I(\tau), \hat{F}]\rangle_B. \end{aligned} \quad (138)$$

Equivalently, in the Lehmann representation (Appendix H 3), the regulator shifts poles into the lower half-plane,

$$\chi_{LF}^{(\eta)}(\omega) = \sum_{m,n} (p_n - p_m) L_{nm} F_{mn} \frac{1}{\omega - \omega_{nm} + i\eta},$$

$$\omega_{nm} := E_n - E_m, \quad (139)$$

so that the spectral lines which are δ -sharp in a strictly closed, finite-dimensional channel are broadened into Lorentzians of width η :

$$\text{Im } \chi_{LF}^{(\eta)}(\omega) = - \sum_{m,n} (p_n - p_m) L_{nm} F_{mn} \frac{\eta}{(\omega - \omega_{nm})^2 + \eta^2}.$$

From this viewpoint, the Kubo's η is both (i) a mathematical convergence device that makes $t_0 \rightarrow -\infty$ well-defined and enforces causality, and (ii) a stand-in for physical level broadening associated with finite lifetimes once the channel is coupled (even weakly) to uncontrolled degrees of freedom. The same object also appears when one derives real-time response from imaginary-time (Matsubara) correlators: one computes $\chi(i\omega_n)$ at discrete Matsubara frequencies ω_n and then analytically continues $i\omega_n \mapsto \omega + i0^+$ to obtain the retarded $\chi^R(\omega)$.[18, 68–70]

Introducing $\eta > 0$ multiplies the time-domain commutator by $e^{-\eta\tau}$, producing an *effective* exponential envelope. However, a single constant η only yields a single exponential scale and should be read as a coarse phenomenology for dissipation.

A more physical route to genuine multi-timescale relaxational decay is precisely the open-channel description: dissipation shifts the relevant poles by *mode-dependent* decay rates. In the Markovian setting discussed above, the adjoint generator \mathcal{L}_0^\dagger has eigenvalues $\lambda_k = -\nu_k + i\omega_k$ with $\nu_k \geq 0$, so that the Kubo-like commutator form (H48) produces

$$\chi_{LF}(\tau) = \Theta(\tau) \sum_k c_k e^{\lambda_k \tau},$$

and in the overdamped regime (relevant for passive RC stacks in-band) one has $\omega_k \approx 0$ and $\chi_{LF}(\tau) \approx \Theta(\tau) \sum_k c_k e^{-\nu_k \tau}$, matching the RC-ladder impulse response. In this sense, the classical RC picture and the “ η -broadened Kubo” picture are two complementary ways to encode the same physical idea: losses in the control stack move the response poles off the real axis, broadening discrete spectral lines into continuous, dissipative features and producing decaying memory kernels. This is exactly the regime in which the c-number filter model for $\Phi(t)$ is justified and in which $\mathcal{A}_{u\Phi}$ isolates the out-of-phase (dissipative) quadrature via (77), thereby connecting our geometric hysteresis measures to standard conductance-like Kubo response functions and their fluctuation-dissipation constraints (Appendix H 3).[17, 18, 39, 68]

Taken together, these results justify modeling the control channel as a classical memory kernel K (generated either by an RC ladder or by an overdamped open-channel response), while keeping the device dynamics unitary to leading order as in (133). Of course, a more careful treatment of the channel's properties is paramount to model the memory appropriately. Here, we simply focus on the simplest case in which the channel is stationary and thermal.

V. DISCUSSION AND CONCLUSIONS

This work isolates a pragmatic and experimentally relevant source of apparent “memory” in driven quantum platforms: the field that enters the device Hamiltonian is often not the commanded waveform $u(t)$, but a *filtered* realized signal $\Phi(t)$ generated by the control stack. The filtering is classical, it reflects finite bandwidth, internal relaxation, and distortion of the control path, yet it can generate pronounced hysteresis in drive-response plots and can strongly shape the “work-like” cyclic integrals considered in this paper.

The paper has two complementary parts. The first part develops a compact *hysteresis language* for separating control-channel memory from intrinsic device dynamics using loop measures in the (u, Φ) , (u, O) , and (Φ, O) planes. The second part provides a *modeling basis* for the control channel itself, connecting the kernel picture $\Phi = (K * u)$ to passive RC-type circuitry (and, more generally, to retarded susceptibilities of a driven control), thereby justifying the exponential-mode embeddings used in the main text.

The loop areas introduced in Sec. II C provide a minimal operational vocabulary. The control-channel area $\mathcal{A}_{u\Phi} = \oint \Phi du$ quantifies hysteresis internal to the control path. The realized-drive area $\mathcal{A}_{\Phi O} = \oint O d\Phi$ isolates history dependence of the observable at fixed realized drive. Finally, the commanded area $\mathcal{A}_{uO} = \oint O du$ is what is typically observed experimentally when one plots an observable against the programmed waveform, and it conflates classical control memory with device response.

A central message is that these loop measures, by themselves, do *not* certify quantum memory in the open-system sense (information backflow). In the kernel-filtered model studied here, the only nonlocality resides in the *classical* map $u(\cdot) \mapsto \Phi(\cdot)$. Once the realized trajectory $\Phi(t)$ is specified, the device evolves unitarily on \mathcal{H}_A . As a consequence, for any two initial device states $\rho_1(0)$ and $\rho_2(0)$ evolved under the same Hamiltonian trajectory, the trace distance

$$D(t) = \frac{1}{2} \|\rho_1(t) - \rho_2(t)\|_1$$

cannot exhibit revivals, since $\|\cdot\|_1$ is invariant under unitary conjugation. [10–12] This separation is experimentally actionable: if one reconstructs (or otherwise controls) the realized $\Phi(t)$ and still observes trace-distance revivals for some pair of preparations, then the reduced

dynamics cannot be explained as a classical filter and must involve additional degrees of freedom.[10]

On the modeling side, the single-pole (single-RC) kernel provides a convenient first parametrization of control memory: it is the minimal causal model that turns the nonlocal relation $u(\cdot) \mapsto \Phi(\cdot)$ into a single auxiliary state variable and introduces one time scale τ_c that can be compared across devices and wiring stacks. Importantly, τ_c need not be introduced as an abstract fit parameter. As summarized in Appendix G, when the small-signal transfer function from u to Φ is well approximated by a first-order low-pass response, the cutoff frequency $f_{3\text{dB}}$ and step-response rise time t_r translate directly into τ_c via $\tau_c \approx 1/2\pi f_{3\text{dB}}$, leading to $t_r \approx 0.3/B_W$, with B_W the (approximately) single-pole bandwidth in hertz. This connects quantities routinely measured in situ (bandwidth, step response, impulse response) to the effective memory scale used in the kernel phenomenology. This was also discussed in [9], in which, for a bandwidth in MHz, they estimated a kernel memory of the order of μs .

As a rough estimate with the modern control stack, an envelope bandwidth in the 0.1–1 GHz range corresponds to $\tau_c \sim 0.16\text{--}1.6\text{ ns}$, placing the most pronounced kernel-induced hysteresis in the regime $\omega\tau_c \sim 1$, i.e. modulation frequencies from hundreds of MHz to a few GHz. Depending on the bandwidth of the control stack, the memory can be as small as $\approx 1\text{ ns}$ to a few μs .

Second, the kernel model suggests a direct route to improved pulse design. If the control path is parameterized by a small set of modes (single RC or a multi-mode realization), one can *embed* the filter dynamics as auxiliary classical state variables and optimize pulses against the *realized* Hamiltonian rather than the commanded waveform. This viewpoint aligns with distortion-aware optimal-control approaches in which hardware response is explicitly incorporated into the forward model used for synthesis and calibration.[2, 9, 13, 14] In gradient-based optimal control, this amounts to augmenting the forward model by the filter ODE(s) and differentiating through them, in the spirit of established quantum-control frameworks.[2, 3]

Third, the kernel at the device is the result of various filters of the stack, including both a classical and a quantum induced kernel, as in Fig. 4. The action of these could be at different timescales. This implies that the filter on the A system is the result of both a quantum K_q and classical K_c filter, e.g. $\mathcal{K}_A = K_q * K_c$, or alternatively $\Phi(t) = (K_q * (K_c * u))(t)$, and thus the stages are modeled using different methods. In practice, realistic wiring stacks are rarely captured by a single pole: connectors, bias tees, impedance mismatches, and distributed dissipation can produce multiple decays and long tails. We provided a principled justification for multi-exponential kernels based on passive RC ladder realizations and for viewing the single-RC model as the leading (slowest-pole) truncation, while we also provided a microscopic justification in which the kernel is identified with a retarded

susceptibility of a driven control in linear response.

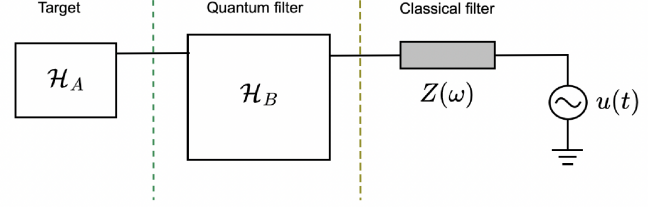


FIG. 4. In practice, the filter at the target device is the result of various stages of the stack.

Two practical consequences follow. First, hysteresis loops in the commanded plane (u, O) should not be over-interpreted: even for a closed, unitary device, classical filtering can generate sizable loop areas through the lag $u \mapsto \Phi$, and coherent nonadiabaticity can generate $\mathcal{A}_{\Phi O} \neq 0$ without invoking any open-system memory. This motivates reporting control-channel diagnostics (at minimum $\mathcal{A}_{u\Phi}$, or an equivalent transfer-function estimate) alongside observable hysteresis plots.

Several extensions are natural. On the diagnostics side, the most informative next step is a systematic numerical sweep of frequency and amplitude across the boundary between adiabatic following and strongly nonadiabatic response, while holding the *control* transfer function fixed [71–77]. This would map, within a unified set of plots, how classical control memory (through K) and coherent dynamics (through H_A) jointly determine $\mathcal{A}_{u\Phi}$, \mathcal{A}_{uO} , and $\mathcal{A}_{\Phi O}$. On the modeling side, pushing the microscopic derivation beyond leading order would clarify how channel fluctuations and backaction modify the effective drive and when truly open-system signatures become unavoidable. We expect the combined hysteresis diagnostics and channel modeling developed here to be useful both for interpreting hysteretic features in experimental data and for designing control strategies that explicitly separate, diagnose, and mitigate classical control memory.

ACKNOWLEDGMENTS

The author is indebted to F. Barrows, C. Nisoli, P. Sathe, A. Adebi, M. Polini, and G. Menichetti for comments regarding this manuscript. This work was partly supported by the U.S. Department of Energy through the Los Alamos National Laboratory. Los Alamos National Laboratory is operated by Triad National Security, LLC, for the National Nuclear Security Administration of U.S. Department of Energy (Contract No. 89233218CNA000001). The research presented in this article was supported by the Laboratory Directed Research and Development program of Los Alamos National Laboratory under project number 20240032DR. The author is currently an employee of Planckian.

[1] Michael A. Nielsen and Isaac L. Chuang. *Quantum Computation and Quantum Information*. Cambridge University Press, 2000.

[2] Steffen J. Glaser, Ugo Boscain, Tommaso Calarco, Christiane P. Koch, Walter K öckenberger, Ronnie Kosloff, Ilya Kuprov, Burkhard Luy, Sophie Schirmer, Thomas Schulte-Herbrüggen, Dominique Sugny, and Frank K. Wilhelm. Training schrödinger's cat: quantum optimal control. *The European Physical Journal D*, 69(12):279, 2015.

[3] Lorenza Viola, Emanuel Knill, and Seth Lloyd. Dynamical decoupling of open quantum systems. *Physical Review Letters*, 82(12):2417–2421, 1999.

[4] Kristan Temme, Sergey Bravyi, and Jay M. Gambetta. Error mitigation for short-depth quantum circuits. *Physical Review Letters*, 119(18):180509, 2017.

[5] Philip Krantz, Morten Kjaergaard, Fei Yan, Terry P. Orlando, Simon Gustavsson, and William D. Oliver. A quantum engineer's guide to superconducting qubits. *Applied Physics Reviews*, 6(2):021318, 2019.

[6] Elijah Pelofske, Pratik Sathe, Cristiano Nisoli, and Frank Barrows. Probing antiferromagnetic hysteresis on programmable quantum annealers. 2025.

[7] Frank Barrows, Elijah Pelofske, Pratik Sathe, Francesco Caravelli, and Cristiano Nisoli. Magnetic memory and hysteresis from quantum transitions: Theory and experiments on quantum annealers. 2025.

[8] Felix Motzoi, Jay M. Gambetta, Patrick Rebentrost, and Frank K. Wilhelm. Simple pulses for elimination of leakage in weakly anharmonic qubits. *Physical Review Letters*, 103(11):110501, 2009.

[9] Troy W. Borneman and David G. Cory. Bandwidth-limited control and ringdown suppression in high-q resonators. *Journal of Magnetic Resonance*, 225:120–129, 2012.

[10] Heinz-Peter Breuer, E.-M. Laine, and J. Piilo. Measure for the degree of non-markovian behavior of quantum processes in open systems. *Physical Review Letters*, 103(21):210401, 2009.

[11] Ángel Rivas, Susana F. Huelga, and Martin B. Plenio. Quantum non-markovianity: Characterization, quantification and detection. *Reports on Progress in Physics*, 77(9):094001, 2014.

[12] Inés de Vega and Daniel Alonso. Dynamics of non-markovian open quantum systems. *Reviews of Modern Physics*, 89(1):015001, 2017.

[13] I. N. Hincks, C. E. Granade, T. W. Borneman, and D. G. Cory. Controlling quantum devices with nonlinear hardware. *Phys. Rev. Applied*, 4:024012, Aug 2015.

[14] Nicolas Wittler, Federico Roy, Kevin Pack, Max Werninghaus, Anurag Saha Roy, Daniel J. Egger, Stefan Filipp, Frank K. Wilhelm, and Shai Machnes. Integrated tool set for control, calibration, and characterization of quantum devices applied to superconducting qubits. *Phys. Rev. Applied*, 15:034080, 2021.

[15] Marco Cattaneo and Gheorghe Sorin Paraoanu. Engineering dissipation with resistive elements in circuit quantum electrodynamics. *Advanced Quantum Technologies*, 4(11), September 2021.

[16] C. W. Gardiner and M. J. Collett. Input and output in damped quantum systems: Quantum stochastic differen-

tial equations and the master equation. *Physical Review A*, 31(6):3761–3774, 1985.

[17] R. Kubo. Statistical-mechanical theory of irreversible processes. i. general theory and simple applications to magnetic and conduction problems. *Journal of the Physical Society of Japan*, 12(6):570–586, 1957.

[18] Dieter Forster. *Hydrodynamic Fluctuations, Broken Symmetry, and Correlation Functions*. W. A. Benjamin, 1975.

[19] Alan V. Oppenheim, Alan S. Willsky, and S. Hamid Nawab. *Signals and Systems*. Prentice Hall, Upper Saddle River, 2nd edition, 1997.

[20] Anant Agarwal and Jeffrey H. Lang. *Foundations of Analog and Digital Electronic Circuits*. Morgan Kaufmann, San Francisco, 2005.

[21] Jan Mikusiński. *The Bochner Integral*. Birkhäuser Basel, 1978.

[22] Tosio Kato. *Perturbation Theory for Linear Operators*. Springer, Berlin, 2nd edition, 1995.

[23] Michael Reed and Barry Simon. *Methods of Modern Mathematical Physics, Vol. I: Functional Analysis*. Academic Press, New York, 1972.

[24] Stephen Boyd and Leon O. Chua. Fading memory and the problem of approximating nonlinear operators with volterra series. *IEEE Transactions on Circuits and Systems*, 32(11):1150–1161, 1985.

[25] L. Magos. Realization of driving-point and transfer functions by r-c ladder networks. *International Journal of Electronics*, 29(3):263–276, 1970.

[26] Thomas Kailath. *Linear Systems*. Prentice Hall, Englewood Cliffs, NJ, 1980.

[27] A. Fialkow and S. Gerst. The routh-hurwitz problem for rational functions of the complex variable. *Transactions of the American Mathematical Society*, 70(3):381–420, 1951.

[28] L. Chua. Memristor-the missing circuit element. *IEEE Transactions on Circuit Theory*, 18(5):507–519, 1971.

[29] Francesco Caravelli and Juan Pablo Carballo. Memristors for the curious outsiders. *Technologies*, 6(4):118, December 2018.

[30] Massimiliano Di Ventra, Yuriy V. Pershin, and Leon O. Chua. Circuit elements with memory: Memristors, mem-capacitors, and meminductors. *Proceedings of the IEEE*, 97(10):1717–1724, October 2009.

[31] M. J. Lighthill. *Introduction to Fourier Analysis and Generalized Functions*. Cambridge University Press, Cambridge, 1958.

[32] Walter Rudin. *Real and Complex Analysis*. McGraw-Hill, New York, 3rd edition, 1987.

[33] Giorgio Bertotti. *Hysteresis in Magnetism: For Physicists, Materials Scientists, and Engineers*. Academic Press, San Diego, 1998.

[34] Isaak D. Mayergoyz. *Mathematical Models of Hysteresis and Their Applications*. Elsevier, Amsterdam, 2003.

[35] F. Preisach. Über die magnetische nachwirkung. *Zeitschrift für Physik*, 94:277–302, 1935.

[36] Max Born and Vladimir Fock. Beweis des adiabatensatzes. *Zeitschrift für Physik*, 51:165–180, 1928.

[37] Tosio Kato. On the adiabatic theorem of quantum mechanics. *Journal of the Physical Society of Japan*, 5(6):435–439, 1950.

[38] Stefan Teufel. Adiabatic perturbation theory in quantum dynamics. *Lecture Notes in Mathematics*, 1821, 2003.

[39] Heinz-Peter Breuer and Francesco Petruccione. *The Theory of Open Quantum Systems*. Oxford University Press, 2002.

[40] J. E. Avron and A. Elgart. Adiabatic theorem without a gap condition. *Communications in Mathematical Physics*, 203(2):445–463, 1999.

[41] Sabine Jansen, Mary Beth Ruskai, and Ruedi Seiler. Bounds for the adiabatic approximation with applications to quantum computation. *Journal of Mathematical Physics*, 48(10):102111, 2007.

[42] Marcos Rigol, Vanja Dunjko, and Maxim Olshanii. Thermalization and its mechanism for generic isolated quantum systems. *Nature*, 452(7189):854–858, 2008.

[43] Anatoli Polkovnikov. Colloquium: Nonequilibrium dynamics of closed interacting quantum systems. *Reviews of Modern Physics*, 83(3):863–883, 2011.

[44] J. J. Sakurai and Jim Napolitano. *Modern Quantum Mechanics*. Cambridge University Press, 3 edition, 2017.

[45] Michele Campisi, Peter Hänggi, and Peter Talkner. Colloquium: Quantum fluctuation relations: Foundations and applications. *Rev. Mod. Phys.*, 83(3):771–791, 2011.

[46] Peter Talkner, Eric Lutz, and Peter Hänggi. Fluctuation theorems: Work is not an observable. *Phys. Rev. E*, 75:050102, 2007.

[47] Heinz-Peter Breuer, Elsi-Mari Laine, Jyrki Piilo, and Bassano Vacchini. Colloquium: Non-markovian dynamics in open quantum systems, 2016.

[48] Ángel Rivas, Susana F. Huelga, and Martin B. Plenio. Quantum non-markovianity: Characterization, quantification and detection. *Rep. Prog. Phys.*, 77(9):094001, 2014.

[49] Carlo De Grandi and Anatoli Polkovnikov. Adiabatic perturbation theory: From landau–zener problem to quenching through a quantum critical point. *Lecture Notes in Physics*, 802:75–114, 2010.

[50] Alexandre Blais, Arne L. Grimsmo, S. M. Girvin, and Andreas Wallraff. Circuit quantum electrodynamics. *Reviews of Modern Physics*, 93(2):025005, 2021.

[51] Anatole Abragam. *The Principles of Nuclear Magnetism*. Oxford University Press, 1961.

[52] Charles P. Slichter. *Principles of Magnetic Resonance*, volume 1 of *Springer Series in Solid-State Sciences*. Springer, 3 edition, 1990.

[53] Mikael Kjaergaard, Mollie E. Schwartz, Jochen Braumüller, Philip Krantz, Joel I.-J. Wang, Simon Gustavsson, and William D. Oliver. Superconducting qubits: Current state of play. *Annual Review of Condensed Matter Physics*, 11:369–395, 2020.

[54] Markus Roth, Jonathan Herrmann, Markus Förster, et al. Cryogenic microwave engineering for scalable superconducting quantum processors. *PRX Quantum*, 2024. To appear; see also arXiv:2311.00000.

[55] Jens Koch, Terri M. Yu, Jay Gambetta, Alexandre A. Houck, D. I. Schuster, J. Majer, Alexandre Blais, M. H. Devoret, S. M. Girvin, and R. J. Schoelkopf. Charge-insensitive qubit design derived from the cooper pair box. *Phys. Rev. A*, 76:042319, 2007.

[56] J. Q. You and Franco Nori. Atomic physics and quantum optics using superconducting circuits. *Nature*, 474:589–597, 2011.

[57] R. Kubo. The fluctuation-dissipation theorem. *Reports on Progress in Physics*, 29(1):255–284, 1966.

[58] Herbert B. Callen and Theodore A. Welton. Irreversibility and generalized noise. *Physical Review*, 83:34–40, 1951.

[59] Bernard Yurke and John S. Denker. Quantum network theory. *Physical Review A*, 29(3):1419–1437, 1984.

[60] A. A. Clerk, M. H. Devoret, S. M. Girvin, F. Marquardt, and R. J. Schoelkopf. Introduction to quantum noise, measurement, and amplification. *Reviews of Modern Physics*, 82(2):1155–1208, 2010.

[61] Michel H. Devoret. Quantum fluctuations in electrical circuits. In Serge Reynaud, Elisabeth Giacobino, and Jean Zinn-Justin, editors, *Quantum Fluctuations*, Les Houches, Session LXIII (1995), pages 351–386. Elsevier (North-Holland), 1997.

[62] Uri Vool and Michel H. Devoret. Introduction to quantum electromagnetic circuits. *International Journal of Circuit Theory and Applications*, 45(7):897–934, 2017.

[63] C. W. Gardiner and M. J. Collett. Input and output in damped quantum systems: Quantum stochastic differential equations and the master equation. *Physical Review A*, 31:3761–3774, 1985.

[64] M. J. Collett and C. W. Gardiner. Squeezing of intracavity and traveling-wave light fields produced in parametric amplification. *Physical Review A*, 30:1386–1391, 1984.

[65] A. A. Clerk, M. H. Devoret, S. M. Girvin, F. Marquardt, and R. J. Schoelkopf. Introduction to quantum noise, measurement, and amplification. *Reviews of Modern Physics*, 82:1155–1208, 2010.

[66] G. W. Ford, M. Kac, and P. Mazur. Statistical mechanics of assemblies of coupled oscillators. *Journal of Mathematical Physics*, 6(4):504–515, 1965.

[67] A. O. Caldeira and A. J. Leggett. Influence of dissipation on quantum tunneling in macroscopic systems. *Physical Review Letters*, 46:211–214, 1981.

[68] Gerald D. Mahan. *Many-Particle Physics*. Springer, 3 edition, 2000.

[69] Alexander L. Fetter and John Dirk Walecka. *Quantum Theory of Many-Particle Systems*. McGraw-Hill, 1971.

[70] Alex Kamenev. *Field Theory of Non-Equilibrium Systems*. Cambridge University Press, 2011.

[71] L. Viola, E. Knill, and S. Lloyd. Dynamical decoupling of open quantum systems. *Phys. Rev. Lett.*, 82:2417, 1999.

[72] L. Viola and E. Knill. Robust dynamical decoupling of quantum systems with bounded controls. *Phys. Rev. Lett.*, 90:037901, 2003.

[73] L. F. Santos and L. Viola. Enhanced convergence and robust performance of randomized dynamical decoupling. *Phys. Rev. Lett.*, 97:150501, 2006.

[74] T. Caneva, M. Murphy, T. Calarco, R. Fazio, S. Montangero, V. Giovannetti, and G. E. Santoro. Optimal control at the quantum speed limit. *Phys. Rev. Lett.*, 103:240501, 2009.

[75] Michael Murphy, Simone Montangero, Vittorio Giovannetti, and Tommaso Calarco. Communication at the quantum speed limit along a spin chain. *Phys. Rev. A*, 82:022318, 2010.

[76] P. Doria, T. Calarco, and S. Montangero. Optimal control technique for many-body quantum dynamics. *Phys. Rev. Lett.*, 106:190501, 2011.

[77] N. Rach, M. M. Müller, T. Calarco, and S. Montangero. Dressing the chopped-random-basis optimization: A bandwidth-limited access to the trap-free landscape. *Phys. Rev. A*, 92:062343, 2015.

[78] Francesco Caravelli. Spectral methods in complex sys-

tems, 2025.

[79] Tektronix. Where does the formula $BW = 0.35 / t_{10\%-90\%}$ come from? Tektronix Support FAQ, 2025. Accessed: 2025-12-29. <https://www.tek.com/en/support/faqs/where-does-formula-bw-035-t10-90-come>.

[80] Keysight Technologies. Bandwidth and rise time requirements for making accurate oscilloscope measurements. Application Note 5991-0662EN, 2017. Published Dec. 1, 2017. Accessed: 2025-12-29. <https://www.acalbfi.com/media/pdf/app-note-Bandwidth-and-Rise-Time-Requirements-for-making-accurate-scope-measurements.5991-0662.pdf>.

Appendix A: Dyson expansion for kernel-filtered control with time-independent drift

This appendix gives a self-contained derivation of the interaction-picture representation and the associated Dyson series for the propagator in the kernel-filtered control model. Throughout this appendix we assume that the drift Hamiltonian \hat{H}_A is time independent.

We start from the model used in the main text,

$$\hat{H}(t) = \hat{H}_A + \hat{H}'_c(t),$$

where the filtered control Hamiltonian is defined by the causal convolution

$$\hat{H}'_c(t) = \int_{-\infty}^t K(t-s) \hat{H}_c(s) ds, \quad K(\tau) = 0 \text{ for } \tau < 0.$$

When convenient one may take the lower limit to be 0 by assuming that the protocol begins at $t = 0$ and that the drive is null for $t < 0$.

The unitary propagator $\hat{U}(t) \equiv U(t, 0)$ is defined by

$$i \frac{d}{dt} \hat{U}(t) = \hat{H}(t) \hat{U}(t), \quad U(0) = \mathbb{1},$$

where we set $\hbar = 1$.

Because \hat{H}_A is time independent, the drift (free) propagator is

$$\hat{U}_0(t) = e^{-i\hat{H}_A t}, \quad i \frac{d}{dt} \hat{U}_0(t) = \hat{H}_A \hat{U}_0(t), \quad \hat{U}_0(0) = \mathbb{1}.$$

Define the interaction-picture propagator by the exact factorization

$$\hat{U}(t) = \hat{U}_0(t) \hat{U}_I(t), \quad \hat{U}_I(t) = \hat{U}_0^\dagger(t) \hat{U}(t) = e^{i\hat{H}_A t} \hat{U}(t).$$

Differentiating $\hat{U}(t) = \hat{U}_0(t) \hat{U}_I(t)$ and using the evolution equations for U and \hat{U}_0 gives

$$i \frac{d}{dt} (\hat{U}_0 \hat{U}_I) = \hat{H}_A \hat{U}_0 \hat{U}_I + \hat{H}'_c \hat{U}_0 \hat{U}_I, \quad i \frac{d}{dt} (\hat{U}_0 \hat{U}_I) = i \dot{\hat{U}}_0 \hat{U}_I + i \hat{U}_0 \dot{\hat{U}}_I.$$

Since $i \dot{\hat{U}}_0 = \hat{H}_A \hat{U}_0$, the \hat{H}_A terms cancel and one obtains

$$i \dot{\hat{U}}_0(t) \dot{\hat{U}}_I(t) = \hat{H}'_c(t) \hat{U}_0(t) \hat{U}_I(t).$$

Multiplying on the left by $\hat{U}_0^\dagger(t)$ yields the interaction-picture equation of motion

$$i \frac{d}{dt} \hat{U}_I(t) = \tilde{H}_{1,I}(t) \hat{U}_I(t), \quad \hat{U}_I(0) = \mathbb{1},$$

where

$$\tilde{H}_{1,I}(t) = \hat{U}_0^\dagger(t) \hat{H}'_c(t) \hat{U}_0(t) = e^{i\hat{H}_A t} \hat{H}'_c(t) e^{-i\hat{H}_A t}.$$

This derivation shows that, under the standing assumption that \hat{H}_A is time independent, the interaction-picture definition used in the main text is exactly equivalent to the Schrödinger-picture evolution.

The formal solution of the interaction-picture equation is

$$\hat{U}_I(t) = \mathcal{T} \exp \left(-i \int_0^t \tilde{H}_{1,I}(\tau) d\tau \right),$$

and expanding the time-ordered exponential yields the Dyson series

$$\hat{U}_I(t) = \mathbb{1} + \sum_{n=1}^{\infty} (-i)^n \int_{0 < \tau_n < \dots < \tau_1 < t} d\tau_1 \cdots d\tau_n \tilde{H}_{1,I}(\tau_1) \cdots \tilde{H}_{1,I}(\tau_n).$$

The full propagator is recovered as

$$\hat{U}(t) = e^{-i\hat{H}_A t} \hat{U}_I(t).$$

A common specialization is a scalar command multiplying a fixed operator,

$$\hat{H}_c(s) = u(s) \hat{M},$$

with $u(s) \in \mathbb{R}$ and $\hat{M} = \hat{M}^\dagger$. In this case,

$$\hat{H}'_c(t) = \int_{-\infty}^t K(t-s) u(s) ds \hat{M} =: w(t) \hat{M},$$

so the filter acts only on the scalar drive, producing the realized field

$$w(t) = \int_{-\infty}^t K(t-s) u(s) ds. \quad (\text{A1})$$

The interaction-picture operator is then

$$\tilde{H}_{1,I}(t) = w(t) \hat{M}_I(t), \quad \hat{M}_I(t) = e^{i\hat{H}_A t} \hat{M} e^{-i\hat{H}_A t},$$

and the Dyson series becomes

$$\hat{U}_I(t) = \mathbb{1} + \sum_{n=1}^{\infty} (-i)^n \int_{0 < \tau_n < \dots < \tau_1 < t} d\tau_1 \cdots d\tau_n \prod_{j=1}^n [w(\tau_j) \hat{M}_I(\tau_j)].$$

Because w is a causal linear functional of the command u through the kernel K , substituting $w = K * u$ into the Dyson series expresses $\hat{U}_I(t)$ as a multilinear functional expansion in the input waveform $u(\cdot)$. This is structurally analogous to classical Volterra (Boyd–Chua) series expansions for nonlinear dynamical systems with memory, where the output is represented as a sum of multilinear functionals of the input with causal integration domains. The present setting differs only in that the kernels are operator-valued and the ordering is quantum (time ordering).

1. Interaction picture and Dyson–Volterra expansion

Let $\hat{U}(t) \equiv \hat{U}(t, 0)$ solve $\dot{\hat{U}}(t) = -i\hat{H}(t)\hat{U}(t)$ (we set $\hbar = 1$). Write $\hat{U}(t) = e^{-i\hat{H}_A t} V(t)$. Then $V(0) = \mathbb{1}$ and

$$\dot{V}(t) = -i w(t) \hat{M}_I(t) V(t), \quad \hat{M}_I(t) := e^{i\hat{H}_A t} \hat{M} e^{-i\hat{H}_A t}. \quad (\text{A2})$$

The formal solution is

$$\hat{V}(t) = \mathcal{T} \exp \left(-i \int_0^t w(\tau) \hat{M}_I(\tau) d\tau \right), \quad (\text{A3})$$

and expanding the time-ordered exponential gives a Dyson series in the *filtered* signal w :

$$\hat{V}(t) = \mathbb{1} + \sum_{n=1}^{\infty} (-i)^n \int_{0 < \tau_n < \dots < \tau_1 < t} d\tau_1 \cdots d\tau_n \prod_{j=1}^n [w(\tau_j) \hat{M}_I(\tau_j)]. \quad (\text{A4})$$

To obtain a Boyd–Chua / Volterra-type functional expansion directly in the *command* $u(\cdot)$, substitute $w(\tau_j) = \int_{-\infty}^{\tau_j} K(\tau_j - s_j) u(s_j) ds_j$ into (A4). One obtains a multilinear functional series

$$\hat{V}(t) = \mathbb{1} + \sum_{n=1}^{\infty} (-i)^n \int_{(-\infty, t]^n} ds_1 \cdots ds_n \left(\prod_{j=1}^n u(s_j) \right) \hat{G}_n(t; s_1, \dots, s_n), \quad (\text{A5})$$

where the *operator-valued Volterra kernels* \hat{G}_n are

$$\hat{G}_n(t; s_1, \dots, s_n) := \int_{0 < \tau_n < \dots < \tau_1 < t} d\tau_1 \cdots d\tau_n \left(\prod_{j=1}^n K(\tau_j - s_j) \right) \hat{M}_I(\tau_1) \cdots \hat{M}_I(\tau_n). \quad (\text{A6})$$

The propagator is then

$$\hat{U}(t) = e^{-i\hat{H}_A t} \hat{V}(t), \quad (\text{A7})$$

with $\hat{V}(t)$ given by (A5).

The kernels admit a simple recursion that mirrors classical Volterra theory:

$$\hat{G}_{n+1}(t; s_1, \dots, s_{n+1}) = \int_{\max(0, s_1)}^t d\tau K(\tau - s_1) \hat{M}_I(\tau) \hat{G}_n(\tau; s_2, \dots, s_{n+1}), \quad (\text{A8})$$

with base case

$$\hat{G}_1(t; s) = \int_{\max(0, s)}^t d\tau K(\tau - s) \hat{M}_I(\tau). \quad (\text{A9})$$

For strictly causal kernels supported on $\tau \geq 0$, the integrands vanish unless $s \leq \tau$, making the causal structure explicit.

If $[\hat{H}_A, \hat{M}] = 0$, then $\hat{M}_I(t) = \hat{M}$ and the time ordering in (A3) becomes irrelevant. In this special case,

$$\hat{U}(t) = e^{-i\hat{H}_A t} \exp\left(-i\hat{M} \int_0^t w(\tau) d\tau\right), \quad (\text{A10})$$

with $w(\tau)$ given by (A1). The noncommuting case is the generic situation, and is captured by the operator-valued kernels \hat{G}_n above.

Appendix B: Time-local ODE embedding for scalar kernel-filtered Hamiltonians

In this appendix we show that when the filtered Hamiltonian enters through a scalar amplitude multiplying a fixed operator, and the kernel is a finite sum of decaying exponentials, the kernel-filtered evolution is equivalent to a time-local system consisting of the Schrödinger equation coupled to a finite set of first-order ODEs for auxiliary filter variables.

Assume a drift-plus-control Hamiltonian of the form

$$\hat{H}(t) = \hat{H}_A + \Phi(t) \hat{M},$$

with \hat{H}_A time independent and \hat{M} Hermitian. The realized control field $\Phi(t)$ is obtained from a commanded waveform $u(t)$ by a causal kernel,

$$\Phi(t) = \int_{-\infty}^t K(t-s) u(s) ds, \quad K(\tau) = 0 \text{ for } \tau < 0.$$

We take $u(t)$ real-valued. If $K(\tau)$ is real-valued, then $\Phi(t)$ is real and $\hat{H}(t)$ is Hermitian.

Suppose the kernel admits a finite exponential representation

$$K(\tau) = \sum_{k=1}^{K_{\max}} c_k e^{-\nu_k \tau} \Theta(\tau), \quad \nu_k > 0, \quad c_k \in \mathbb{R}.$$

Define auxiliary mode variables by

$$\Phi_k(t) := \int_{-\infty}^t c_k e^{-\nu_k(t-s)} u(s) ds, \quad \Phi(t) = \sum_{k=1}^{K_{\max}} \Phi_k(t).$$

Causality is explicit: only values $s \leq t$ contribute.

Differentiate $\Phi_k(t)$ under the integral sign. Write the integrand as $c_k e^{-\nu_k(t-s)} u(s)$ and note that

$$\frac{\partial}{\partial t} e^{-\nu_k(t-s)} = -\nu_k e^{-\nu_k(t-s)}.$$

Using Leibniz' rule for differentiation of an integral with variable upper limit gives

$$\dot{\Phi}_k(t) = c_k e^{-\nu_k(t-t)} u(t) + \int_{-\infty}^t c_k \frac{\partial}{\partial t} \left(e^{-\nu_k(t-s)} \right) u(s) ds.$$

The boundary term is $c_k u(t)$. The remaining term evaluates to

$$\int_{-\infty}^t c_k \left(-\nu_k e^{-\nu_k(t-s)} \right) u(s) ds = -\nu_k \int_{-\infty}^t c_k e^{-\nu_k(t-s)} u(s) ds = -\nu_k \Phi_k(t).$$

Hence each mode satisfies the first-order ODE

$$\dot{\Phi}_k(t) = -\nu_k \Phi_k(t) + c_k u(t).$$

The corresponding initial condition depends on how the protocol is started. If one assumes $u(t) = 0$ for $t < 0$ and begins the evolution at $t = 0$, then

$$\Phi_k(0) = \int_{-\infty}^0 c_k e^{-\nu_k(0-s)} u(s) ds = 0.$$

More generally, prehistory in $u(s)$ for $s < 0$ produces a nonzero $\Phi_k(0)$, which is the correct way to encode nontrivial initial filter memory.

The quantum state obeys the Schrödinger equation

$$i \frac{d}{dt} |\psi(t)\rangle = \left(\hat{H}_A + \Phi(t) \hat{M} \right) |\psi(t)\rangle = \left(\hat{H}_A + \left[\sum_{k=1}^{K_{\max}} \Phi_k(t) \right] \hat{M} \right) |\psi(t)\rangle.$$

Together with the mode equations, the kernel-filtered dynamics is therefore equivalent to the time-local system

$$\begin{cases} i \frac{d}{dt} |\psi(t)\rangle = \left(\hat{H}_A + \left[\sum_{k=1}^{K_{\max}} \Phi_k(t) \right] \hat{M} \right) |\psi(t)\rangle, \\ \dot{\Phi}_k(t) = -\nu_k \Phi_k(t) + c_k u(t), \quad k = 1, \dots, K_{\max}. \end{cases}$$

This embedding replaces the convolutional memory in the Hamiltonian by a finite-dimensional classical state $(\Phi_1, \dots, \Phi_{K_{\max}})$. The resulting evolution remains unitary because the instantaneous Hamiltonian acting on the quantum state is Hermitian for real $\Phi(t)$.

Let us now introduce the special case of a RC kernel. For $K_{\max} = 1$ one has $K(\tau) = ce^{-\nu\tau}\Theta(\tau)$ and $\Phi(t) = \Phi_1(t)$, so the filter reduces to the familiar relaxation equation

$$\dot{\Phi}(t) = -\nu \Phi(t) + c u(t),$$

coupled to the Schrödinger equation with $\hat{H}(t) = \hat{H}_A + \Phi(t) \hat{M}$.

Many kernels that arise in practice are not exactly finite sums of exponentials but can be accurately approximated by such sums on a relevant time window, either from physics (e.g. a Matsubara-like decompositions) or from system-identification procedures. In that case, the above embedding provides a controlled time-local approximation to the kernel-filtered dynamics, with the approximation quality inherited from the kernel fit.

Appendix C: Expression for $f'(0)$ in adiabatic case

Starting from

$$f(\Phi) = \sum_i \frac{p_i}{\text{Tr } \Pi_i(\Phi)} \text{Tr}(\Pi_i(\Phi) \hat{O}), \quad H(\Phi) = \hat{H}_A + \Phi \hat{M}, \quad (\text{C1})$$

and assuming an iso-degenerate spectral path (so $\text{Tr } \Pi_i(\Phi)$ is constant) and that \hat{O} has no explicit Φ -dependence, one has

$$f'(0) = \sum_i \frac{p_i}{d_i} \text{Tr}(\Pi'_i(0) \hat{O}), \quad d_i := \text{Tr } \Pi_i(0), \quad (\text{C2})$$

where $\Pi'_i(\Phi) = \partial_\Phi \Pi_i(\Phi)$.

Assume the i -th spectral band of $H(0)$ is separated by a nonzero gap from the rest of the spectrum. Let

$$Q_i(0) := \mathbb{1} - \Pi_i(0), \quad R_i(0) := Q_i(0) (H(0) - \varepsilon_i(0))^{-1} Q_i(0), \quad (\text{C3})$$

(the inverse is taken on the range of $Q_i(0)$). A standard Kato/analytic-perturbation identity gives

$$\Pi'_i(0) = R_i(0) \hat{M} \Pi_i(0) + \Pi_i(0) \hat{M} R_i(0). \quad (\text{C4})$$

Substituting into (C2) yields the explicit resolvent form

$$f'(0) = \sum_i \frac{p_i}{d_i} \text{Tr} \left([R_i(0) \hat{M} \Pi_i(0) + \Pi_i(0) \hat{M} R_i(0)] \hat{O} \right). \quad (\text{C5})$$

Using cyclicity of the trace and Hermiticity ($R_i(0) = R_i(0)^\dagger$, $\hat{M} = \hat{M}^\dagger$, $\hat{O} = \hat{O}^\dagger$), this can be written as a manifestly real expression,

$$f'(0) = 2 \sum_i \frac{p_i}{d_i} \text{Re} \text{Tr} \left(\Pi_i(0) \hat{O} R_i(0) \hat{M} \Pi_i(0) \right). \quad (\text{C6})$$

where Re implies the real part.

If $H(0)$ has a spectral decomposition into band projectors

$$H(0) = \sum_j \varepsilon_j(0) \Pi_j(0), \quad (\text{C7})$$

then on the complement of band i the reduced resolvent admits the expansion

$$R_i(0) = \sum_{j \neq i} \frac{1}{\varepsilon_j(0) - \varepsilon_i(0)} \Pi_j(0), \quad (\text{C8})$$

which, inserted into (C4), gives the familiar first-order perturbation-theory formula for the derivative of the spectral projector:

$$\Pi'_i(0) = \sum_{j \neq i} \frac{\Pi_j(0) \hat{M} \Pi_i(0) + \Pi_i(0) \hat{M} \Pi_j(0)}{\varepsilon_i(0) - \varepsilon_j(0)}. \quad (\text{C9})$$

Substituting (C9) into (C2) yields

$$f'(0) = \sum_i \frac{p_i}{d_i} \sum_{j \neq i} \frac{\text{Tr} \left([\Pi_j(0) \hat{M} \Pi_i(0) + \Pi_i(0) \hat{M} \Pi_j(0)] \hat{O} \right)}{\varepsilon_i(0) - \varepsilon_j(0)}. \quad (\text{C10})$$

A slightly cleaner (and again manifestly real) form is obtained by cyclicity of the trace:

$$f'(0) = 2 \sum_i \frac{p_i}{d_i} \sum_{j \neq i} \frac{\text{Re} \text{Tr} \left(\Pi_i(0) \hat{O} \Pi_j(0) \hat{M} \Pi_i(0) \right)}{\varepsilon_i(0) - \varepsilon_j(0)}. \quad (\text{C11})$$

If the spectrum is nondegenerate, $\Pi_i(0) = |i\rangle\langle i|$ and $d_i = 1$, then (C11) reduces to the standard first-order eigenstate perturbation formula:

$$f'(0) = 2 \sum_i p_i \sum_{j \neq i} \frac{\text{Re} \left(\langle i | \hat{O} | j \rangle \langle j | \hat{M} | i \rangle \right)}{\varepsilon_i(0) - \varepsilon_j(0)}. \quad (\text{C12})$$

Equations (C4)–(C12) require a nonzero gap separating the chosen band(s) at $\Phi = 0$. At degeneracy crossings, $f'(0)$ need not be well-defined without specifying how the band(s) are tracked through the crossing (and adiabaticity itself becomes subtle).

Appendix D: Loop integrals, uniqueness, and bounds

1. Setup and definitions

Let $u \in [0, T]$ be a cycle parameter (e.g. time or sweep parameter). Assume

$$\Phi : [0, T] \rightarrow \mathbb{R}, \quad O : [0, T] \rightarrow \mathbb{R}. \quad (\text{D1})$$

We consider the (oriented) loop integral

$$A_{uO} := \oint O d\Phi, \quad (\text{D2})$$

interpreted as a Riemann–Stieltjes integral along the closed cycle. Throughout, we assume the cycle is closed in Φ :

$$\Phi(0) = \Phi(T). \quad (\text{D3})$$

A sufficient condition for reducing (D2) to an ordinary integral is absolute continuity of Φ .

Lemma 1 (Parameterization formula). *If Φ is absolutely continuous on $[0, T]$, then $\Phi'(u)$ exists for almost every u and is integrable, and*

$$A_{uO} = \oint O d\Phi = \int_0^T O(u) \Phi'(u) du. \quad (\text{D4})$$

Proof. For absolutely continuous Φ , the differential $d\Phi$ is represented by $\Phi'(u) du$ thus, the integral reduces to the integral:

$$\int_0^T O d\Phi = \int_0^T O(u) \Phi'(u) du. \quad (\text{D5})$$

For a closed cycle, the loop integral $\oint O d\Phi$ is understood as the integral over one period, i.e. the same expression on $[0, T]$. \square

We also define the *total variation* (total sweep) of Φ with respect to u :

$$V_{u\Phi} := \int_0^T |\Phi'(u)| du, \quad (\text{D6})$$

well-defined whenever Φ is absolutely continuous.

Proposition 1 (Single-valued $O = f(\Phi) \Rightarrow$ zero loop integral). *Assume Φ is absolutely continuous, (D3) holds, and there exists a single-valued function $f : \mathbb{R} \rightarrow \mathbb{R}$ such that*

$$O(u) = f(\Phi(u)) \quad \text{for all } u \in [0, T]. \quad (\text{D7})$$

If f is continuous (or merely integrable) so that an antiderivative F exists with $F'(\Phi) = f(\Phi)$ almost everywhere, then

$$A_{uO} = \oint f(\Phi) d\Phi = 0. \quad (\text{D8})$$

Proof. Let F be an antiderivative of f , i.e. $F'(\Phi) = f(\Phi)$ (a.e.). Along the trajectory,

$$dF = F'(\Phi) d\Phi = f(\Phi) d\Phi. \quad (\text{D9})$$

Therefore,

$$\oint f(\Phi) d\Phi = \oint dF = F(\Phi(T)) - F(\Phi(0)). \quad (\text{D10})$$

Using $\Phi(T) = \Phi(0)$ from (D3) yields $F(\Phi(T)) - F(\Phi(0)) = 0$, hence $A_{uO} = 0$. \square

Remark 1. Proposition 1 formalizes the standard statement: a nonzero loop area $\oint O d\Phi$ requires that O is *not* a single-valued function of Φ along the cycle (i.e. there is hysteresis / multibranch behavior).

Theorem 1 (Variation bound). *Assume Φ is absolutely continuous, (D3) holds, and O is bounded:*

$$O_{\min} \leq O(u) \leq O_{\max} \quad \text{for all } u \in [0, T]. \quad (\text{D11})$$

Define $\Delta O := O_{\max} - O_{\min}$ and $V_{u\Phi}$ as in (D6). Then

$$|A_{uO}| \leq \frac{\Delta O}{2} V_{u\Phi} = \frac{\Delta O}{2} \int_0^T |\Phi'(u)| du. \quad (\text{D12})$$

Equivalently,

$$-\frac{\Delta O}{2} V_{u\Phi} \leq A_{uO} \leq \frac{\Delta O}{2} V_{u\Phi}. \quad (\text{D13})$$

Proof. We set the midrange constant $O_c := \frac{1}{2}(O_{\max} + O_{\min})$ and define $\tilde{O}(u) := O(u) - O_c$. Then $|\tilde{O}(u)| \leq \Delta O/2$ for all u .

Using Lemma 1,

$$A_{uO} = \int_0^T O(u) \Phi'(u) du = \int_0^T (O_c + \tilde{O}(u)) \Phi'(u) du. \quad (\text{D14})$$

The constant part vanishes because

$$\int_0^T O_c \Phi'(u) du = O_c (\Phi(T) - \Phi(0)) = 0 \quad (\text{D15})$$

by (D3). Thus

$$A_{uO} = \int_0^T \tilde{O}(u) \Phi'(u) du. \quad (\text{D16})$$

Taking absolute values and applying the triangle inequality,

$$|A_{uO}| \leq \int_0^T |\tilde{O}(u)| |\Phi'(u)| du \leq \frac{\Delta O}{2} \int_0^T |\Phi'(u)| du = \frac{\Delta O}{2} V_{u\Phi}. \quad (\text{D17})$$

This proves (D12). The two-sided bound follows immediately. \square

Corollary 1 (Sup-norm and Cauchy–Schwarz bounds). *Under the assumptions of Lemma 1,*

$$|A_{uO}| \leq \|O\|_{\infty} \int_0^T |\Phi'(u)| du, \quad (\text{D18})$$

and, if additionally $O \in L^2(0, T)$ and $\Phi' \in L^2(0, T)$,

$$|A_{uO}| \leq \|O\|_2 \|\Phi'\|_2. \quad (\text{D19})$$

Proof. From (D4),

$$|A_{uO}| = \left| \int_0^T O \Phi' du \right| \leq \int_0^T |O| |\Phi'| du \leq \|O\|_{\infty} \int_0^T |\Phi'| du, \quad (\text{D20})$$

proving the sup-norm bound. The L^2 bound is Cauchy–Schwarz:

$$\left| \int_0^T O \Phi' du \right| \leq \left(\int_0^T |O|^2 du \right)^{1/2} \left(\int_0^T |\Phi'|^2 du \right)^{1/2}. \quad (\text{D21})$$

\square

The loop-area becomes particularly transparent when the cycle consists of an “up-sweep” in Φ followed by a “down-sweep”.

Lemma 2 (Two-branch formula for a single turning point). *Assume Φ is absolutely continuous and there exists $u_* \in (0, T)$ such that:*

$$\Phi \text{ is strictly increasing on } [0, u_*], \quad \Phi \text{ is strictly decreasing on } [u_*, T], \quad (\text{D22})$$

and $\Phi(0) = \Phi(T) = \Phi_{\min}$, $\Phi(u_*) = \Phi_{\max}$. Define the two branches as single-valued functions of Φ on $[\Phi_{\min}, \Phi_{\max}]$ by

$$O_{\uparrow}(\varphi) := O(u_{\uparrow}(\varphi)), \quad O_{\downarrow}(\varphi) := O(u_{\downarrow}(\varphi)), \quad (\text{D23})$$

where u_{\uparrow} is the inverse of $\Phi|_{[0, u_*]}$ and u_{\downarrow} is the inverse of $\Phi|_{[u_*, T]}$. Then

$$A_{uO} = \oint O d\Phi = \int_{\Phi_{\min}}^{\Phi_{\max}} (O_{\uparrow}(\varphi) - O_{\downarrow}(\varphi)) d\varphi. \quad (\text{D24})$$

Proof. Split the loop integral into two parts and use Lemma 1:

$$A_{uO} = \int_0^{u_*} O(u) \Phi'(u) du + \int_{u_*}^T O(u) \Phi'(u) du. \quad (\text{D25})$$

On $[0, u_*]$, Φ is strictly increasing, so the change of variables $\varphi = \Phi(u)$ is valid and $d\varphi = \Phi'(u) du$:

$$\int_0^{u_*} O(u) \Phi'(u) du = \int_{\Phi_{\min}}^{\Phi_{\max}} O(u_{\uparrow}(\varphi)) d\varphi = \int_{\Phi_{\min}}^{\Phi_{\max}} O_{\uparrow}(\varphi) d\varphi. \quad (\text{D26})$$

On $[u_*, T]$, Φ is strictly decreasing, so the same substitution yields reversed limits:

$$\int_{u_*}^T O(u) \Phi'(u) du = \int_{\Phi_{\max}}^{\Phi_{\min}} O(u_{\downarrow}(\varphi)) d\varphi = - \int_{\Phi_{\min}}^{\Phi_{\max}} O_{\downarrow}(\varphi) d\varphi. \quad (\text{D27})$$

Adding both expressions gives (D24). \square

Proposition 2 (Lower bound from uniform branch separation). *Under the assumptions of Lemma 2, suppose there exists $\delta > 0$ such that*

$$O_{\uparrow}(\varphi) - O_{\downarrow}(\varphi) \geq \delta \quad \text{for all } \varphi \in [\Phi_{\min}, \Phi_{\max}]. \quad (\text{D28})$$

Then

$$A_{uO} \geq \delta (\Phi_{\max} - \Phi_{\min}). \quad (\text{D29})$$

If instead $O_{\downarrow}(\varphi) - O_{\uparrow}(\varphi) \geq \delta$, then $A_{uO} \leq -\delta (\Phi_{\max} - \Phi_{\min})$.

Proof. From (D24),

$$A_{uO} = \int_{\Phi_{\min}}^{\Phi_{\max}} (O_{\uparrow}(\varphi) - O_{\downarrow}(\varphi)) d\varphi \geq \int_{\Phi_{\min}}^{\Phi_{\max}} \delta d\varphi = \delta (\Phi_{\max} - \Phi_{\min}), \quad (\text{D30})$$

which proves (D29). The second case is identical after swapping the branches. \square

Remark 2 (Why lower bounds need extra assumptions). Without a condition such as a sign-definite branch difference $O_{\uparrow} - O_{\downarrow}$, cancellations may occur and one cannot guarantee any strictly positive lower bound on $|A_{uO}|$ from bounds on $|O|$ and $|\Phi'|$ alone; the universal lower bound is then 0.

Appendix E: Nonadiabatic cyclic integrals for filtered control: identities and bounds

This appendix provides the derivations underlying the bounds for I in the main text. The only assumption is unitary evolution generated by the time-dependent Hamiltonian.

Let \hat{O} be time independent and define

$$I = \oint dt \operatorname{Tr}(\rho(t)\hat{O}) \dot{u}(t) \quad (\text{E1})$$

over one cycle of duration T in steady periodic response, $u(T) = u(0)$ and $\rho(T) = \rho(0)$. Integration by parts gives

$$I = \left[u(t) \operatorname{Tr}(\rho(t)\hat{O}) \right]_0^T - \int_0^T dt u(t) \frac{d}{dt} \operatorname{Tr}(\rho(t)\hat{O}) = - \oint dt u(t) \operatorname{Tr}(\dot{\rho}(t)\hat{O}). \quad (\text{E2})$$

Under unitary dynamics,

$$\dot{\rho}(t) = -i[\hat{H}(t), \rho(t)],$$

and by cyclicity of the trace,

$$\operatorname{Tr}(\dot{\rho}(t)\hat{O}) = -i \operatorname{Tr}(\rho(t)[\hat{O}, \hat{H}(t)]) = -i \langle [\hat{O}, \hat{H}(t)] \rangle_t. \quad (\text{E3})$$

Substituting yields

$$I = i \oint dt u(t) \langle [\hat{O}, \hat{H}(t)] \rangle_t. \quad (\text{E4})$$

Let us now assume the scalar filtered-control model

$$\hat{H}(t) = \hat{H}_A + \Phi(t)\hat{M}, \quad \Phi(t) = \int_0^t K(t-s) u(s) ds, \quad (\text{E5})$$

with real causal kernel K . Define the commutator weights

$$a(t) = \langle [\hat{O}, \hat{H}_A] \rangle_t, \quad b(t) = \langle [\hat{O}, \hat{M}] \rangle_t. \quad (\text{E6})$$

Then

$$\langle [\hat{O}, \hat{H}(t)] \rangle_t = a(t) + \Phi(t)b(t),$$

and the cyclic functional splits exactly as

$$I = i \oint_0^T dt u(t) a(t) + i \oint_0^T dt u(t) \Phi(t) b(t). \quad (\text{E7})$$

The first term depends on correlations between the drive and $a(t)$ and is present even when $K(t)$ approaches a delta function. The second term is the contribution in which the control history enters explicitly through the convolution; it is the term that reduces to the quadratic functional studied in the main text, when $b(t)$ may be treated as constant.

To be concrete, we write the memory contribution as

$$I_{\text{mem}} = i \int_0^T dt b(t) u(t) \Phi(t) = i \int_0^T dt b(t) u(t) \int_0^t ds K(t-s) u(s). \quad (\text{E8})$$

Introducing

$$v(t) = b(t)u(t)$$

gives the triangular bilinear form

$$I_{\text{mem}} = i \int_0^T dt \int_0^t ds v(t) K(t-s) u(s), \quad (\text{E9})$$

which makes the temporal nonlocality explicit: values of the drive at earlier times $s < t$ contribute to the response at time t with weight $K(t - s)$. When $b(t)$ is constant, $v(t) \propto u(t)$ and the expression becomes a genuine quadratic functional of the command waveform.

We now bound the norm of the memory content. The bias term obeys Cauchy–Schwarz:

$$|I_{\text{bias}}| = \left| \int_0^T dt u(t) a(t) \right| \leq \|u\|_{L^2(0,T)} \|a\|_{L^2(0,T)}. \quad (\text{E10})$$

For the memory term, first bound

$$|b(t)| \leq \|b\|_\infty$$

to obtain

$$|I_{\text{mem}}| \leq \|b\|_\infty \int_0^T dt |u(t)\Phi(t)| \leq \|b\|_\infty \|u\|_{L^2(0,T)} \|\Phi\|_{L^2(0,T)}. \quad (\text{E11})$$

Since $\Phi = K_c * u$ with $K_c(\tau) = K(\tau)\Theta(\tau) \in L^1(\mathbb{R}_+)$, Young's inequality yields

$$\|\Phi\|_{L^2(0,T)} \leq \|K_c\|_{L^1(\mathbb{R}_+)} \|u\|_{L^2(0,T)}. \quad (\text{E12})$$

Combining these two gives

$$|I_{\text{mem}}| \leq \|b\|_\infty \|K_c\|_{L^1(\mathbb{R}_+)} \|u\|_{L^2(0,T)}^2, \quad (\text{E13})$$

and therefore

$$|I| \leq \|u\|_{L^2(0,T)} \|a\|_{L^2(0,T)} + \|b\|_\infty \|K_c\|_{L^1(\mathbb{R}_+)} \|u\|_{L^2(0,T)}^2, \quad (\text{E14})$$

which is the inequality we report in the paper.

In the instantaneous-control limit $K(\tau) \rightarrow \delta(\tau)$, $\Phi(t) \rightarrow u(t)$ and the memory contribution becomes local,

$$I_{\text{mem}} \rightarrow i \int_0^T dt b(t) u(t)^2. \quad (\text{E15})$$

Departures from this local reduction quantify the role of the control-channel memory kernel.

For completeness, we provide exact formulae in the case of sinusoidal control and an exponential kernel function; consider the kernel

$$K(\tau) = \frac{1}{\tau_c} e^{-\tau/\tau_c} \Theta(\tau), \quad (\text{E16})$$

so that Φ satisfies $\tau_c \dot{\Phi} + \Phi = u$. For $u(t) = A \cos(\omega t)$, the solution with $\Phi(0) = 0$ is

$$\Phi(t) = \frac{A}{1 + (\omega\tau_c)^2} \left[\cos(\omega t) + \omega\tau_c \sin(\omega t) - e^{-t/\tau_c} \right]. \quad (\text{E17})$$

The quadratic functional $J(T) = \int_0^T u(t)\Phi(t) dt$ and its special cases (integer numbers of periods and long-time limit) follow by direct integration, recovering the expressions stated in the main text when $b(t)$ is treated as constant and the bias term is suppressed by symmetry or design.

Appendix F: Classical control channel: RC synthesis, pole structure, and exponential-mode kernels

This appendix motivates the use of RC ladder models for the control channel and connects the associated transfer function to the exponential-mode representation used in the main text. The essential point is that the class of transfer functions produced by passive RC networks has a highly constrained analytic structure (stability, real coefficients, and pole/zero restrictions). That same structure implies that the corresponding impulse response is a nonnegative mixture of decaying exponentials (discrete for finite ladders, continuous in the distributed limit). This is precisely the statement that the realized field $\Phi(t) = (K * u)(t)$ can be represented (exactly or to controlled accuracy) by a finite set of auxiliary modes obeying first-order ODEs.

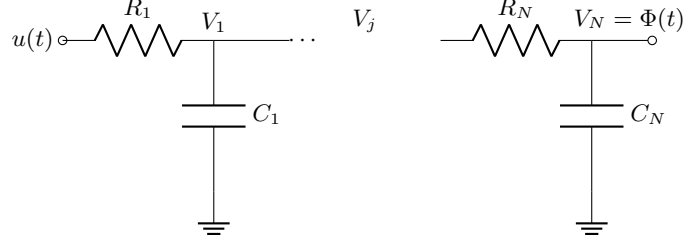


FIG. 5. Discrete RC ladder (lossy line) model of the control channel. The commanded input voltage $u(t)$ drives a chain of series resistors with shunt capacitors to ground. The delivered device-node voltage is $\Phi(t) = V_N(t)$.

We model the control line and bias circuitry as a passive linear time-invariant two-port that maps an input voltage waveform $u(t)$ to the voltage $\Phi(t)$ at the device node. In the Laplace domain (with s in the right half-plane), this defines a transfer function

$$G(s) := \frac{\Phi(s)}{u(s)}.$$

Passivity and causality imply that the network is stable (no poles in $\text{Re}(s) > 0$) and that $G(s)$ is analytic there with real coefficients. For RC networks (resistors and capacitors only), the pole structure is even more restricted: the transfer function of a passive RC two-port is a real rational function whose poles lie on the negative real axis (and, in the generic case, are simple). A detailed characterization of the transfer functions of general RC ladder topologies is classical; for the ladder class relevant here, these restrictions are derived and discussed in [27].

For synthesis, one often specifies a desired voltage-ratio function $G(s)$ and asks when it is realizable by an RC ladder. A standard criterion is that voltage-ratio functions with negative poles and nonpositive zeros fall into the RC ladder realizability class; one constructive route proceeds by selecting an appropriate driving-point function (an impedance or admittance) whose numerator and denominator are matched to the prescribed transfer denominator and then performing a ladder extraction step-by-step [25]. In other words, the analytic restrictions are not merely consequences of RC ladders; they are also the design constraints that ensure a ladder realization exists.

In the present work we use these results in the forward direction: if the control channel is well described by a passive RC network (a common and physically motivated assumption for wiring, filters, bias tees, and distributed lossy lines at the relevant frequencies), then $G(s)$ belongs to the above class, and therefore its time-domain impulse response necessarily has an exponential-mode representation.

Assume first that $G(s)$ is rational and strictly proper or proper. Under the RC restrictions, all poles lie on the negative real axis. For a finite ladder, there are finitely many poles, and one may write a partial-fraction expansion of the form

$$G(s) = g_\infty + \sum_{k=1}^K \frac{c_k}{s + \nu_k}, \quad \nu_k > 0,$$

where g_∞ accounts for any instantaneous feedthrough (if present). The corresponding causal impulse response is

$$K(t) = g_\infty \delta(t) + \sum_{k=1}^K c_k e^{-\nu_k t} \Theta(t).$$

Consequently,

$$\Phi(t) = (K * u)(t) = g_\infty u(t) + \sum_{k=1}^K c_k \int_{-\infty}^t e^{-\nu_k(t-s)} u(s) ds.$$

Introducing auxiliary coordinates

$$\Phi_k(t) := \int_{-\infty}^t c_k e^{-\nu_k(t-s)} u(s) ds, \quad \Phi(t) = g_\infty u(t) + \sum_{k=1}^K \Phi_k(t),$$

one obtains the time-local realization

$$\dot{\Phi}_k(t) = -\nu_k \Phi_k(t) + c_k u(t), \quad k = 1, \dots, K.$$

This is the ODE embedding used in the main text. For a finite RC ladder, it is not an approximation: it is simply the state-space realization implied by the pole expansion of $G(s)$.

The memoryless (instantaneous) limit corresponds to $K(t) \propto \delta(t)$, i.e. $G(s) \rightarrow \text{const}$ (up to a static gain convention). In the exponential-mode picture, a convenient sufficient condition for this limit is: (i) the total weight satisfies $g_\infty + \sum_k c_k = 1$, and (ii) all time scales collapse, in the sense that $\max_k \nu_k^{-1} \rightarrow 0$. Then K concentrates at $t = 0$ and $\Phi(t)$ approaches $u(t)$ uniformly on protocols that do not vary on vanishing time scales.

Conversely, the longest memory time is controlled by the slowest mode

$$\tau_{\text{mem}} \sim \nu_{\min}^{-1}, \quad \nu_{\min} := \min_k \nu_k.$$

Retaining only this slowest pole is precisely the single-RC approximation: it keeps the dominant long-time relaxation channel and discards faster components of the line response.

To make the preceding discussion concrete, we now write explicitly the dynamics of a discrete RC ladder (a lumped-element model of a lossy line). Consider the N -stage network sketched in Fig. 5: the commanded input voltage $u(t)$ drives a chain of series resistors, and each intermediate node is shunted to ground by a capacitor. Let $V_j(t)$ denote the voltage at node j for $j = 1, \dots, N$, with the boundary condition $V_0(t) = u(t)$, and identify the delivered device-node voltage as

$$\Phi(t) = V_N(t).$$

For clarity we allow the component values to vary by stage (R_j, C_j), and recover the uniform case by setting $R_j \equiv R$, $C_j \equiv C$.

Kirchhoff's current law at node j equates the capacitor current to the net resistive current flowing into that node. For the first node one obtains

$$C_1 \dot{V}_1(t) = \frac{V_0(t) - V_1(t)}{R_1} - \frac{V_1(t) - V_2(t)}{R_2},$$

for interior nodes $j = 2, \dots, N-1$ one has

$$\begin{aligned} C_j \dot{V}_j(t) &= i_j - i_{j+1} \\ &= \frac{V_{j-1}(t) - V_j(t)}{R_j} - \frac{V_j(t) - V_{j+1}(t)}{R_{j+1}}, \end{aligned} \tag{F1}$$

and for the terminal node (open end beyond node N) one finds

$$C_N \dot{V}_N(t) = \frac{V_{N-1}(t) - V_N(t)}{R_N}.$$

In this model, thus, at equilibrium the currents $i_j = i_{j+1}$ and the shunted capacitances do not leak currents into the ground. In the uniform ladder case ($R_j \equiv R, C_j \equiv C$) these equations reduce to the familiar discrete-diffusion form

$$C \dot{V}_j(t) = \frac{1}{R} (V_{j-1}(t) - 2V_j(t) + V_{j+1}(t)), \quad j = 1, \dots, N-1,$$

together with the terminal condition

$$C \dot{V}_N(t) = \frac{1}{R} (V_{N-1}(t) - V_N(t)).$$

Writing $\vec{V}(t) = (V_1(t), \dots, V_N(t))^\top$, the ladder is a finite-dimensional linear time-invariant system

$$\dot{\vec{V}}(t) = A \vec{V}(t) + \vec{b} u(t), \quad \Phi(t) = \vec{e}_N^\top \vec{V}(t),$$

where \vec{e}_N is the N th standard basis vector, $\vec{b} = (1/(R_1 C_1), 0, \dots, 0)^\top$, and A is tridiagonal with entries determined by $\{R_j, C_j\}$ (explicitly: $A_{11} = -(1/(R_1 C_1) + 1/(R_2 C_1))$, $A_{12} = 1/(R_2 C_1)$; for $2 \leq j \leq N-1$, $A_{j,j-1} = 1/(R_j C_j)$, $A_{j,j} = -(1/(R_j C_j) + 1/(R_{j+1} C_j))$, $A_{j,j+1} = 1/(R_{j+1} C_j)$; and $A_{N,N-1} = 1/(R_N C_N)$, $A_{N,N} = -1/(R_N C_N)$).

At this point, it is obvious to see that for any locally integrable input u and any initial condition $V(0)$, the unique solution is given by variation of constants [78],

$$V(t) = e^{At} V(0) + \int_0^t e^{A(t-s)} b u(s) ds,$$

and therefore the readout node satisfies

$$\Phi(t) = \vec{e}_N^T e^{At} \vec{V}(0) + \int_0^t K_N(t-s) u(s) ds, \quad K_N(t) := \vec{e}_N^T e^{At} \vec{b}.$$

Thus the input–output map $u \mapsto \Phi$ is a causal convolution with kernel K_N , up to an exponentially decaying transient term determined by $\vec{V}(0)$. In particular, if one initializes the ladder in its steady state for $u \equiv 0$ (i.e. $\vec{V}(0) = 0$), then $\Phi(t) = (K_N * u)(t)$ exactly.

Taking the Laplace transform for $\text{Re}(s) > 0$ gives

$$(sI - A)V(s) = V(0) + b u(s), \quad \Phi(s) = \vec{e}_N^T \vec{V}(s),$$

hence

$$\Phi(s) = \vec{e}_N^T (sI - A)^{-1} \vec{V}(0) + G_N(s) u(s), \quad G_N(s) := \frac{\Phi(s)}{u(s)} = \vec{e}_N^T (sI - A)^{-1} \vec{b}.$$

The scalar transfer function $G_N(s)$ is a real rational function whose poles are the eigenvalues of A . Since the ladder is passive, all eigenvalues satisfy $\text{Re}(\lambda) < 0$, so G_N is stable (analytic for $\text{Re}(s) > 0$). For RC ladders, one in fact has the stronger property that the poles lie on the negative real axis (and generically are simple) [25, 27]. Equivalently, the eigenvalues of $-A$ are real and strictly positive.

Assume for simplicity that A is diagonalizable with distinct eigenvalues $\lambda_k \in \mathbb{R}$ ($k = 1, \dots, N$), with $\lambda_k < 0$. Writing $\nu_k := -\lambda_k > 0$, the transfer function admits a partial-fraction expansion

$$G_N(s) = \sum_{k=1}^N \frac{\alpha_k}{s + \nu_k},$$

where the residues α_k depend on the overlaps of the input and readout vectors with the eigenmodes of A . Inverting the Laplace transform yields the impulse response as a finite sum of decaying exponentials,

$$K_N(t) = \sum_{k=1}^N \alpha_k e^{-\nu_k t} \Theta(t),$$

so the realized field is

$$\Phi(t) = \int_0^t \left(\sum_{k=1}^N \alpha_k e^{-\nu_k(t-s)} \right) u(s) ds.$$

This is the precise sense in which a finite RC ladder produces an exponential-mode kernel: its poles $\{-\nu_k\}$ are real and negative, and each pole contributes one relaxation mode. In the language of the main text, one can define auxiliary modes

$$\Phi_k(t) := \int_0^t \alpha_k e^{-\nu_k(t-s)} u(s) ds, \quad \Phi(t) = \sum_{k=1}^N \Phi_k(t),$$

which satisfy the time-local realization

$$\dot{\Phi}_k(t) = -\nu_k \Phi_k(t) + \alpha_k u(t), \quad k = 1, \dots, N.$$

The same result follows without partial fractions by expanding the matrix exponential. If $A = Q \Lambda Q^{-1}$ with $\Lambda = \text{diag}(\lambda_1, \dots, \lambda_N)$, then

$$K_N(t) = \vec{e}_N^T Q e^{\Lambda t} Q^{-1} \vec{b} = \sum_{k=1}^N \left(\vec{e}_N^T q_k \right) \left(\vec{q}_k^T \vec{b} \right) e^{\lambda_k t} \Theta(t),$$

where q_k and \vec{q}_k are right and left eigenvectors. For symmetric ladders (e.g. uniform R, C), one can take Q orthogonal so that $\vec{q}_k = q_k$.

On the imaginary axis $s = i\omega$, the steady-state sinusoidal response is governed by $G_N(i\omega)$, whose magnitude and phase encode attenuation and lag. The negative real pole structure implies a monotone low-pass character and

guarantees that $K_N(t)$ is a linear combination of decaying exponentials. This pole/impulse-response correspondence is the direct bridge from circuit realizability to the exponential-mode kernels used to embed the control memory as a finite set of auxiliary ODEs in the main text.

The input–output transfer function is

$$G_N(s) := \frac{\Phi(s)}{u(s)} = e_N^T (sI - A)^{-1} b.$$

Hence the poles of G_N are the eigenvalues of A . For a passive RC ladder the dynamics is stable, so these poles lie in $\text{Re}(s) < 0$, and for the ladder families of interest they occur on the negative real axis; the associated realizability and synthesis constraints are classical and are treated in detail in [27] and from a constructive synthesis viewpoint in [25].

The corresponding causal impulse response kernel is

$$K_N(t) = e_N^T e^{At} b \Theta(t),$$

and diagonalizing A yields an explicit exponential-mode decomposition,

$$K_N(t) = \sum_{k=1}^N \alpha_k e^{-\nu_k t} \Theta(t), \quad \nu_k > 0,$$

where $\{-\nu_k\}$ are the eigenvalues of A and the weights α_k are fixed by the overlaps of the input vector b and the readout vector e_N with the corresponding eigenvectors. Note that $\alpha_k = (e_N^T q_k) (\tilde{q}_k^T b)$. Consequently, the delivered voltage is a causal convolution $\Phi(t) = (K_N * u)(t)$ and therefore admits the finite-dimensional time-local realization used in the main text:

$$\dot{\Phi}_k(t) = -\nu_k \Phi_k(t) + \alpha_k u(t), \quad \Phi(t) = \sum_{k=1}^N \Phi_k(t).$$

For a finite ladder this representation is exact: it is simply the modal form of the ladder state-space dynamics.

The longest memory time is governed by the slowest decay rate,

$$\tau_{\text{mem}} \sim \nu_{\min}^{-1}, \quad \nu_{\min} := \min_k \nu_k.$$

For the uniform ladder one recovers diffusive scaling of the slowest mode, $\nu_{\min} \propto (RC)^{-1} N^{-2}$ for large N , so adding ladder stages increases the longest memory time quadratically in N . In this precise sense, a long line naturally produces a hierarchy of relaxation rates rather than a single RC constant, and the single-pole (single-RC) model corresponds to retaining only the slowest relaxation channel.

Let us now discuss the diffusive regime. A long ladder with many small sections approaches a distributed RC line. In that limit, voltage propagation along the line is governed by a diffusion equation, and the transfer function from the input to a point a distance x away is no longer rational. Nevertheless, it remains passive and stable, and its impulse response is still completely monotone: it can be written as a nonnegative mixture of decaying exponentials.

Concretely, for a distributed line with resistance r and capacitance c per unit length, the voltage $V(x, t)$ satisfies

$$\partial_t V(x, t) = D \partial_x^2 V(x, t), \quad D := \frac{1}{rc}. \quad (\text{F2})$$

For boundary drive $V(0, t) = u(t)$ and a readout at position $x = L$, the input–output relation is again a causal convolution $\Phi(t) = \int_{-\infty}^t K_L(t-s)u(s) ds$. In the Laplace domain one finds

$$G_L(s) = \frac{\Phi(s)}{u(s)} = \exp(-L\sqrt{s/D}),$$

which has no right-half-plane singularities and is strictly decaying with frequency. The corresponding time-domain kernel has a long tail (slower than an exponential), reflecting the continuum of diffusive time scales in the line. Equivalently, $G_L(s)$ admits a Laplace–Stieltjes representation

$$G_L(s) = \int_0^\infty \frac{d\mu_L(\nu)}{s + \nu}, \quad d\mu_L(\nu) \geq 0,$$

and therefore

$$K_L(t) = \int_0^\infty e^{-\nu t} d\mu_L(\nu).$$

This shows that the “sum of exponentials” representation used in the main text is the discrete counterpart of a more general statement: passive RC channels produce kernels that are nonnegative mixtures of exponentials. A finite auxiliary-mode model corresponds to approximating the measure μ_L by a finite quadrature rule, i.e. replacing the continuum by finitely many effective relaxation rates $\{\nu_k\}$ with weights $\{c_k\}$.

The control-channel model in the main text assumes that the realized field is generated by a passive, stable filter with a hierarchy of relaxation rates,

$$K(t) \approx \sum_{k=1}^{K_{\max}} c_k e^{-\nu_k t} \Theta(t).$$

For a finite ladder, this is exact after lumped-element modeling; for a long distributed line, it is a controlled approximation obtained by rational (modal) approximation of the transfer function. The single-RC case corresponds to retaining only the slowest relaxation rate and is therefore the minimal model that captures a nontrivial memory time. Finally, the nomenclature “mode” is literal in the ladder picture: the rates ν_k are the decay rates of the ladder’s internal linear modes, i.e. the channels through which the line stores and releases past drive history [25, 27].

It is worth noting that the same passive RC-line model also applies to the *readout* (or more generally the wiring-mediated observation) of signals generated at a quantum device node. In the distributed (diffusive) limit, the voltage along a lossy line with resistance r and capacitance c per unit length satisfies eqn. (F2) with a boundary drive (or device-generated signal) imposed at $x = 0$ and a readout taken at $x = l$. This defines a linear, causal input–output relation between the waveform $u(t) := V(0, t)$ and the measured voltage $\Phi(t) := V(l, t)$.

Passing to the Laplace domain (with $\text{Re}(s) > 0$), the diffusion equation gives

$$V(x, s) = V(0, s) \exp\left(-x\sqrt{\frac{s}{D}}\right), \quad \Rightarrow \quad G_l(s) := \frac{\Phi(s)}{u(s)} = \exp\left(-l\sqrt{\frac{s}{D}}\right).$$

Therefore the readout is a convolution $\Phi = K_l * u$ with an impulse response $K_l(t)$ defined by the inverse Laplace transform of $G_l(s)$. Using the standard inversion formula for $\exp(-a\sqrt{s})$, one obtains the explicit kernel

$$K_l(t) = \frac{l}{2\sqrt{\pi D}} t^{-3/2} \exp\left(-\frac{l^2}{4Dt}\right) \Theta(t).$$

This kernel is strictly causal and normalized (it has unit DC gain), but it is *not* concentrated at a single time: the diffusive line does not behave as an ideal delay element. Instead, it realizes a broad distribution of effective delays, reflecting the continuum of internal relaxation time scales.

A convenient operational notion of the readout time is obtained from the step response. For a step input $u(t) = u_0 \Theta(t)$ one finds

$$\Phi(t) = u_0 \text{erfc}\left(\frac{l}{2\sqrt{Dt}}\right),$$

so the time to reach a fraction $\eta \in (0, 1)$ of the final value satisfies

$$\Phi(\tau_\eta) = \eta u_0 \iff \tau_\eta = \frac{l^2}{4D (\text{erfc}^{-1}(\eta))^2}.$$

In particular, any reasonable “readout/settling time” definition scales as

$$\tau_{\text{ro}} \sim \frac{l^2}{D} = r c l^2 = (rl)(cl) = R_{\text{tot}} C_{\text{tot}},$$

up to an $O(1)$ factor that depends on the chosen threshold (e.g. 50%, 90%, or a 10–90% rise time).

Finally, it is sometimes useful (but only as an approximation) to describe the diffusive kernel as an effective delay for band-limited waveforms. Writing the frequency response $G_l(i\omega)$, its phase implies a frequency-dependent group delay

$$\tau_g(\omega) := -\frac{d}{d\omega} \arg G_l(i\omega) = \frac{l}{2\sqrt{2D\omega}},$$

so around a narrow carrier band one may heuristically view the readout as an attenuated, delayed version of the drive together with additional smoothing. The exact time-domain description, however, remains the causal convolution with $K_l(t)$ above rather than a delta-function delay.

Appendix G: Single-pole bandwidth, time constant, and rise-time conversions

Let us briefly describe how to model the controller using the specifications from the classical controller device sitting in the laboratory - e.g. how to turn this manuscript into a practical rule. We assume for simplicity here that this is classical, i.e. finding the specifications of the RC ladder channel and the dominant contribution, in which the kernel can be written as $K(\tau) = \tau_c^{-1} e^{-\tau/\tau_c}$. Here we use the make the assumption that there is a unique RC channel. In this case, the engineering literature comes to help to estimate the time τ_c [79, 80].

In practice the control channel is often characterized *in situ* by a small-signal frequency response (e.g. a measured transfer function magnitude or a 3 dB bandwidth), whereas in our model the same channel is parameterized in the time domain by a memory scale τ_c (for instance, via an exponential kernel or an equivalent first-order ODE). When the small-signal map from the commanded waveform $u(t)$ to the realized field $\Phi(t)$ is well described by a *dominant single pole*, these characterizations are equivalent and one can translate between them without ambiguity.

A first-order low-pass response with unit DC gain has transfer function

$$H(i\omega) = \frac{1}{1 + i\omega\tau_c},$$

where $\tau_c > 0$ is the characteristic time constant. The magnitude is

$$|H(i\omega)| = \frac{1}{\sqrt{1 + (\omega\tau_c)^2}}.$$

The 3 dB cutoff is defined as the frequency where the *power* has dropped by a factor of two relative to DC. Equivalently, the magnitude has dropped to $1/\sqrt{2}$ of its DC value:

$$|H(i\omega_{3\text{dB}})| = \frac{1}{\sqrt{2}}.$$

Substituting the magnitude formula gives

$$\frac{1}{\sqrt{1 + (\omega_{3\text{dB}}\tau_c)^2}} = \frac{1}{\sqrt{2}} \implies 1 + (\omega_{3\text{dB}}\tau_c)^2 = 2 \implies \omega_{3\text{dB}}\tau_c = 1.$$

Thus

$$\omega_{3\text{dB}} = \frac{1}{\tau_c}, \quad f_{3\text{dB}} = \frac{\omega_{3\text{dB}}}{2\pi} = \frac{1}{2\pi\tau_c}, \quad \tau_c = \frac{1}{2\pi f_{3\text{dB}}}.$$

This identity is exact for the single-pole model. In more complicated lines with multiple poles (or weak resonances), one may still report an *effective* τ_c by fitting a dominant-pole approximation over the relevant bandwidth.

The same first-order system has a standard time-domain interpretation. Let the input be a unit step, and denote by $y(t)$ the normalized output (so that $y(\infty) = 1$). The first-order low-pass step response is

$$y(t) = 1 - e^{-t/\tau_c}.$$

As stated in the text, we define the 10% and 90% times, t_{10} and t_{90} , by $y(t_{10}) = 0.1$ and $y(t_{90}) = 0.9$. Solving gives

$$0.1 = 1 - e^{-t_{10}/\tau_c} \implies e^{-t_{10}/\tau_c} = 0.9 \implies t_{10} = \tau_c \ln\left(\frac{1}{0.9}\right),$$

and

$$0.9 = 1 - e^{-t_{90}/\tau_c} \implies e^{-t_{90}/\tau_c} = 0.1 \implies t_{90} = \tau_c \ln\left(\frac{1}{0.1}\right).$$

Therefore the 10%–90% rise time is

$$t_r = t_{90} - t_{10} = \tau_c \left[\ln\left(\frac{1}{0.1}\right) - \ln\left(\frac{1}{0.9}\right) \right] = \tau_c \ln\left(\frac{0.9}{0.1}\right) = \tau_c \ln 9 \approx 2.197 \tau_c.$$

If the channel is approximately single-pole, it is standard to identify the bandwidth \mathcal{B}_w (in hertz) with the 3 dB cutoff,

$$\mathcal{B}_w \approx f_{3\text{dB}} = \frac{1}{2\pi\tau_c}.$$

Combining this with $t_r \approx (\ln 9)\tau_c$ yields

$$t_r \approx (\ln 9)\tau_c = \frac{\ln 9}{2\pi} \frac{1}{\mathcal{B}_w} \approx \frac{2.197}{2\pi} \frac{1}{\mathcal{B}_w} \approx \frac{0.349}{\mathcal{B}_w} \approx \frac{0.35}{\mathcal{B}_w}.$$

This is the origin of the widely used bandwidth–rise-time conversion for first-order limited responses in the engineering context, which we also use in the text. In our context it provides a direct translation between measurable small-signal characterizations of the line (a 3 dB bandwidth or step/impulse response) and the effective memory scale τ_c used to parameterize the kernel or its ODE embedding in the main text.

The relations above are exact for a true first-order response. For transfer functions with multiple comparable poles/zeros, the 3 dB point and the 10%–90% rise time generally do not correspond to a unique τ_c ; nevertheless, over a limited frequency range one can often fit a dominant pole and use the same conversions to report an effective memory scale appropriate for the drive waveforms considered in this work. The specifications provided in the literature suggest that [79, 80] τ_c is in the range of 500ps – 1500 ps for a scope in the Ghz regime.

Appendix H: Quantum control channel: Kubo–Born–Oppenheimer derivation of a filtered control Hamiltonian (with weak dissipation)

This appendix derives, from a microscopic quantum model, the effective description used throughout the paper in which the device is driven by a *realized* classical field $\Phi(t)$ that is a causal convolution of the commanded waveform $u(t)$. The key steps are: (i) model the control hardware as a (large) quantum “channel” driven at an input port by a classical source $u(t)$; (ii) identify the delivered device-node field with the expectation value of an output-port operator \hat{B} ; (iii) use linear response (Kubo) to obtain $\Phi(t) = (K * u)(t)$ with K a retarded susceptibility; and (iv) under weak device–channel coupling, show that the device evolves under an effective Hamiltonian $\hat{H}_{\text{eff}}(t) = \hat{H}_A + \Phi(t)\hat{M}$, with any Lindblad contribution appearing as a separate (weak) correction generated by channel fluctuations.

1. Closed system case (no dissipation)

Let \mathcal{H}_A be the device Hilbert space (a qubit in the main text) and \mathcal{H}_B the Hilbert space of the control channel (wiring/filter stack). We assume a classical command $u(t)$ acts at the *input port* of the channel as a c-number source, and the device couples to the *output port* field at the chip.

We take the total Hamiltonian (setting $\hbar = 1$) to be

$$\hat{H}(t) = \hat{H}_A + \hat{H}_B + g \hat{M} \otimes \hat{L} - u(t) \mathbb{I}_A \otimes \hat{F}, \quad (\text{H1})$$

where: \hat{F} is the channel operator conjugate to the applied input waveform $u(t)$ (generalized force at the boundary); \hat{L} is the channel operator representing the delivered field at the device node (generalized coordinate at the output port); \hat{M} is the device coupling operator (e.g. σ_x or σ_z); and g quantifies device loading of the channel.

We assume a bipartite Hilbert space $\mathcal{H} = \mathcal{H}_A \otimes \mathcal{H}_B$ and an initial product state at time t_0 ,

$$\hat{\rho}(t_0) = \hat{\rho}_A(t_0) \otimes \hat{\rho}_B, \quad [\hat{\rho}_B, \hat{H}_B] = 0, \quad (\text{H2})$$

with exact unitary evolution

$$\hat{\rho}(t) = \hat{U}(t, t_0) \hat{\rho}(t_0) \hat{U}^\dagger(t, t_0), \quad \hat{U}(t, t_0) = \mathcal{T} \exp \left(-i \int_{t_0}^t \hat{H}(s) ds \right). \quad (\text{H3})$$

The reduced state is $\hat{\rho}_A(t) := \text{Tr}_B[\hat{\rho}(t)]$.

To derive $\dot{\hat{\rho}}_A(t)$, we will use only standard identities for the partial trace. Fix an orthonormal basis $\{|n\rangle\}$ of \mathcal{H}_B . By definition,

$$\text{Tr}_B[\hat{X}] := \sum_n (\mathbb{I}_A \otimes \langle n |) \hat{X} (\mathbb{I}_A \otimes |n\rangle), \quad \hat{X} \in \mathcal{B}(\mathcal{H}_A \otimes \mathcal{H}_B). \quad (\text{H4})$$

From (H4) one immediately checks the following identities (for \hat{A} acting on \mathcal{H}_A , \hat{Z} acting on \mathcal{H}_B , and \hat{X} arbitrary on $\mathcal{H}_A \otimes \mathcal{H}_B$):

$$\text{Tr}_B[(\hat{A} \otimes \mathbb{I}_B) \hat{X}] = \hat{A} \text{Tr}_B[\hat{X}], \quad (\text{H5})$$

$$\text{Tr}_B[\hat{X}(\hat{A} \otimes \mathbb{I}_B)] = \text{Tr}_B[\hat{X}] \hat{A}, \quad (\text{H6})$$

$$\text{Tr}_B[(\mathbb{I}_A \otimes \hat{Z}) \hat{X}] = \text{Tr}_B[\hat{X}(\mathbb{I}_A \otimes \hat{Z})]. \quad (\text{H7})$$

(Identity (H7) is the ‘‘cyclicity’’ of the trace on subsystem B for operators acting *only* on B . It follows from (H4) by inserting a resolution of the identity on \mathcal{H}_B and relabeling dummy indices.) A useful corollary of (H7) is

$$\mathrm{Tr}_B([\mathbb{I}_A \otimes \hat{Z}, \hat{X}]) = 0 \quad \text{for all } \hat{Z} \in \mathcal{B}(\mathcal{H}_B), \hat{X} \in \mathcal{B}(\mathcal{H}_A \otimes \mathcal{H}_B). \quad (\text{H8})$$

Now use the Liouville–von Neumann equation $\dot{\hat{\rho}}(t) = -i[\hat{H}(t), \hat{\rho}(t)]$ and differentiate under the partial trace, we get

$$\dot{\hat{\rho}}_A(t) = \mathrm{Tr}_B[\dot{\hat{\rho}}(t)] = -i \mathrm{Tr}_B([\hat{H}(t), \hat{\rho}(t)]). \quad (\text{H9})$$

Assume the usual decomposition

$$\hat{H}(t) = \hat{H}_A \otimes \mathbb{I}_B + \mathbb{I}_A \otimes \hat{H}_B + g \hat{M} \otimes \hat{L} + \text{(possible drive terms acting only on } B\text{)}. \quad (\text{H10})$$

We now insert (H10) into (H9) and treat each contribution.

Using (H5)–(H6),

$$\begin{aligned} \mathrm{Tr}_B([\hat{H}_A \otimes \mathbb{I}_B, \hat{\rho}]) &= \mathrm{Tr}_B((\hat{H}_A \otimes \mathbb{I}_B)\hat{\rho}) - \mathrm{Tr}_B(\hat{\rho}(\hat{H}_A \otimes \mathbb{I}_B)) \\ &= \hat{H}_A \mathrm{Tr}_B[\hat{\rho}] - \mathrm{Tr}_B[\hat{\rho}] \hat{H}_A \\ &= [\hat{H}_A, \hat{\rho}_A]. \end{aligned} \quad (\text{H11})$$

For any operator \hat{Z} acting only on B , (H8) gives

$$\mathrm{Tr}_B([\mathbb{I}_A \otimes \hat{Z}, \hat{\rho}]) = 0. \quad (\text{H12})$$

Hence $\mathbb{I}_A \otimes \hat{H}_B$ (and likewise any classical-drive term of the form $\mathbb{I}_A \otimes \hat{Z}(t)$) does not contribute *directly* to $\dot{\hat{\rho}}_A$ at this stage; it affects the reduced dynamics only indirectly through the full state $\hat{\rho}(t)$.

We compute the partial trace of the commutator $[\hat{M} \otimes \hat{L}, \hat{\rho}]$ explicitly:

$$\mathrm{Tr}_B([\hat{M} \otimes \hat{L}, \hat{\rho}]) = \mathrm{Tr}_B((\hat{M} \otimes \hat{L})\hat{\rho}) - \mathrm{Tr}_B(\hat{\rho}(\hat{M} \otimes \hat{L})). \quad (\text{H13})$$

For the first term, pull \hat{M} out using (H5):

$$\begin{aligned} \mathrm{Tr}_B((\hat{M} \otimes \hat{L})\hat{\rho}) &= \mathrm{Tr}_B((\hat{M} \otimes \mathbb{I}_B)(\mathbb{I}_A \otimes \hat{L})\hat{\rho}) \\ &= \hat{M} \mathrm{Tr}_B((\mathbb{I}_A \otimes \hat{L})\hat{\rho}). \end{aligned} \quad (\text{H14})$$

For the second term, first use cyclicity on subsystem B , (H7), to move $(\mathbb{I}_A \otimes \hat{L})$ to the left, and then pull \hat{M} out on the right using (H6):

$$\begin{aligned} \mathrm{Tr}_B(\hat{\rho}(\hat{M} \otimes \hat{L})) &= \mathrm{Tr}_B(\hat{\rho}(\hat{M} \otimes \mathbb{I}_B)(\mathbb{I}_A \otimes \hat{L})) \\ &= \mathrm{Tr}_B((\mathbb{I}_A \otimes \hat{L})\hat{\rho}(\hat{M} \otimes \mathbb{I}_B)) \quad (\text{by (H7)}) \\ &= \mathrm{Tr}_B((\mathbb{I}_A \otimes \hat{L})\hat{\rho}) \hat{M} \quad (\text{by (H6)}). \end{aligned} \quad (\text{H15})$$

Subtracting (H15) from (H14) yields

$$\mathrm{Tr}_B([\hat{M} \otimes \hat{L}, \hat{\rho}]) = [\hat{M}, \mathrm{Tr}_B((\mathbb{I}_A \otimes \hat{L})\hat{\rho})]. \quad (\text{H16})$$

Combining (H9), (H11), (H12), and (H16) gives the exact identity

$$\dot{\hat{\rho}}_A(t) = -i[\hat{H}_A, \hat{\rho}_A(t)] - ig [\hat{M}, \mathrm{Tr}_B((\mathbb{I}_A \otimes \hat{L})\hat{\rho}(t))]. \quad (\text{H17})$$

The nontrivial object is the operator-valued ‘‘field’’

$$\hat{X}_L(t) := \mathrm{Tr}_B((\mathbb{I}_A \otimes \hat{L})\hat{\rho}(t)) \in \mathcal{B}(\mathcal{H}_A), \quad (\text{H18})$$

which depends on the full joint state $\hat{\rho}(t)$ and therefore, in general, on device–channel correlations.

We now impose the common but physically motivated *weak-loading* assumption [39], or Born–Oppenheimer approximation. There exists a regime in which the device perturbs the channel only weakly, so that to leading order

$$\hat{\rho}(t) = \hat{\rho}_A(t) \otimes \hat{\rho}_B^{(u)}(t) + \mathcal{O}(g), \quad (\text{H19})$$

where $\hat{\rho}_B^{(u)}(t)$ is the channel state produced by the drive $u(t)$ *in the absence of the device*, i.e. under the driven channel Hamiltonian

$$\hat{H}_B^{(u)}(t) = \hat{H}_B - u(t)\hat{F}. \quad (\text{H20})$$

Under (H19),

$$\text{Tr}_B(\hat{B}\hat{\rho}(t)) = \hat{\rho}_A(t)\Phi(t) + \mathcal{O}(g), \quad \Phi(t) := \text{Tr}_B(\hat{\rho}_B^{(u)}(t)\hat{L}), \quad (\text{H21})$$

and (H9) becomes, to leading order in g ,

$$\dot{\rho}_A(t) = -i[\hat{H}_A + g\Phi(t)\hat{M}, \hat{\rho}_A(t)] + \mathcal{O}(g^2). \quad (\text{H22})$$

Thus, at the Hamiltonian level, the device is driven by the c-number realized field $\Phi(t)$ generated by the channel. We now compute $\Phi(t)$ from (H21) in *linear response* in the source u , being explicit about which time each density operator refers to.

Fix an initial time t_0 at which the drive is specified and the channel is prepared in a stationary reference state for the unforced Hamiltonian \hat{H}_B :

$$\hat{\rho}_B^{(u)}(t_0) = \hat{\rho}_B, \quad [\hat{\rho}_B, \hat{H}_B] = 0. \quad (\text{H23})$$

Here $\hat{\rho}_B$ is time-independent in the Schrödinger picture under \hat{H}_B , but it is the *initial condition* for the driven evolution under $\hat{H}_B - u(t)\hat{F}$.

We work in the interaction picture with respect to \hat{H}_B :

$$\hat{O}_I(t) = e^{i\hat{H}_B(t-t_0)}\hat{O}e^{-i\hat{H}_B(t-t_0)}. \quad (\text{H24})$$

In particular,

$$\hat{F}_I(t) = e^{i\hat{H}_B(t-t_0)}\hat{F}e^{-i\hat{H}_B(t-t_0)}, \quad \hat{L}_I(t) = e^{i\hat{H}_B(t-t_0)}\hat{L}e^{-i\hat{H}_B(t-t_0)}. \quad (\text{H25})$$

Let $\hat{\rho}_B^{(u)}(t)$ denote the channel density operator at *observation time* t in the Schrödinger picture, evolved from the initial condition (H23) under the time-dependent Hamiltonian $\hat{H}_B - u(t)\hat{F}$. Define its interaction-picture counterpart

$$\hat{\rho}_I(t) = e^{i\hat{H}_B(t-t_0)}\hat{\rho}_B^{(u)}(t)e^{-i\hat{H}_B(t-t_0)}. \quad (\text{H26})$$

Then $\hat{\rho}_I(t_0) = \hat{\rho}_B$ and $\hat{\rho}_I(t)$ satisfies

$$\frac{d}{dt}\hat{\rho}_I(t) = iu(t)[\hat{F}_I(t), \hat{\rho}_I(t)]. \quad (\text{H27})$$

Integrating (H27) from t_0 to t and expanding to first order in u gives

$$\hat{\rho}_I(t) = \hat{\rho}_B + i \int_{t_0}^t ds u(s)[\hat{F}_I(s), \hat{\rho}_B] + \mathcal{O}(u^2). \quad (\text{H28})$$

Transforming back to the Schrödinger picture at time t ,

$$\hat{\rho}_B^{(u)}(t) = e^{-i\hat{H}_B(t-t_0)}\hat{\rho}_I(t)e^{i\hat{H}_B(t-t_0)} = \hat{\rho}_B(t) + \delta\hat{\rho}_B(t) + \mathcal{O}(u^2), \quad (\text{H29})$$

where, because $[\hat{\rho}_B, \hat{H}_B] = 0$,

$$\hat{\rho}_B(t) := e^{-i\hat{H}_B(t-t_0)}\hat{\rho}_B e^{i\hat{H}_B(t-t_0)} = \hat{\rho}_B, \quad (\text{H30})$$

and the first-order correction is

$$\delta\hat{\rho}_B(t) = i \int_{t_0}^t ds u(s)e^{-i\hat{H}_B(t-t_0)}[\hat{F}_I(s), \hat{\rho}_B]e^{i\hat{H}_B(t-t_0)}. \quad (\text{H31})$$

Equivalently (and often more convenient), one can keep the correction in the interaction picture as in (H28).

By definition,

$$\Phi(t) = \text{Tr}_B(\hat{\rho}_B^{(u)}(t)\hat{L}) = \text{Tr}_B(\hat{\rho}_I(t)\hat{L}_I(t)), \quad (\text{H32})$$

where the second equality follows from (H26) and cyclicity of trace. Insert the linearized state (H28):

$$\begin{aligned} \Phi(t) &= \text{Tr}_B(\hat{\rho}_B\hat{L}_I(t)) + i \int_{t_0}^t ds u(s) \text{Tr}_B([\hat{F}_I(s), \hat{\rho}_B]\hat{L}_I(t)) + \mathcal{O}(u^2) \\ &= \Phi_0 + i \int_{t_0}^t ds u(s) \langle [\hat{L}_I(t), \hat{F}_I(s)] \rangle_B + \mathcal{O}(u^2), \end{aligned} \quad (\text{H33})$$

with

$$\Phi_0 := \text{Tr}_B(\hat{\rho}_B\hat{L}) = \text{Tr}_B(\hat{\rho}_B\hat{L}_I(t)), \quad \langle \cdot \rangle_B := \text{Tr}_B(\hat{\rho}_B \cdot). \quad (\text{H34})$$

In the second line of (H33) we used the trace identity $\text{Tr}_B([\hat{F}_I(s), \hat{\rho}_B]\hat{L}_I(t)) = \text{Tr}_B(\hat{\rho}_B[\hat{L}_I(t), \hat{F}_I(s)])$.

Because $[\hat{\rho}_B, \hat{H}_B] = 0$, the correlator depends only on the time difference $\tau = t - s$, so we define

$$\chi_{LF}(\tau) := i \Theta(\tau) \langle [\hat{L}_I(\tau), \hat{F}] \rangle_B = i \Theta(\tau) \langle [\hat{L}_I(t), \hat{F}_I(s)] \rangle_B, \quad \tau = t - s. \quad (\text{H35})$$

Therefore,

$$\Phi(t) = \Phi_0 + \int_{t_0}^t ds \chi_{LF}(t-s) u(s) + \mathcal{O}(u^2). \quad (\text{H36})$$

Taking $t_0 \rightarrow -\infty$ (with the usual adiabatic switch-on prescription if desired) yields the causal convolution form

$$\Phi(t) = \Phi_0 + \int_{-\infty}^t K(t-s) u(s) ds + \mathcal{O}(u^2), \quad K(\tau) \equiv \chi_{LF}(\tau). \quad (\text{H37})$$

Equation (H37) is precisely the kernel model used in the main text: the control-channel memory kernel is the retarded susceptibility of the driven channel between the input-port operator \hat{F} and the output-port operator \hat{B} .

2. Closed versus open control channels: structure of the retarded kernel

In this appendix we treat the *control channel* B as the only system whose input–output map carries memory. The device A may be treated separately (and may remain unitary); the kernel below is defined purely in terms of B . We consider a classical command $u(t)$ that couples at the *input port* to a Hermitian channel operator \hat{F} , and we define the *delivered field* at the device node by a Hermitian channel operator \hat{L} (notation $\hat{L} \equiv \hat{B}$ in other parts of the manuscript). In linear response the realized field $\Phi(t) := \langle \hat{L} \rangle_t$ is governed by a retarded susceptibility.

We now treat the channel. Let $\hat{\rho}_B$ be a stationary reference state for the unforced channel dynamics. The retarded response function is

$$\chi_{LF}(\tau) := i \Theta(\tau) \langle [\hat{L}_I(\tau), \hat{F}_I(0)] \rangle_B, \quad \langle \cdot \rangle_B := \text{Tr}_B(\hat{\rho}_B \cdot), \quad (\text{H38})$$

where the interaction-picture operators $\hat{O}_I(t)$ are defined with respect to the *unforced* channel generator (Hamiltonian for the closed case, Liouvillian for the open case). In frequency domain we write $\chi_{LF}(\omega)$ for the Fourier transform of $\chi_{LF}(\tau)$ (under the usual convergence prescription).

The question addressed here is: *under what conditions can $\chi_{LF}(\tau)$ be written (or well approximated) as a sum of decaying exponentials, as assumed in the RC-like model of the main text?* We distinguish two cases.

a. Closed (lossless) channel: unitary kernel and Lehmann representation

Assume first that the channel B is *closed*, so its unforced dynamics is unitary under a time-independent Hamiltonian \hat{H}_B . Take the reference state to commute with \hat{H}_B , hence diagonal in the energy basis. Let $\hat{H}_B |n\rangle = E_n |n\rangle$ and

$$\hat{\rho}_B = \sum_n p_n |n\rangle\langle n|, \quad p_n \geq 0, \quad \sum_n p_n = 1. \quad (\text{H39})$$

Then $\hat{L}_I(\tau) = e^{i\hat{H}_B\tau} \hat{L} e^{-i\hat{H}_B\tau}$ admits the expansion

$$\hat{L}_I(\tau) = \sum_{m,n} e^{i(E_m - E_n)\tau} L_{mn} |m\rangle\langle n|, \quad L_{mn} := \langle m| \hat{L} |n\rangle. \quad (\text{H40})$$

Using (H39)–(H40), the commutator expectation becomes

$$\langle [\hat{L}_I(\tau), \hat{F}] \rangle_B = \sum_{m,n} (p_n - p_m) L_{nm} F_{mn} e^{i(E_n - E_m)\tau}, \quad F_{mn} := \langle m| \hat{F} |n\rangle. \quad (\text{H41})$$

Therefore the retarded kernel has the Lehmann representation

$$\chi_{LF}(\tau) = i \Theta(\tau) \sum_{m,n} (p_n - p_m) L_{nm} F_{mn} e^{i(E_n - E_m)\tau}. \quad (\text{H42})$$

We now list a few consequences of this description. First, for finite-dimensional B , (H42) is a finite sum of purely oscillatory terms $e^{i\omega_{nm}\tau}$ with Bohr frequencies $\omega_{nm} = E_n - E_m$. Hence $\chi_{LF}(\tau)$ does not generically decay as $\tau \rightarrow \infty$ (except for special degeneracies or cancellations). In frequency space, the imaginary part is a sum of delta-peaked spectral lines rather than a smooth dissipative response. Second, the factor $\Theta(\tau)$ enforces causality. For Hermitian \hat{L}, \hat{F} , $\langle [\hat{L}_I(\tau), \hat{F}] \rangle_B$ is purely imaginary, so $\chi_{LF}(\tau)$ is real for $\tau > 0$. The Fourier transform satisfies the reality condition $\chi_{LF}(\omega)^* = \chi_{LF}(-\omega)$ and Kramers–Kronig relations (analyticity in the upper half-plane). Lastly, a closed channel can still exhibit *memory* (phase lag, propagation delay, reactive distortion), but its kernel is not generically a sum of *decaying* exponentials. Effective decay can occur only in a macroscopic limit (continuous spectrum) through dephasing (destructive interference), in which case $\chi_{LF}(\tau)$ typically has non-exponential tails and corresponding branch-cut structure in Laplace/Fourier space. Thus the RC-like *relaxational* kernels of the main text require either genuine dissipation or an effective coarse-graining that produces such an irreversible semigroup.

This said, we now provide a general overview of how model dissipation in the *control channel* B itself (resistive losses, thermalized attenuators, leakage into many uncontrolled degrees of freedom) by treating B as an *open* system with an undriven GKLS generator \mathcal{L}_0 . Let $\hat{\rho}_{B,ss}$ be a stationary state, $\mathcal{L}_0 \hat{\rho}_{B,ss} = 0$. We drive the channel at the input port by the classical command $u(t)$ through the Hamiltonian perturbation $-u(t)\hat{F}$, so the channel master equation is

$$\dot{\hat{\rho}}_B(t) = \mathcal{L}_0 \hat{\rho}_B(t) - i u(t) [\hat{F}, \hat{\rho}_B(t)]. \quad (\text{H43})$$

Define the realized field and its linear response about stationarity:

$$\Phi(t) := \text{Tr}_B(\hat{\rho}_B(t)\hat{L}), \quad \delta\Phi(t) := \Phi(t) - \text{Tr}_B(\hat{\rho}_{B,ss}\hat{L}). \quad (\text{H44})$$

We then write $\hat{\rho}_B(t) = \hat{\rho}_{B,ss} + \delta\hat{\rho}_B(t)$ and keep only terms linear in u :

$$\dot{\delta\hat{\rho}}_B(t) = \mathcal{L}_0 \delta\hat{\rho}_B(t) - i u(t) [\hat{F}, \hat{\rho}_{B,ss}]. \quad (\text{H45})$$

Assuming the steady-state (no-transient) regime, the causal solution is

$$\delta\hat{\rho}_B(t) = \int_{-\infty}^t ds e^{\mathcal{L}_0(t-s)} \left(-i[\hat{F}, \hat{\rho}_{B,ss}] \right) u(s). \quad (\text{H46})$$

Taking the expectation of \hat{L} yields the convolution form

$$\delta\Phi(t) = \int_{-\infty}^t ds K(t-s) u(s), \quad K(\tau) := \text{Tr}_B \left(\hat{L} e^{\mathcal{L}_0\tau} \left(-i[\hat{F}, \hat{\rho}_{B,ss}] \right) \right), \quad \tau \geq 0. \quad (\text{H47})$$

Introduce the adjoint semigroup $e^{\mathcal{L}_0^\dagger\tau}$ acting on observables via $\text{Tr}(\hat{X} e^{\mathcal{L}_0\tau} \hat{Y}) = \text{Tr}((e^{\mathcal{L}_0^\dagger\tau} \hat{X}) \hat{Y})$. Then

$$K(\tau) = i \text{Tr}_B \left(\hat{\rho}_{B,ss} [e^{\mathcal{L}_0^\dagger\tau} \hat{L}, \hat{F}] \right), \quad \chi_{LF}(\tau) = \Theta(\tau) K(\tau). \quad (\text{H48})$$

Equation (H48) is the Markovian open-channel analogue of the unitary Kubo formula (H38): dissipation enters through the semigroup $e^{\mathcal{L}_0^\dagger\tau}$.

At this point, we assume that, on the operator subspace relevant for the port observables, \mathcal{L}_0^\dagger admits a discrete spectral decomposition (e.g. after a finite-mode truncation of the channel):

$$\mathcal{L}_0^\dagger \hat{R}_k = \lambda_k \hat{R}_k, \quad \text{Re}(\lambda_k) \leq 0, \quad (\text{H49})$$

and expand $e^{\mathcal{L}_0^\dagger \tau} \hat{L}$ in this eigenbasis. Inserting into (H48) yields

$$\chi_{LF}(\tau) = \Theta(\tau) \sum_k c_k e^{\lambda_k \tau}, \quad (H50)$$

with coefficients c_k determined by the overlaps of \hat{L} and \hat{F} with the eigenoperators and by the stationary state $\hat{\rho}_{B,ss}$. Stability implies that all non-steady modes decay: $\text{Re}(\lambda_k) < 0$ for $k \neq 0$. In general $\lambda_k = -\nu_k + i\omega_k$, producing damped oscillations.

The exponential (classical) kernels used in the main text correspond to a *relaxational* regime in which the relevant channel modes are overdamped and non-oscillatory in the drive band. Concretely, the dominant eigenvalues satisfy $\lambda_k = -\nu_k$ with $\nu_k > 0$, so

$$\chi_{LF}(\tau) = \Theta(\tau) \sum_{k=1}^{K_{\max}} c_k e^{-\nu_k \tau}, \quad \nu_k > 0. \quad (H51)$$

Keeping only the slowest rate ν_{\min} yields the single-pole (single-RC) approximation.

This purely relaxational spectral structure is exactly what is enforced by passive RC ladder models of the control stack: the transfer function is stable with poles on the negative real axis, implying a sum (finite ladder) or mixture (distributed line) of decaying exponentials (Appendix F). Thus the RC-like approximation employed in the main text may be read equivalently as: (i) a classical network-synthesis statement about passive RC transfer functions; or (ii) an open-channel statement that the effective generator \mathcal{L}_0^\dagger has a dominantly real, negative spectrum on the relevant port-observable subspace.

3. Thermal Lehmann representation of the kernel and its temperature dependence

In this subsection, we make the kernel $K(\tau) \equiv \chi_{LF}(\tau)$ in (H38) fully explicit for a *closed* control channel in a thermal state. This yields a concrete expression for how the temperature and the channel energy spectrum determine the linear filter seen by the commanded waveform $u(t)$.

Assume the unforced channel Hamiltonian \hat{H}_B is time independent and the reference state is thermal,

$$\hat{\rho}_B = \frac{e^{-\beta \hat{H}_B}}{Z}, \quad Z = \text{Tr}_B(e^{-\beta \hat{H}_B}), \quad \beta = (k_B T)^{-1}. \quad (H52)$$

Let $\{|n\rangle\}$ be an eigenbasis of \hat{H}_B ,

$$\hat{H}_B |n\rangle = E_n |n\rangle, \quad p_n := \langle n| \hat{\rho}_B |n\rangle = \frac{e^{-\beta E_n}}{Z}. \quad (H53)$$

We write the interaction-picture operators (with respect to \hat{H}_B) as $\hat{O}_I(t) = e^{i\hat{H}_B(t-t_0)} \hat{O} e^{-i\hat{H}_B(t-t_0)}$ and define the output-port observable \hat{L} (device-side field) and input-port drive operator \hat{F} (boundary generalized force), consistent with Sec. H 1.

Stationarity implies

$$K(\tau) \equiv \chi_{LF}(\tau) = i \Theta(\tau) \text{Tr}_B \left(\hat{\rho}_B [\hat{L}_I(\tau), \hat{F}_I(0)] \right). \quad (H54)$$

We now expand (H54) in the energy eigenbasis.

Insert resolutions of the identity into $\hat{L}_I(\tau)$ and $\hat{F}_I(0) = \hat{F}$. Writing $L_{mn} := \langle m| \hat{L} |n\rangle$ and $F_{mn} := \langle m| \hat{F} |n\rangle$, we have

$$\hat{L}_I(\tau) = e^{i\hat{H}_B \tau} \hat{L} e^{-i\hat{H}_B \tau} = \sum_{m,n} e^{i(E_m - E_n)\tau} L_{mn} |m\rangle \langle n|. \quad (H55)$$

Similarly,

$$\hat{F} = \sum_{m,n} F_{mn} |m\rangle \langle n|. \quad (H56)$$

We compute the thermal correlators. We have $\langle \hat{L}_I(\tau) \hat{F} \rangle_\beta$ and $\langle \hat{F} \hat{L}_I(\tau) \rangle_\beta$ with $\langle \cdot \rangle_\beta := \text{Tr}_B(\hat{\rho}_B \cdot)$. Using $\hat{\rho}_B = \sum_n p_n |n\rangle \langle n|$ from (H53),

$$\begin{aligned} \langle \hat{L}_I(\tau) \hat{F} \rangle_\beta &= \sum_n p_n \langle n | \hat{L}_I(\tau) \hat{F} | n \rangle \\ &= \sum_{n,m} p_n e^{i(E_n - E_m)\tau} L_{nm} F_{mn}, \end{aligned} \quad (\text{H57})$$

$$\begin{aligned} \langle \hat{F} \hat{L}_I(\tau) \rangle_\beta &= \sum_n p_n \langle n | \hat{F} \hat{L}_I(\tau) | n \rangle \\ &= \sum_{n,m} p_n e^{i(E_m - E_n)\tau} F_{nm} L_{mn} \\ &= \sum_{n,m} p_m e^{i(E_n - E_m)\tau} L_{nm} F_{mn}, \end{aligned} \quad (\text{H58})$$

where the last step in (H58) is a relabeling $n \leftrightarrow m$.

Subtracting (H58) from (H57) yields

$$\langle [\hat{L}_I(\tau), \hat{F}] \rangle_\beta = \sum_{n,m} (p_n - p_m) L_{nm} F_{mn} e^{i(E_n - E_m)\tau}. \quad (\text{H59})$$

Therefore the thermal kernel is

$$K(\tau) = i \Theta(\tau) \sum_{n,m} (p_n - p_m) L_{nm} F_{mn} e^{i(E_n - E_m)\tau}, \quad p_n = \frac{e^{-\beta E_n}}{Z}. \quad (\text{H60})$$

This is the thermal specialization of (H42).

Using now the explicit exponential form $p_n = \frac{e^{-\beta E_n}}{Z}$, we can rewrite the weight difference as

$$p_n - p_m = \frac{e^{-\beta E_m}}{Z} \left(e^{-\beta(E_n - E_m)} - 1 \right) = -\frac{e^{-\beta E_m}}{Z} \left(1 - e^{-\beta \omega_{nm}} \right), \quad \omega_{nm} := E_n - E_m. \quad (\text{H61})$$

Thus each Bohr frequency ω_{nm} is weighted by an explicit thermal factor $1 - e^{-\beta \omega_{nm}}$, encoding detailed balance.

At this point, we define the (two-sided) Fourier transform of the retarded kernel

$$K(\omega) := \int_{-\infty}^{\infty} d\tau e^{i\omega\tau} K(\tau). \quad (\text{H62})$$

Using $\int_0^\infty d\tau e^{i(\omega - \omega_{nm})\tau} = \pi\delta(\omega - \omega_{nm}) + i\mathcal{P}\frac{1}{\omega - \omega_{nm}}$, (H60) implies

$$K(\omega) = \sum_{n,m} (p_n - p_m) L_{nm} F_{mn} \left(\mathcal{P}\frac{1}{\omega - \omega_{nm}} - i\pi\delta(\omega - \omega_{nm}) \right). \quad (\text{H63})$$

The dissipative (loss) part is therefore

$$\text{Im } K(\omega) = -\pi \sum_{n,m} (p_n - p_m) L_{nm} F_{mn} \delta(\omega - \omega_{nm}). \quad (\text{H64})$$

It is often convenient to introduce the (non-symmetrized) dynamical correlation spectrum

$$S_{LF}(\omega) := \int_{-\infty}^{\infty} d\tau e^{i\omega\tau} \langle \hat{L}_I(\tau) \hat{F} \rangle_\beta = 2\pi \sum_{n,m} p_n L_{nm} F_{mn} \delta(\omega - \omega_{nm}), \quad (\text{H65})$$

for which thermal weights imply the KMS/detailed-balance relation

$$S_{LF}(-\omega) = e^{-\beta\omega} S_{FL}(\omega). \quad (\text{H66})$$

Comparing (H64) with (H65) gives the standard fluctuation-dissipation relation between the retarded response and equilibrium fluctuations:

$$\text{Im } K(\omega) = -\frac{1}{2} \left(1 - e^{-\beta\omega} \right) S_{LF}(\omega). \quad (\text{H67})$$

Equivalently, in terms of the symmetrized spectrum $S_{LF}^{\text{sym}}(\omega) := \frac{1}{2}(S_{LF}(\omega) + S_{FL}(-\omega))$,

$$S_{LF}^{\text{sym}}(\omega) = -\coth\left(\frac{\beta\omega}{2}\right) \text{Im } K(\omega), \quad (\text{H68})$$

(up to the sign convention relating K to χ ; here $K \equiv \chi_{LF}$ as in discussed earlier).

Equations (H60)–(H68) show that, for a closed channel, the kernel is determined by (i) the frequencies ω_{nm} , (ii) the port matrix elements $L_{nm}F_{mn}$, and (iii) the thermal factors $p_n - p_m$, or equivalently the detailed-balance weights $1 - e^{-\beta\omega}$. In particular, for a finite-dimensional closed channel, $K(\tau)$ is a quasi-periodic sum of purely oscillatory terms and does not generically decay as $\tau \rightarrow \infty$. Thus thermal equilibrium alone does not yield an RC-like relaxational kernel; obtaining sums of *decaying* exponentials requires either dissipation (open channel) or an effective continuum/coarse-graining limit, as discussed above.

Let us now observe that the general kernel $K(\tau) = \chi_{LF}(\tau)$ becomes a familiar linear-response *admittance* (or more generally a *transadmittance*) once we identify the input and output operators with standard port variables.

At an electrical input port, a classical voltage drive $u(t)$ couples to the port charge operator \hat{q} via the work term

$$\hat{H}_{\text{drive}}(t) = -u(t)\hat{q}. \quad (\text{H69})$$

Comparing with $\hat{V}(t) = -u(t)\hat{F}$, we identify the input operator as $\hat{F} = \hat{q}$.

If we choose the output observable to be the port current $\hat{I} := \dot{\hat{q}} = \frac{i}{\hbar}[\hat{H}_B, \hat{q}]$ (here $\hbar = 1$), then the kernel

$$\chi_{Iq}(\tau) = i\Theta(\tau)\langle[\hat{I}_I(\tau), \hat{q}]\rangle_{\beta} \quad (\text{H70})$$

governs the linear response $\delta\langle\hat{I}(t)\rangle = \int_{-\infty}^t ds \chi_{Iq}(t-s)u(s)$. In the frequency domain,

$$\delta\langle\hat{I}(\omega)\rangle = Y(\omega)u(\omega), \quad Y(\omega) \equiv \chi_{Iq}(\omega), \quad (\text{H71})$$

so the complex admittance $Y(\omega)$ is exactly a retarded susceptibility.

Using $\hat{I} = \dot{\hat{q}}$, one may integrate by parts (or use $\hat{I}(\omega) = -i\omega\hat{q}(\omega)$ at the level of linear response) to write

$$Y(\omega) = -i\omega\chi_{qq}(\omega), \quad \chi_{qq}(\tau) = i\Theta(\tau)\langle[\hat{q}_I(\tau), \hat{q}]\rangle_{\beta}. \quad (\text{H72})$$

This is the standard Kubo identification of admittance with a retarded correlator.

It follows that the cycle-averaged power delivered by a monochromatic drive $u(t) = \text{Re}(u_{\omega}e^{-i\omega t})$ is

$$\bar{P}(\omega) = \frac{1}{2}\text{Re } Y(\omega)|u_{\omega}|^2. \quad (\text{H73})$$

For a passive channel, $\bar{P}(\omega) \geq 0$, hence $\text{Re } Y(\omega) \geq 0$. In Lehmann form, one sees this nonnegativity transparently: specializing (H64) to $L = I$, $F = q$, and using $\hat{I}_{nm} = i(E_n - E_m)q_{nm} = i\omega_{nm}q_{nm}$, the dissipative part $\text{Re } Y(\omega)$ can be expressed in terms of squared matrix elements $|q_{nm}|^2$ with thermal weights and delta functions, ensuring that the absorption at $\omega > 0$ is nonnegative for physical port couplings.

In thermal equilibrium, the symmetrized current noise spectrum

$$S_{II}^{\text{sym}}(\omega) := \int_{-\infty}^{\infty} d\tau e^{i\omega\tau} \frac{1}{2}\langle\{\delta\hat{I}_I(\tau), \delta\hat{I}\}\rangle_{\beta} \quad (\text{H74})$$

is related to the dissipative response by the fluctuation–dissipation theorem,

$$S_{II}^{\text{sym}}(\omega) = \omega \coth\left(\frac{\beta\omega}{2}\right) \text{Re } Y(\omega), \quad (\text{H75})$$

(where $\hbar = 1$). In the classical (high-temperature) limit $\beta\omega \ll 1$, this reduces to the Johnson–Nyquist form $S_{II}^{\text{sym}}(\omega) \approx 2k_B T \text{Re } Y(\omega)$. Thus, the same susceptibility that determines the deterministic filtering of the control waveform also fixes the equilibrium fluctuations of the channel output.

More generally, if \hat{L} is a downstream voltage/flux (node coordinate) or a current at a different port, then χ_{LF} is a *transfer* response (transimpedance/transadmittance). In this interpretation, the kernel K used in the main text is precisely an input–output response function between an input-port drive operator (e.g. \hat{q}) and an output-port readout operator (e.g. a downstream node flux $\hat{\varphi}$ or current \hat{I}). This provides a direct bridge between the Kubo kernel $K(\tau)$ and the usual circuit notion of frequency-dependent transfer functions.

4. Adiabatic switch-on in Kubo: from discrete lines to RC-like kernels

The GKLS/semi-group viewpoint in Sec. H 2 makes dissipation explicit through the spectrum of \mathcal{L}_0^\dagger and yields sums of decaying exponentials directly. There is a complementary (and historically standard) linear-response viewpoint, often phrased in terms of an $\eta \downarrow 0^+$ prescription in Kubo theory, which clarifies how a strictly closed thermal channel fails to produce decay and how even infinitesimal damping broadens the spectrum. This is useful here because our goal is precisely to justify why an experimentally observed control stack behaves like a classical causal filter $K(\tau)$ rather than a quasi-periodic kernel without resorting to the open channel.

In the Kubo setup, the channel is assumed to be in an equilibrium (e.g. thermal) state in the remote past, and the perturbation is switched on adiabatically so that the state is not abruptly driven out of equilibrium at $t_0 \rightarrow -\infty$. Concretely, one replaces the drive by an adiabatically switched source, for example

$$u(t) \mapsto u_\eta(t) := e^{\eta t} u(t), \quad \eta > 0,$$

and only at the end takes $\eta \downarrow 0^+$. This implements (i) convergence of integrals from $t_0 = -\infty$, and (ii) selection of the retarded (causal) solution. This is the same physical role played by the $+i0^+$ prescription in retarded Green functions and susceptibilities. (See Kubo's original development of linear response.) [17] In this context, we start from the closed-channel retarded response (unitary interaction picture w.r.t. H_B),

$$K(\tau) \equiv \chi_{LF}(\tau) = i \Theta(\tau) \langle [L_I(\tau), F_I(0)] \rangle_B.$$

With the adiabatic switch-on, the same derivation yields an η -regularized retarded kernel

$$K_\eta(\tau) = i \Theta(\tau) e^{-\eta\tau} \langle [L_I(\tau), F] \rangle_B.$$

Thus, even before invoking any bath, each oscillatory component acquires a factor $e^{-\eta\tau}$: the η prescription is literally an (infinitesimal) exponential damping in the time domain.

For a closed thermal channel, the Lehmann form produces discrete spectral lines at ω_{mn} frequencies. With $\eta > 0$, denominators acquire a finite imaginary part:

$$K_\eta(\omega) = \sum_{n,m} (p_n - p_m) L_{nm} F_{mn} \frac{1}{\omega - \omega_{nm} + i\eta}, \quad \omega_{nm} := E_n - E_m.$$

Taking the imaginary part makes the broadening explicit:

$$\text{Im } K_\eta(\omega) = -\pi \sum_{n,m} (p_n - p_m) L_{nm} F_{mn} \delta_\eta(\omega - \omega_{nm}), \quad \delta_\eta(x) := \frac{1}{\pi} \frac{\eta}{x^2 + \eta^2}.$$

So the δ -peaks of the strictly closed channel are replaced by Lorentzians of width η . In condensed-matter and transport practice, one often replaces η by a physical relaxation rate to model dissipation, i.e. $\eta \rightarrow \Gamma$, producing the same kind of spectral broadening but with a non-infinitesimal width.

A strictly closed finite-dimensional channel has purely real frequencies, so $K(\tau)$ is a sum of oscillatory terms and does not generically decay. To obtain a classical-looking memory kernel, the spectral lines must be broadened by genuine relaxation mechanisms: leakage into uncontrolled degrees of freedom, resistive losses, thermalization in attenuators, or (equivalently) an effective continuum/coarse-graining limit. Operationally, this means that the retarded response is controlled by poles displaced into the lower half-plane,

$$\omega \mapsto \omega + i\gamma_k, \quad \gamma_k > 0,$$

so that each contribution behaves like a damped oscillation

$$K_k(\tau) \propto \Theta(\tau) e^{-\gamma_k \tau} e^{i\omega_k \tau}.$$

In the relaxational (overdamped) regime relevant for an RC-like control stack, the dominant poles in the drive band are approximately on the imaginary axis,

$$K(\omega) \approx \sum_k \frac{c_k}{\nu_k - i\omega}, \quad \nu_k > 0,$$

and the inverse transform gives a sum of pure decays,

$$K(\tau) \approx \Theta(\tau) \sum_k c_k e^{-\nu_k \tau}.$$

This is exactly the same functional form obtained from the GKLS semigroup expansion in Eq. (H51) and in the RC-ladder case; the two viewpoints differ only in language. First, in the open-channel/GKLS picture, the decay rates ν_k are $\nu_k = -\text{Re}(\lambda_k)$ from the spectrum of \mathcal{L}_0^\dagger (microscopic dissipation made explicit). Second, in the η -regularized Kubo picture, η is the adiabatic retarded prescription, and replacing η by a physical linewidth Γ amounts to modeling the same pole displacement caused by dissipation/broadening mechanisms in the channel.

Both routes justify reading the experimentally observed control line as a causal filter with a stable pole structure; the RC-ladder approximation used in the main text corresponds to the special case where the relevant poles are dominantly real and negative in the bandwidth of interest.